4 RESULTS AND DISCUSSION

Present research on significant grindability indices, including grinding forces, specific grinding energy, grinding temperature, force ratio, and surface integrity, is reported under different environments in the following subsection. Understanding the relationship between surface properties and MBN parameters requires a thorough comprehension of the basic grindability indices, such as grinding forces, specific energy, the temperature of grinding, etc. Details of the experimental setup, grinding conditions, and all instruments regarding the grindability and surface integrity indices measurements have been discussed in Chapter 3 for Sections 4.1, 4.2, and 4.3.

4.1 Performance analysis of grinding parameters under grinding environment for ground AISI D2 tool steel

The grindability of an AISI D2 tool steel under dry, wet, and cryogenic cooling conditions at a constant table feed rate of 9 m/min with an Al_2O_3 (aluminum oxide) wheel depend upon many aspects, such as grinding forces (tangential and normal), specific grinding energy, 2D and 3D roughness parameters, etc. These aspects were precisely examined and analyzed in the investigational work to define the applicability of the cryogenic method during grinding workpieces with an alumina wheel. Later, SEM, EDX, AFM and bearing area curve analysis were used to characterize the samples of the ground surface received after grinding under various environments. The observations are recorded after three passes with five repetitions for the entire trial.

4.1.1 Grinding environment on grinding force

Forces are generated when the workpiece is ground against the abrasive wheel during the grinding operation. Grinding forces, namely, tangential force (F_t) and normal force (F_n),

were measured using a 3D force dynamometer during each pass and noted the value of grinding force, as indicated in Fig. 4.1.

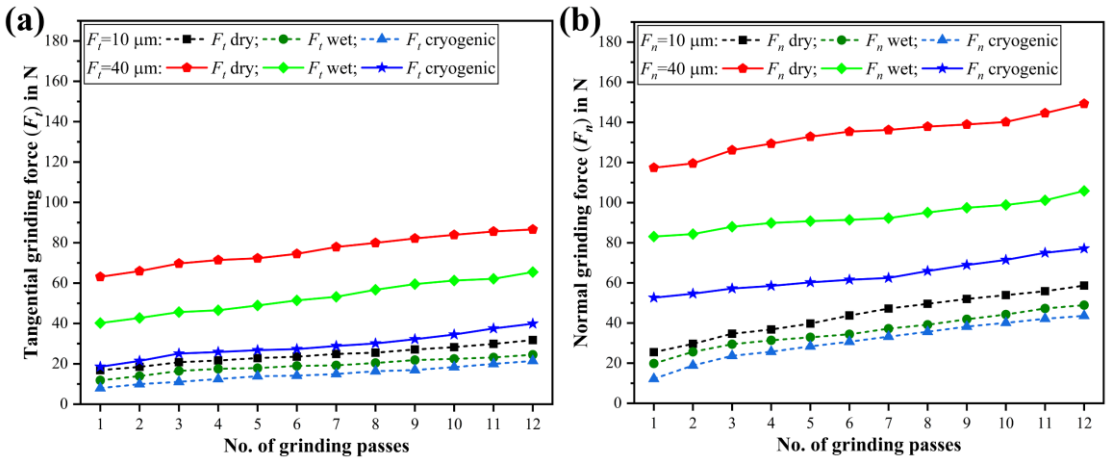

Fig. 4.1: Variations in grinding forces with number of grinding passes at different downfeed: (a) Tangential grinding force; (b) Normal grinding force.

This figure shows increased force with an increase in the number of grinding passes in tangential and normal directions at low (10 µm) and high (40 µm) downfeed under dry, wet, and cryogenic conditions. This may be related to the wear of abrasive grits as the number of grinding passes increases [209]. The normal force is still more elevated than the tangential force, as presented in Fig. 4.1 (a) and (b), because of more abrasive grits in the abrasive wheel with a large negative rake angle [210]. Furthermore, increased downfeed in all grinding environments led to larger grinding forces. A rise in downfeed increased wheel loading due to increased friction at the abrasive wheel and workpiece interface, resulting in high heat production. More heat generation, lack of lubrication, and grit fracture under dry grinding produced higher grinding force. Thus, wet, and cryogenic cooling effectively reduced the grinding force magnitude compared to dry grinding due to better cooling and lubrication results. Compared to cryogenic cooling, wet cooling has higher grinding force, while it has lower grinding force than dry. Under high-speed grinding operation, cutting fluid failed to maintain effective cooling and lubrication in the interface zone area at a

higher downfeed. Because of the wedge effect between the abrasive wheel and the workpiece surface, a stiff air layer, also known as the hydrodynamic boundary layer, may form in front of the interface zone area. Therefore, the fluid's energy was insufficient to penetrate the stiff air boundary layer around the abrasive wheel.

Li et al. [19] reported that the hydrodynamic pressure of the fluid is generated in front of the interface area owing to the wedge effect where the grinding wheel–workpiece meets. The findings demonstrated that hydrodynamic pressure increases with increased abrasive wheel speed and decreased distance between the abrasive wheel and workpiece. Thus, based on the results, they found less effective machining performance related to less penetration in the hydrodynamic boundary layer at higher downfeed. In particular, cryogenic cooling using LN_2 coolant even decreased grinding forces significantly. It may be because the LN_2 coolant penetrates deeper into the grinding zone, lowering the grinding temperature and friction between abrasive grit and workpiece and improving grit's fracture and cutting edge sharpness [211].

In other words, less grinding force was obtained at low downfeed (10 μm) compared to the high downfeed (40 μm), as shown in Fig. 4.1. During the 1st pass, under cryogenic grinding, a reduction in F_t was obtained by 52.87% and 32.85% at 10 μm and by 70.60% and 53.82% at 40 μm, and F_n was reduced by 52.08% and 38.49% at 10 μm and by 55.17%, and 36.68% at 40 μm as compared to dry and wet environments, respectively. During the 12th pass, at 10 μm, the F_t and F_n in cryogenic environment decreased to about 32.61% and 25.69% than dry and 12.67% and 10.88% over wet, and at 40 μm, F_t and F_n reduced to approximately 53.95% and 48.32% to dry and 39.09% and 27.11% than wet. Similarly, Awale et al. [166] conducted a grinding experiment on AISI H13 die steel under small quantity lubrication (SQL) grinding process. They reported a higher grinding force at 32 μm downfeed with each number of grinding passes in comparison to 8 μm downfeed under

all SQL conditions. Owing to the maximum uncut/undeformed chip thickness or wheel loading by debris particles, a higher grinding force was found.

The grinding force is a crucial response parameter to evaluate the effectiveness of a process. Fig. 4.2 revealed that both forces (i.e., tangential, and normal) increase with an increase in downfeed; downfeed is the most influential parameter for the grinding force. These forces have decreasing trends concerning the various environments: dry, wet, and cryogenic, respectively. Due to the absence of cutting fluid in dry environment, the abrasive wheel becomes worn out. Therefore, more contact was covered between the abrasive wheel and the workpiece during rubbing by dull grits over the workpiece surface, resulting in higher grinding force.

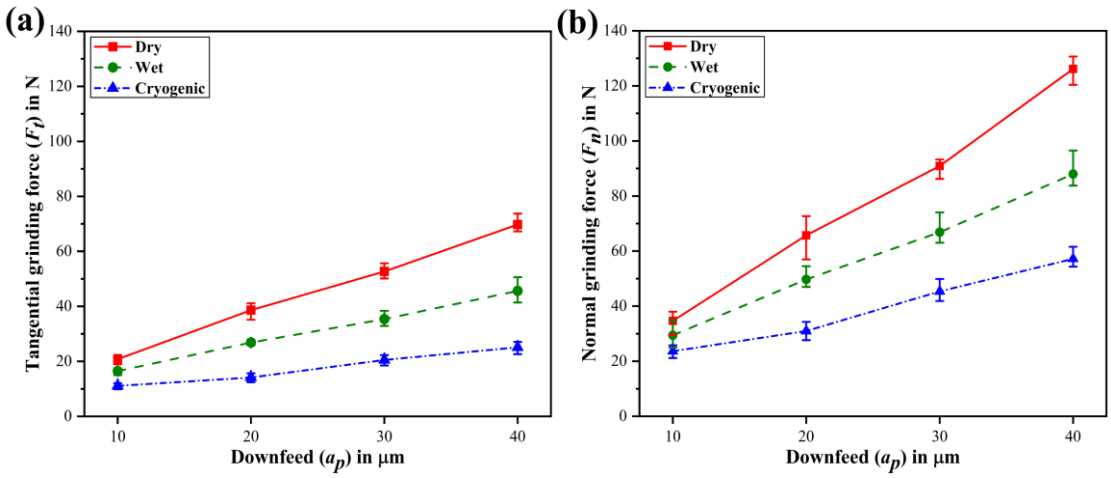

Fig. 4.2: Variations in grinding forces with downfeed under different environments at table feed rate of 9 m/min.

Similarly, Manimaran et al. [211] also reported that higher tangential and normal grinding forces were observed at higher downfeed in the dry grinding over wet and cryogenic grinding of AISI 316 stainless due to the excessive rubbing action of grinding wheel without lubrication media. Conversely, lower grinding forces were obtained due to the retention of the grit's sharpness in the wet grinding process. The cutting fluids also

efficiently controlled the temperature, but at higher a_p, cutting fluids faced a problem in reaching the contact zone. These problems occurred mainly due to the stiff boundary layer of the air around the alumina wheel. Generally, a stiff air boundary layer (hydrodynamic boundary layer) can be developed ahead of the grinding zone due to the wedge between the grinding wheel and the ground surface. The reason was that the hydrodynamic boundary layer is inversely proportional to the smaller space between the abrasive wheel and the ground sample [83].

On the other hand, the ease of the liquid nitrogen in reaching the contact area and the impact of the reduction in temperature resulted in better outcomes of the grinding forces to other environmental conditions. In cryogenic grinding, the F_t decreased by 46–64% related to dry and nearby 32–48% related to wet grinding, and the reduction was 31–54% and 20–38% in F_n over dry and wet grinding, respectively. The grinding forces are induced mainly from the more contribution of shearing action of the abrasive hard particles, i.e., the action of cutting edges on the workpiece, and consequently depends on the grits sharpness and fracturing of edges during the grinding process [212]. According to Manimaran et al. [30], the main factor for the sharpness variation of the grits is the temperature which is generated at the grinding zone area and due to adhered work material with grits. The adhesion is also developed due to the temperature at the newly grind surface, and induced chips react with the grinding wheel or workpiece at high temperature.

4.1.2 Grinding environment on specific grinding energy

Specific grinding energy is the most important response variable throughout the material removal process, especially when grinding difficult-to-machine materials. It varies inversely to the undeformed chip thickness and reflects the degree of interference between the workpiece and the abrasive grit [61]. Fig. 4.3 indicated that specific grinding energy (U_g) for dry, wet, and cryogenic cooling decreases with an increase in process variables

such as downfeed. From Fig. 4.3, it is noted that cryogenic cooling required less specific energy compared to dry and wet conditions during the whole domain of process variables. The influence of better cooling at the contact zone in liquid nitrogen conditions may be credited for reducing grinding zone temperature and sustaining grit sharpness for an extended duration. At the lower a_p, the U_g was high as at such a_p, the effective abrasive grit rake becomes more negative, leading to higher F_t. Therefore, the percentage contribution of rubbing and ploughing actions at lower a_p predominated over shearing action, and with the result that increased the requirement of U_g [59]. Cryogenic cooling induced 46.63% reduction over dry and 32.68% over wet conditions in U_g at a_p of 10 µm. In cryogenic grinding, low U_g signified that grinding operation is more ecological and power-saving, whereas grits deteriorate in dry grinding. Due to the lowest work softening, lower grinding forces, grit sharpness retention, and favourable chip formation, the low grinding energy may be attributed to cryogenic cooling [213]. Further, rubbing action does not support any material removal. Hence, a higher U_g is required in dry grinding for removing material. In comparison, wet grinding consumes less U_g than dry as an effect of cooling at the contact area.

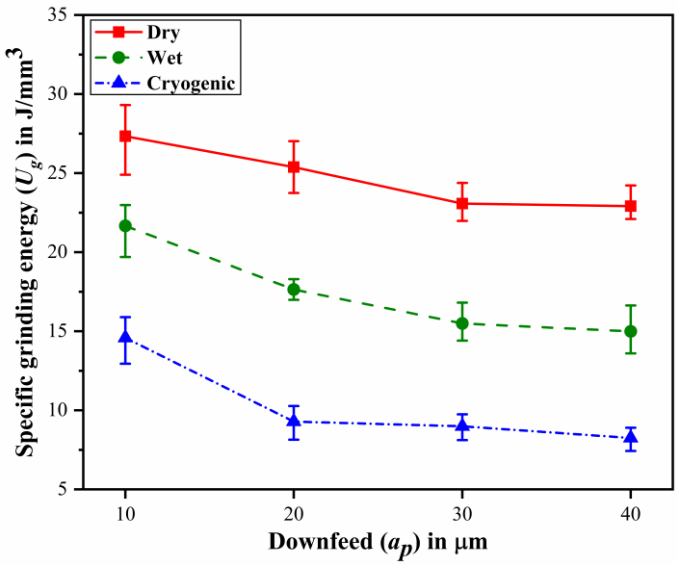

Fig. 4.3: Specific grinding energy versus downfeed under different environments.

4.1.3 Grinding environment on grinding temperature

The grinding temperature plays an essential role in specifying the surface quality and integrity of the finished product. The liquid nitrogen injected at the grinding zone forms a liquid/gaseous cushion between the abrasive grits and chips, providing cooling and lubrication through excellent heat absorption [214]. The abrasive grits' mechanical properties change due to the effective temperature reduction, and when combined with the lubricating effect, the abrasive grits' sharpness is extended. Therefore, sharper abrasive grits produce lower friction and lead to a decrease in the temperature [136]. When the cryogenic coolant is in gaseous form, it can reduce the friction between the abrasive grit and the work material by lubricating well and penetrating better. The decrease in the grinding temperature at the grinding zone by cryogenic cooling leads to improvements in the other grinding parameters.

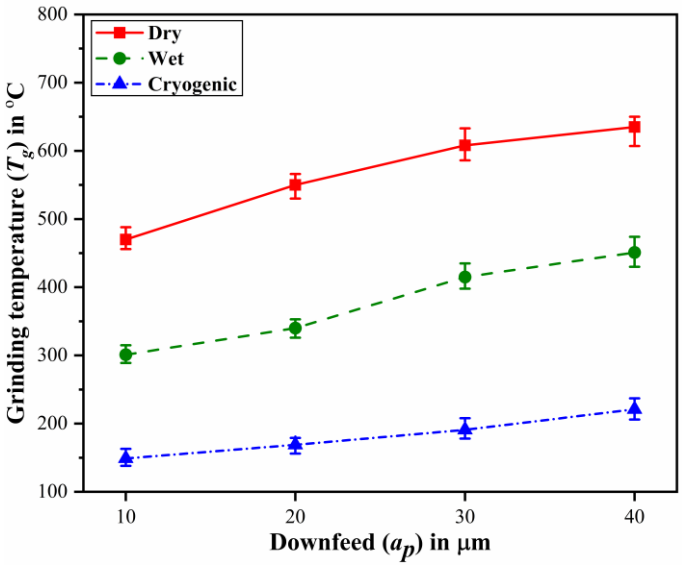

Fig. 4.4: Grinding temperature versus downfeed under different environments.

The variations in the grinding zone temperature with downfeed, when grinding AISI D2 tool steel with Al_2O_3 grinding wheel under distinct grinding environments (i.e., dry, wet, and cryogenic) is shown in Fig. 4.4. Grinding temperature increased with an increase in

downfeed. It can be seen from Fig. 4.4 that the grinding temperature was noticeably greater when dry grinding, which was caused by the increased wheel loading that occurred in the lack of cutting fluid. However, in wet grinding, a major portion of heat is removed by cutting fluid from the grinding zone area by convection heat transfer phenomena. It is further observable that the temperature achieved in a cryogenic environment is much lower than in dry and wet. It has an even lower boiling point of LN_2, which recommends its usage during grinding. The LN_2 coolant generated about 65-70% and a 50-54% reduction in grinding temperature compared to dry and wet grinding, respectively. The temperature reductions of 68.29% and 50.49% at a downfeed of 10 μm and 65.19% and 50.99% at a downfeed of 40 μm were observed in dry and wet grinding, respectively, for cryogenic grinding.

4.1.4 Grinding environment on force ratio

Force ratio is another parameter that gives unobserved details about the efficiency of grinding. Force ratio is the ratio of F_t and F_n. The ratio of grinding force (F_t / F_n) indicates the abrasive-workpiece interaction or nature of wheel-workpiece interaction and sharpness of the grains [166], [215]. Fig. 4.5 indicates the effect of the downfeed on force ratio for the AISI D2 tool steel material. The reduction in force ratio was obtained with an increase in a_p. It may be ascribed to the more contribution of shearing action by the hard abrasive particles during the chip formation process with large contact length at a higher a_p, resulting in decreased force ratio [216].

Based on the error bar chart in Fig. 4.5, the range of force ratio was observed from 0.43 to 0.60. Compared to dry and wet environmental conditions, the lower force ratio was obtained in the LN_2 grinding process at all scales of a_p. It was mainly due to the generation of low temperatures at the contact zone area. The low temperature generated during grinding enhances the durability of the workpiece and makes it less tacky due to less

adhesion between the workpiece and the wheel [145]. Still, in the dry grinding process, the maximum force ratio was obtained due to non-lubrication from the viewpoint of tribology. The grinding force ratios in wet and cryogenic grinding were 6.23% and 20.63% lower than dry grinding at higher a_p, respectively.

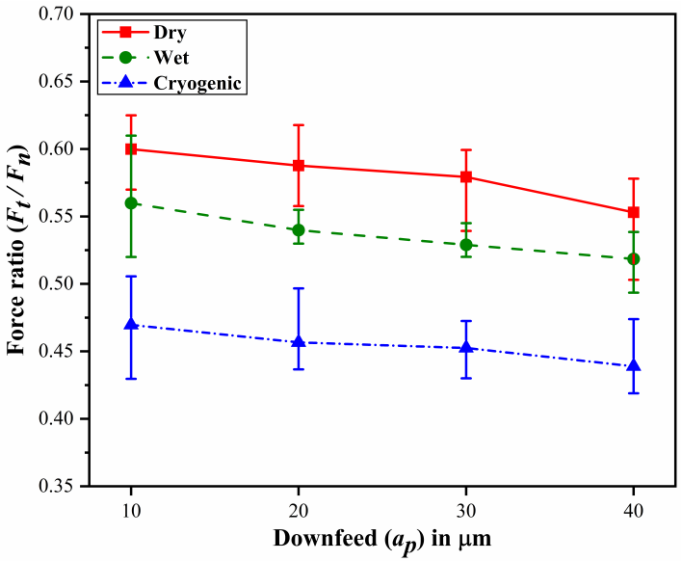

Fig. 4.5: Grinding force ratio versus downfeed under different environments.

4.1.5 Grinding environment on surface roughness

The LN_2 coolant has lesser roughness values at all downfeed due to the control of temperature at the grinding zone. Fig. 4.6 depict the characterization of the micro-geometrical property of the ground surface of AISI D2 tool steel with the help of arithmetical mean roughness or average surface roughness (R_a), root mean square of the surface roughness (R_q) and mean roughness depth (R_z) parameters under dry, wet, and cryogenic environments. The roughness parameters (R_a, R_q and R_z) increased with an increase in downfeed for all the environments. A small roughness value was found at lower a_p. This may be attributed to the fact that downfeed is directly proportional to undeformed chip thickness. In other words, decreasing downfeed caused minimum abrasive cutting edges contact with the nascent ground surface, resulted in minimum friction between

interaction surfaces by rubbing and ploughing [217]. Conversely, at higher a_p, the softening of the workpiece increased during the presence of high temperatures at the grinding area under dry condition, which results in the movement of the material near the abrasive particles. Further, these materials adhered in the void between abrasive particles during consecutive passes of the grinding wheel over the surface, then, smeared particle weld to the machined area, forming metal re-deposition. Hence, higher surface roughness or poor surface quality was observed at higher a_p.

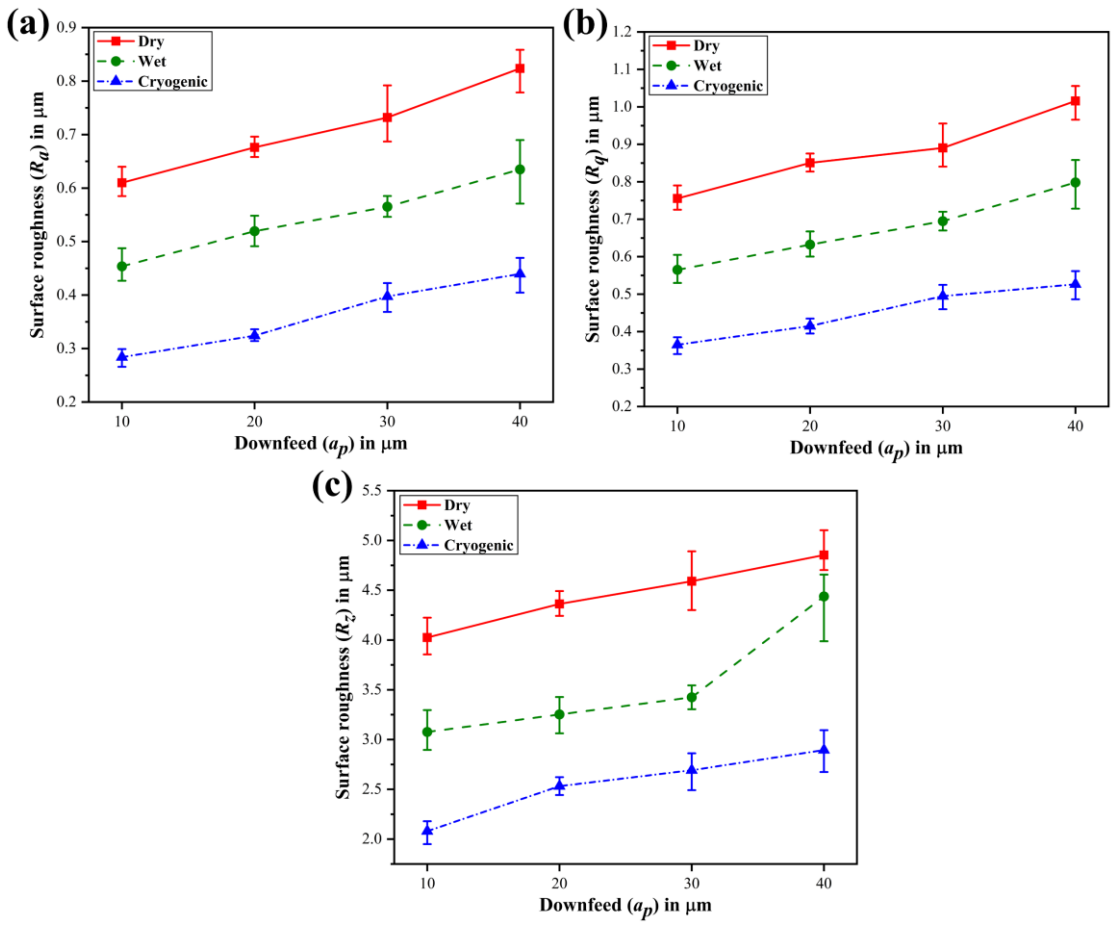

Fig. 4.6: Surface roughness (R_a, R_q and R_z) versus downfeed under different environmental conditions.

This result is in agreement with the Awale et al. [26]. They observed poor surface quality in deeper grooves and metal re-deposition layer over the ground surface under dry grinding. Cutting fluid enhances grinding performance in terms of minimum heat generation in two

ways, such as lubrication and cooling. In the present study, the coolant used in the contact area significantly improved the sharpness of the edges of grits and further decreased the softening of the workpiece. The higher grit sharpness produced good surface quality. This effect smoothly worked up to low a_p; after that, the cutting fluids encountered a challenge near entering the grinding zone at high a_p. Thus, frictional force increased; further, it increased the temperature. The elevated temperature relocated on the machined surface, and then, grits generated marks and thermal damage over the ground surface [218]. The reason is poor lubrication performance in friction surfaces of wheel and workpiece.

Conversely, cutting fluid minimizes the heat generation in the workpiece and maintaining the abrasive wheel cutting efficiency with effective cooling characteristics at higher downfeed [5]. Therefore, a lower grinding force was obtained at all respective downfeed in wet grinding compared to dry grinding. In contrast, more heat dissipation was observed during cryogenic cooling, which offered better surface quality or small surface roughness values at all levels of a_p in comparison to dry and wet environments. Mist of liquid nitrogen out from the nozzle formed a layer among the chips, workpiece, and grits of the wheel, producing a smaller friction coefficient. The 45–54%, 44–52%, and 40–49% reduction in R_a, R_q and R_z, respectively, were achieved by using cryogenic cooling over the dry grinding, and also improvements in R_a, R_q and R_z were observed 29–38%, 28–36%, and 21–35% as compared to wet grinding. Similarly, Kara et al. [219] also reported that optimal surface roughness of ground AISI 5140 steel was obtained at cryogenic treatment over conventional heat treatment.

Fig. 4.7 shows the 2D profiles of the ground surface at 40 µm downfeed under different environments, i.e., LN_2, wet and dry conditions with alumina wheel. In dry grinding, the deformed surface was found due to dull abrasive grits. The circles showed a maximum peak to valley height (i.e., more ups and downs), resulting in higher roughness (refer to Fig. 4.7

(a)). It was mainly induced due to the absence of coolant. Fig. 4.7 (b) indicates the less magnitude of roughness when compared to dry grinding because wet grinding decreased the rubbing action between the grinding wheel and workpiece due to enough lubrication. But at higher a_p, roughness increased due to the failure of cutting fluids at the contact zone area. Besides, the 2D surface profiles with a few peaks and valleys heights generated better surface roughness at higher a_p as compared to dry and wet conditions, as is apparent from Fig. 4.7 (c). Because of lower cryogenic temperature, it produced better abrasive grits sharpness and excellent surface quality.

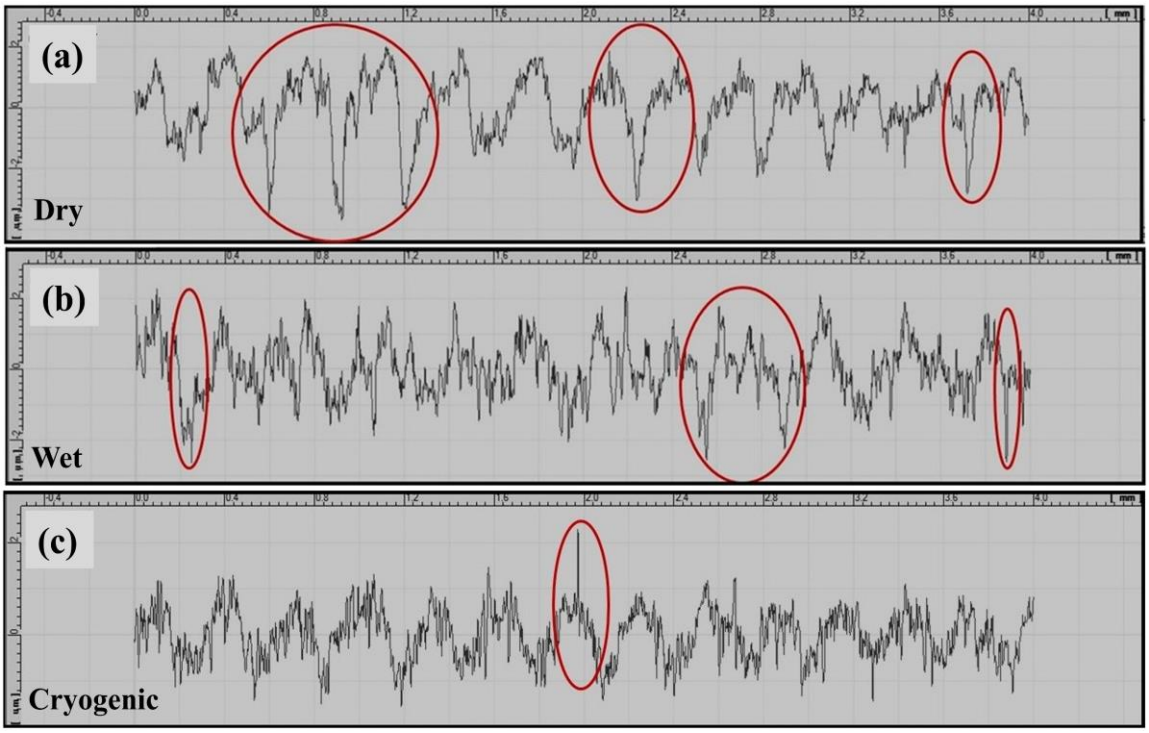

Fig. 4.7: 2D profiles generated by grinding over the surface at 40 µm downfeed under various environments: (a) Dry; (b) Wet; (c) Cryogenic conditions.

4.1.6 Grinding environment on ground surface characteristics

4.1.6.1 Surface morphology

Fig. 4.8 represents the SEM images of the ground surface at maximum downfeed (40 µm) under dry, wet, and cryogenic conditions. Grinding marks, surface burn, redeposition,

pull out and side flow materials were seen during dry grinding, as revealed in Fig. 4.8 (a). Because of the interaction of alumina grits with the workpiece surface in the lack of cooling and lubricating actions, more heat was induced in the interface zone area. Raising the workpiece's temperature increased its adhesion to the wheel, causing metal redeposition. Also, high temperatures generated grinding marks/scratches and surface burn. Therefore, as a result of the above effects, the surface quality was diminished. In other words, with the cooling and lubricating effect of water-based soluble oil, the ground surface has fewer defects than in dry conditions, as shown in Fig. 4.8 (b). The sharpness of the grits was significantly enhanced by the coolant that was applied to the interface zone area. Thus, the higher grit sharpness provided better surface quality [30]. In order to reach a high downfeed (40 µm), wet coolants have challenges entering the interface zone. The lack of coolant raised frictional force, which raised the temperature. Hence, under wet cooling, pull out, and redeposition materials were found to decrease. As perceived in Fig. 4.8 (c), a smooth surface under cryogenic cooling was obtained due to the controlled temperature and high grits sharpness. Sharper grits lead to more shearing action. Due to better shearing or cutting action by the sharper grits, except for side flow, no further defects were noticeable.

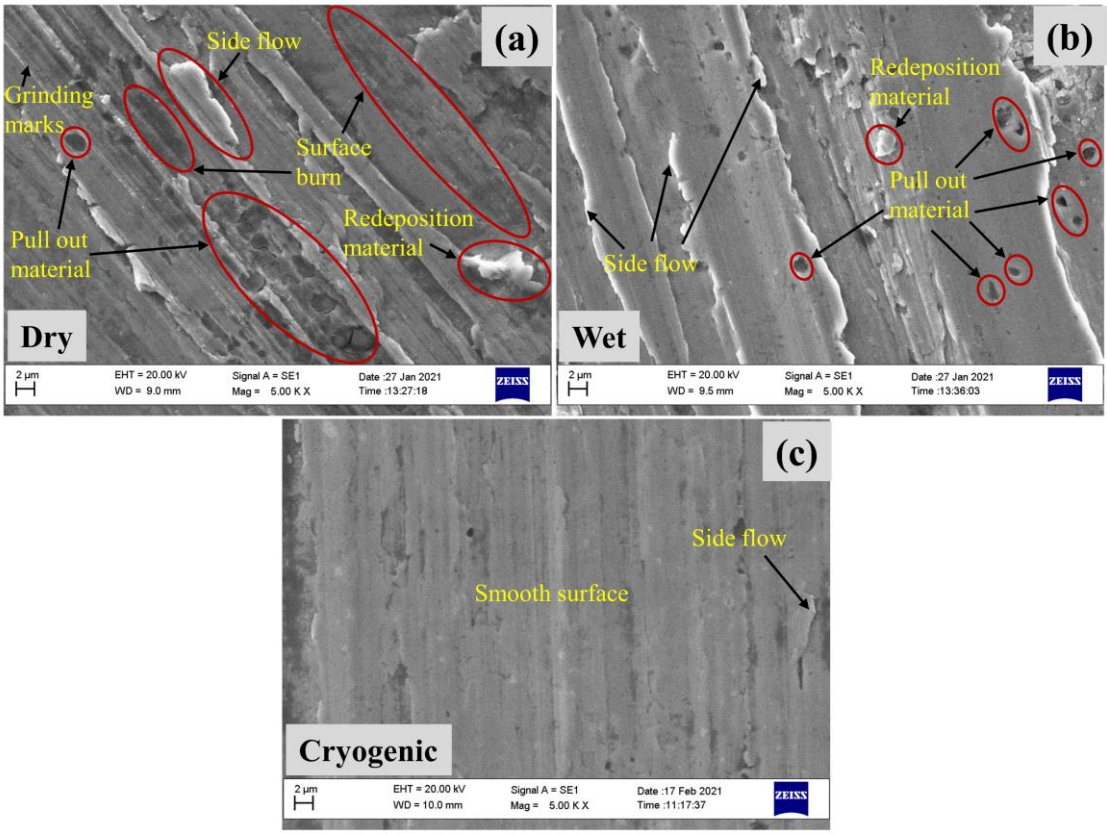

Fig. 4.8: SEM images of the ground surface at 40 µm downfeed under (a) Dry; (b) Wet; (c) Cryogenic environments.

Fig. 4.9 displays the EDX results of the ground surface under three environments, i.e., dry, wet, and cryogenic conditions. Under dry grinding, maximum heat was transferred to the workpiece due to the relatively poor thermal conductivity of the AISI D2 tool steel and the lack of cutting fluid. Furthermore, the redeposited grinding chips on the ground surface were oxidised or carbonised due to the intense flash heat. This redeposited layer indicates transferred atoms, with dominant C and O elements (26.14% and 6.87%). While in wet grinding, grinding chips take away the maximum amount of heat because of the high heat transfer coefficient of water. The grinding temperature in wet grinding condition was observed lower along with less carbon element (C: 20.45%) in comparison to dry grinding. Cryogenic grinding resulted in lower temperature at the grinding zone area without any thermal damage, restricting the redeposition layer over the workpiece surface. EDX results

of cryogenic ground sample reported less carbon element (C: 11.40%) than dry and wet grinding. This low carbon content also indicates the absence of thermal damage in cryogenic grinding.

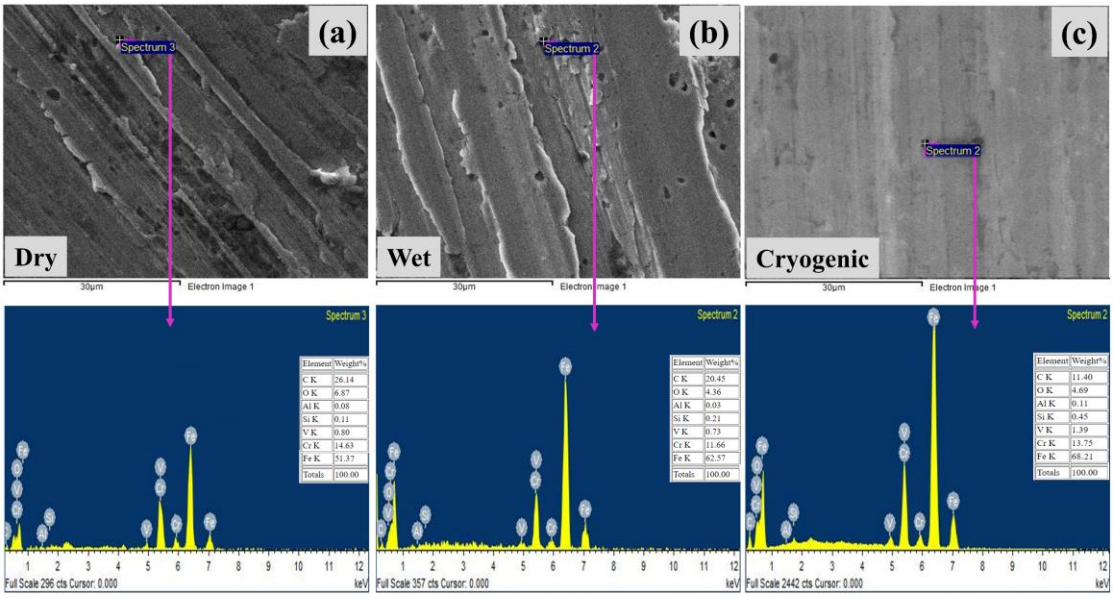

Fig. 4.9: EDX analysis of ground surface at 40 µm downfeed under (a) Dry; (b) Wet; (c) Cryogenic environments.

4.1.6.2 Surface topography

A three-dimensional atomic force micrograph (AFM) was used to examine the topography of the three-dimensional surface of the ground surface in three different environments, i.e., dry, wet, and cryogenic cooling (refer to Fig. 4.10). Surface topography and surface roughness investigations at the nano-scale level were performed in different environments on an equal region of all ground samples (70 × 70 µm^2). Atomic force micrograph outcomes with reference to average surface roughness (S_a) and root mean square roughness (S_q) were recorded. Average surface roughness values were 517.23, 401.17 and 283.12 nm for dry, wet, and cryogenic, respectively. Root mean square roughness values for dry, wet, and cryogenic values were 690.47, 464.07 and 344.05 nm, respectively. According to the S_a and S_q measured data, it was observed that temperature at

the abrasive wheel–workpiece interface plays a crucial role in the grinding process because the dry grinding process has a high temperature in comparison to wet and cryogenic grinding. These findings (roughness parameters, i.e., S_a and S_q) demonstrated that cryogenic coolant performed admirable effects owing to the cooling and lubrication factors during the grinding operation. Compared to dry and wet, less height of peak and valley was found in the cryogenic environment because of the generation of low temperature at the interface area with the workpiece and abrasive grits interface.

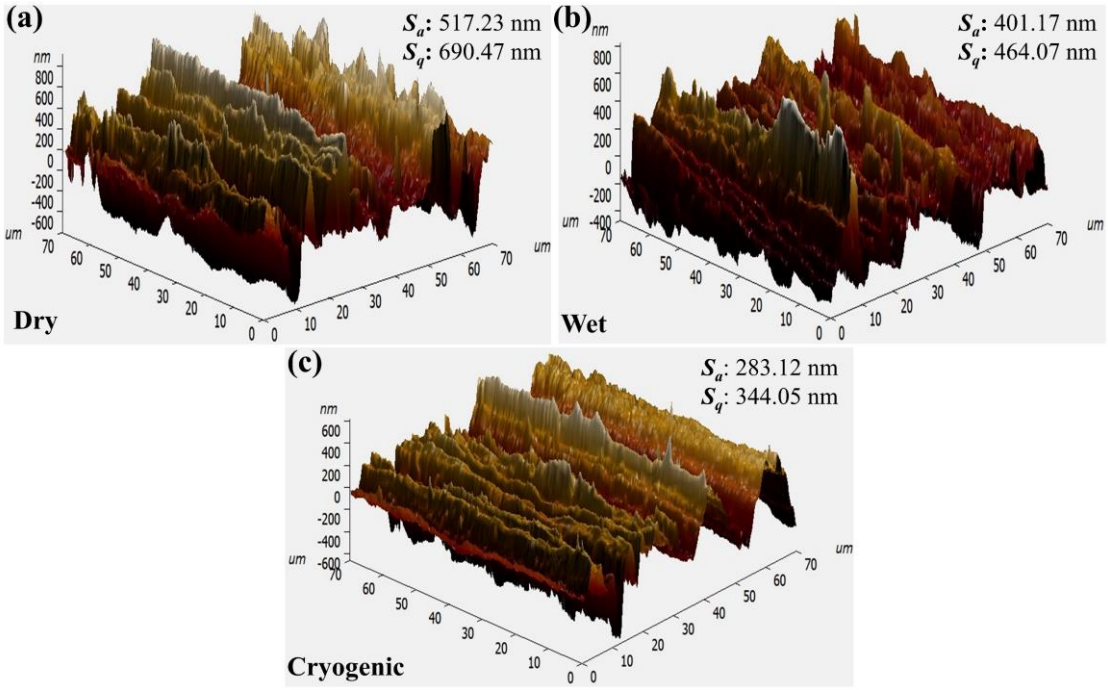

Fig. 4.10: 3D AFM images of the ground sample at 40 µm downfeed under (a) Dry; (b) Wet; (c) Cryogenic environments.

4.1.6.3 Bearing area curve analysis

The solid black lines depicted in the graph (refer to Fig. 4.11 (a)) reflect the bearing area curve (BAC), also called the Abbott-Firestone curve. This curve has a S-shaped appearance, as with many engineering surfaces. The horizontal axis indicates the bearing area lengths as a percentage of the total assessment length of the profile, and the vertical axis represents the surface height. BAC analysis is a technique used to characterize an

object's surface texture. With regard to better perceiving the effects of roughness characteristics, it may be helpful to divide the bearing area curve into subgroups. A straight line may be drawn using a best-fit line across 40% of the bearing area curve's centre part and then shifted along the curve until the slope is as slight as possible [220]. The divided section of the bearing area curve included reduced peak height (R_{pk}), core roughness depth (R_k) and reduced valley depth (R_{vk}). The bearing area curve and its three subgroups are depicted in Fig. 4.11 (a).

Using the bearing area curve based on the ISO 13565-2 standard [221], the parameters (R_{pk}, R_k, R_{vk}, M_{r1} and M_{r2}) were calculated with the help of the profile of the bearing area curve. Core roughness depth, R_k, denoted the roughness profile that excludes fine protrusion peaks and deep steep-sided troughs. A 40% line was placed on the central portion of the bearing area curve by the best-fit line with the smallest gradient. The lines were then drawn to the 0% and 100% points (refer to Fig. 4.11 (a)). Reduced peak height, R_{pk}, represents the average height of the protrusion over the upper limit of R_k and also indicates the top region of the surface (hatched area A_1) that will be rapidly worn away. An average depth of the deep steep-sided valleys profile (hatched area A_2) below the lower limit of the R_k stands for reduced valley depth, R_{vk}, which was a subsurface that retains the lubricant. The smallest material ratio, M_{r1}, denoted the bearing area curve percentage that meets the core roughness's upper limit on the profile of the bearing area curve. A similar concept, the greatest material ratio, M_{r2}, described the bearing area curve percentage that intersects the core roughness's lower limit on the profile of the bearing area curve. The side of the right-angle triangle represents the R_{pk} and R_{vk} parameters. These parameters are calculated based on the triangle's same area (peak area, A_1 and valley area, A_2). The right-angle triangle corresponding to the "peak area, A_1" has M_{r1} as its base, and that corresponding to the "valley area, A_2" has 100%–M_{r2} as its base, as shown in Fig. 4.11 (a).

In other words, the need for a surface with a low R_{pk} was based on the fact that peak heights were worn away in the initial phases of operation, whereas R_k can become the long-term feature (i.e., roughness profile: peak and valley) of a surface.

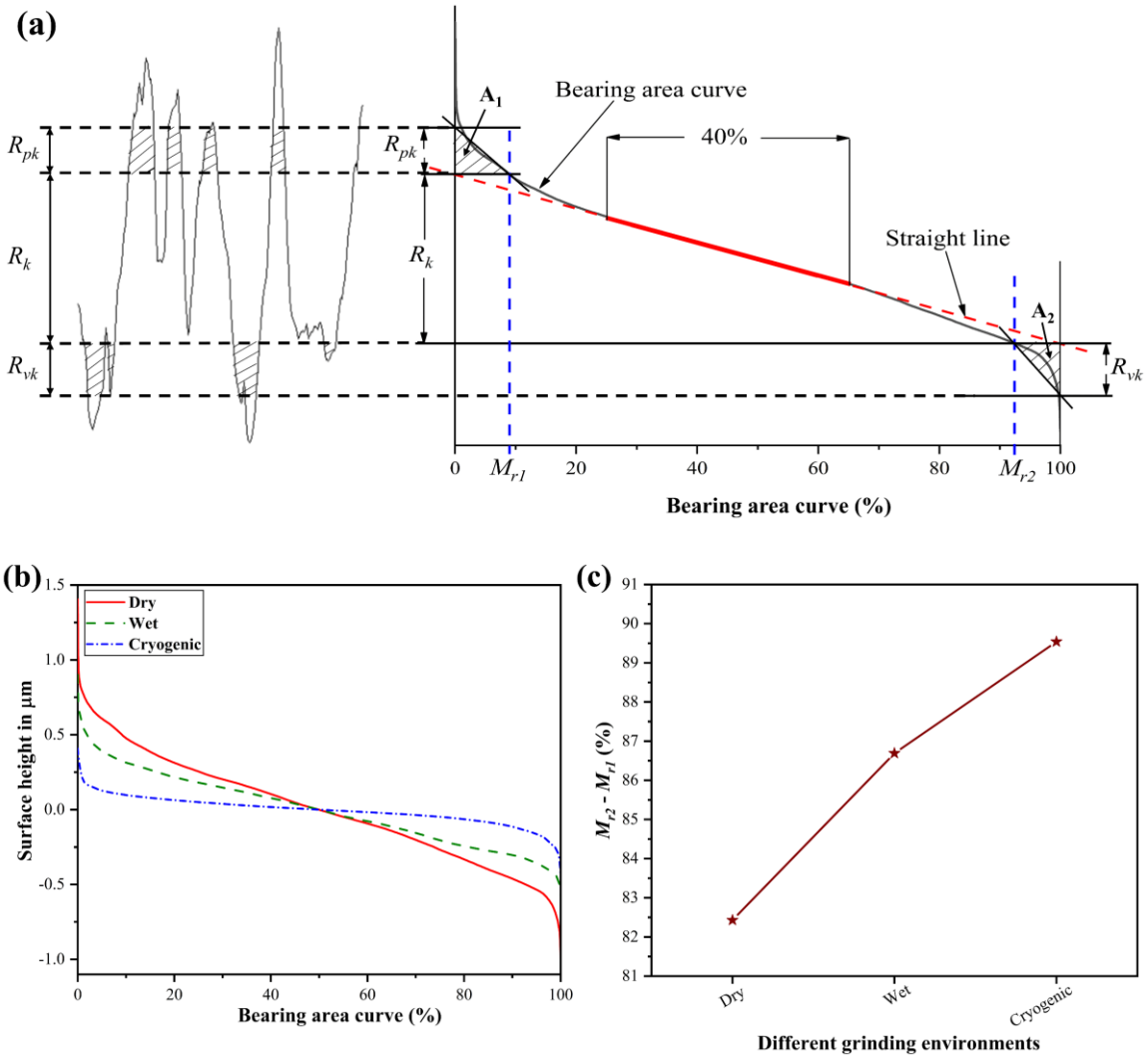

Fig. 4.11: Bearing area curve analysis: (a) Filtering and parameters of the bearing area curve; (b) Bearing area curve at different environments; (c) Bearing area ratio at different environments.

Fig. 4.11 (b) and (c) illustrate the bearing area curve and bearing area ratio with the different environments at maximum downfeed. The measured bearing area curves were investigated and evaluated. Fig. 4.11 (b) shows the ground surface curvature of different environments, i.e., dry, wet, and cryogenic, at 40 µm downfeed. Clearly, there was a

substantial variance in the bearing area curves of the dry, wet, and cryogenic ground sample. According to Fig. 4.11 (b), the dry bearing area curve is more irregular than cryogenic but slightly irregular than wet conditions. Fig. 4.11 (c) indicates the bearing area ratio (M_{r2}–M_{r1}) in different environments. From Fig. 4.11 (a), by crossing a line that divided the valley depth profile and peak height profile from the core roughness profile, the bearing area ratio is defined. It represents the percentage area of the bearing area curve. The bearing area ratio increased with the sequence of dry, wet, and cryogenic environments. A minimum bearing area ratio (82.43%) in dry and maximum bearing area ratio (89.54%) in cryogenic environments was noticed. The higher bearing area ratio revealed a larger bearing area, resulting in lower wear and friction in the finished parts, generating better surface roughness [220]. It generally happens due to dependence on the temperature and grit's sharpness. Owing to more heat generation in dry condition, the sharpness of the grits become worn out (occurrence of blunt edges), which produces more friction between two surfaces (i.e., workpiece and abrasive wheel) during rubbing action. The presence of the cooling and lubrication indicated more bearing area ratio in wet and cryogenic environments as compared to dry. Compared to wet conditions, a higher bearing area ratio (refer to Fig. 4.11 (c)) was found in cryogenic due to low temperature, which provided good sharpness of grits, inducing improvement in surface roughness.

4.1.7 Grinding environment on chip morphology

Grinding removes material from several cutting edges with varying removal properties owing to many grains. Malkin and Guo [68] stated that alumina grit geometry may produce the chip formation that occurred in cutting action mode. Fig. 4.12 illustrates the scanning electron micrographs of the grinding chips collected on carbon tape under various grinding conditions.

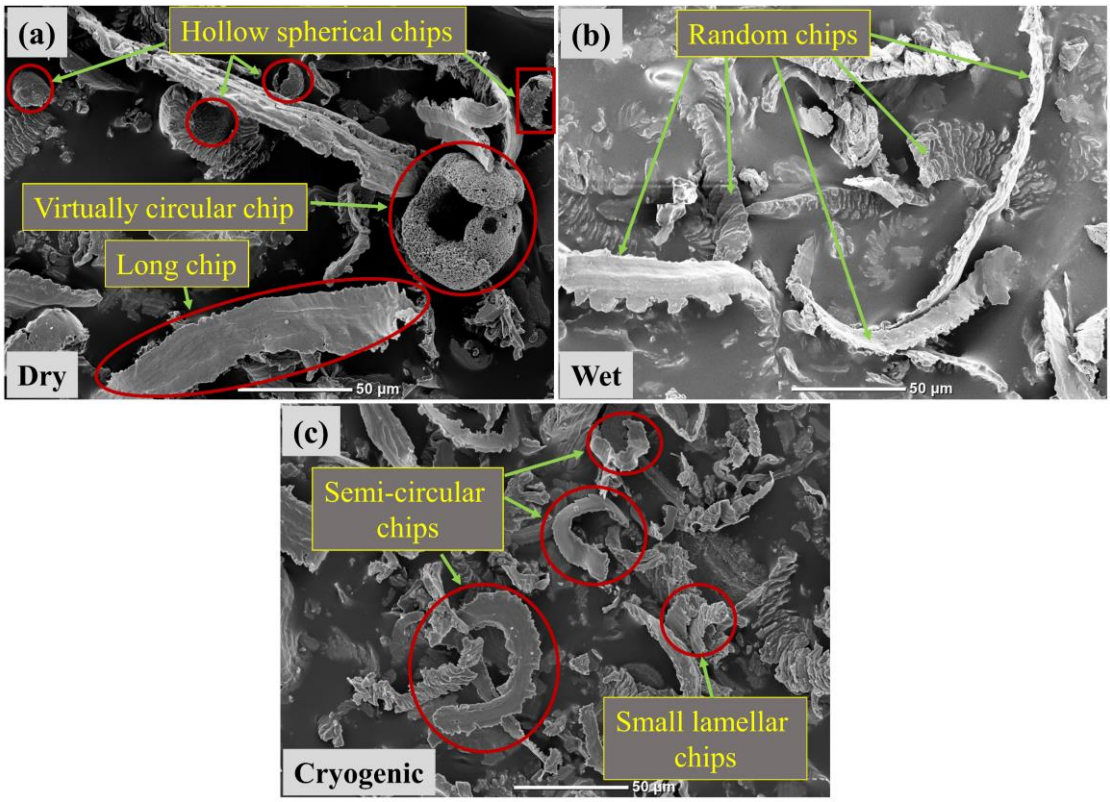

Fig. 4.12: SEM micrographs of chips under: (a) Dry; (b) Wet; (c) Cryogenic environments.

As can be seen from Fig. 4.12 (a), dry grinding resulted in virtually completely curled chips (i.e., chips that are almost circular), which was evidence of significant oxidation and large heat production. The chips tend to curl more often when using typical grinding wheels, such as an alumina wheel with low heat conductivity [222]. Also, it generated elongated leafy and hollow spherical chips at a high interface zone temperature during the grinding operation. The enhanced ductility and material's softness cause the long chips. Compared to dry grinding, wet grinding resulted in random chips with larger and smaller chips, as shown in Fig. 4.12 (b). Chips in small size were seen due to chip breakability because of supplying greater cooling impact at the interface area (alumina wheel-chips). However, while using LN_2 cryogen for grinding, basically C-type or semi-circular chips or small lamellar chips have been identified. This was due to the chips being subjected to abrupt and intense cooling, causing them to break apart in the center (refer to Fig. 4.12 (c)).

4.1.8 Grinding environment on microstructural analysis

In the grinding, the work material is gone through large thermal, mechanical, and chemical action, which induced to strain hardening effect and recrystallization of the ground surface. Fig. 4.13 shows the microstructural image of various ground samples and base metal in a plane perpendicular to the machined surface. As shown in Fig. 4.13 (a), a typical microstructure of AISI D2 tool steel shows evenly dispersed chromium-rich alloy carbides in a matrix of pearlite. The chromium-rich carbide makes it one of the hardest steels.

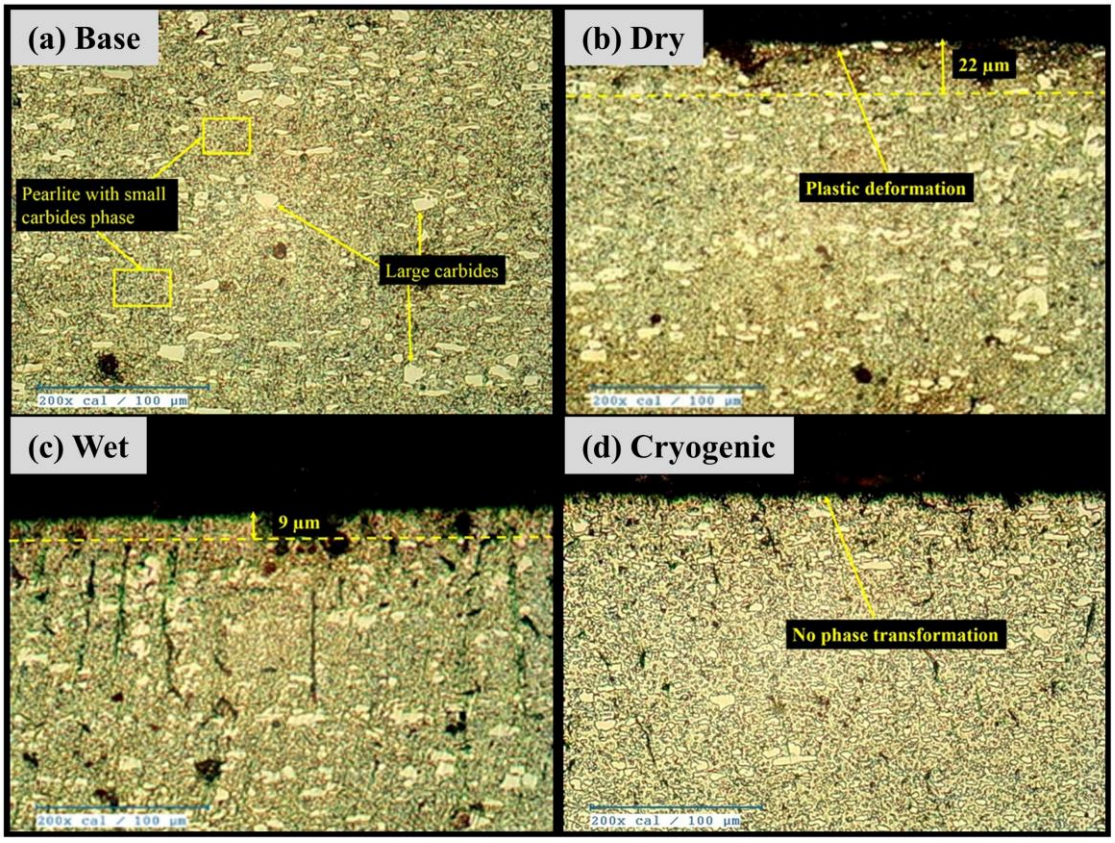

Fig. 4.13: Transverse sectional micrographs of ground samples under different environments: (a) Base; (b) Dry; (c) Wet; (d) Cryogenic.

At 24 µm downfeed, slightly grain elongation was observed near the ground surface under each grinding environment. The reason is more cutting edges contact with workpiece as an increase in downfeed, which results in more friction between the grinding wheel and

workpiece surface, and drastic heat was generated in the grinding zone. Therefore, large thermal damage in terms of grain elongation or phase transformation near the ground region was observed. From Fig. 4.13 (b), maximum plastic deformation near about 22 μm depth from the ground surface was observed under dry grinding. It is expected because huge heat developed in the grinding zone by continuous shearing, ploughing, and rubbing action under the absence of coolant. Xavier et al. [223] also pointed out dry machining is responsible for serious phase transformation as followed by wet and cryogenic machining of AISI 52100 steel. In wet grinding, small thermal damage layer (approximately, 9 μm) was observed on the finished surface owing to effective lubrication and cooling. On the other hand, no surface alteration like plastic deformation or grain elongation was found on the ground surface owing to minimum thermo-mechanical loading during cryogenic grinding. This happens due to LN_2 drastically reduced deformation temperature; grain dislocation becomes much difficult, resulting in very small or negligible thermal damage region. Similarly, Klocke et al. [224] reported that cryogenic machining minimizes the thermal damage depth of machined surface and subsurface as compared to conventional wet machining of gamma titanium aluminides.

4.1.9 Effect of cryogenic coolant delivery pressure on grindability indices

Grinding experiments were carried out with AISI D2 tool steel with an alumina wheel at a different downfeed with a constant table feed rate of 9 m/min under cryogenic cooling conditions. The influences of the LN_2 delivery pressure of 2, 3, and 4 bars in the cryogenic grinding have been compared for the variations in the grinding forces, specific grinding energy, and surface roughness. The LN_2 coolant was supplied at various pressures using a nozzle orifice diameter of 3 mm at the grinding zone at a constant stand-off distance of 50 mm.

4.1.9.1 Grinding forces and specific grinding energy

The variation in the tangential and normal forces when grinding AISI D2 tool steel at 9 m/min table feed rate while using cryogenic cooling with different supply pressures are depicted in Fig. 4.14. At a lower downfeed, the LN_2 delivery pressure has a much less impact. A high liquid nitrogen delivery pressure has a very important role in producing more coolant at the grinding zone. It penetrates the air boundary layer generated by the high-speed alumina wheel. Fig. 4.14 indicates the changes in the grinding forces to LN_2 delivery pressure. High delivery pressure at 4 bar offered a reduction of 8% in F_t and 6% in F_n at 40 µm downfeed compared to 2 bar delivery pressure. It was mainly due to more effective ejection of the coolant from the flat spray nozzle at the grinding zone area and sufficient lubrication at the tip of grits, resulting in decreased forces [140].

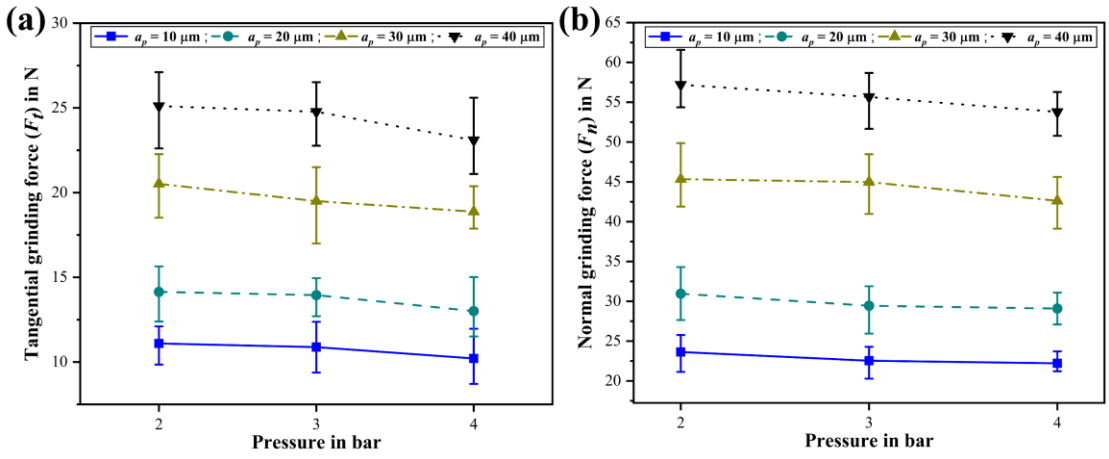

Fig. 4.14: Grinding forces versus delivery pressure under different downfeed.

Fig. 4.15 compares the specific grinding energy with different delivery pressure at various downfeed under cryogenic grinding. This graph also showed a reduction in energy consumption or specific grinding energy with increasing delivery pressure, which happened due to effective cooling and lubrication in the interaction of abrasive wheel and workpiece at higher delivery pressure (4 bar). Furthermore, this pressure was significantly affected by rubbing and ploughing action as followed by shearing, which means reduced

friction forces by rubbing and ploughing action on the ground surface through a uniform cooling. Therefore, minimum energy consumption or lower specific grinding energy was found at 4 bar delivery pressure than 2 and 3 bar delivery pressure. The LN_2 coolant delivery pressure at 4 bar reduced specific grinding energy by approximately 8 % over the coolant at 2 bar pressure.

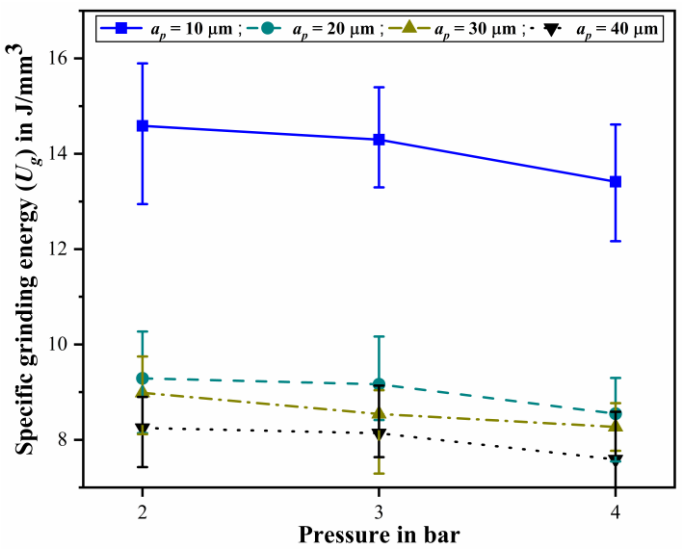

Fig. 4.15: Specific grinding energy versus delivery pressure under different downfeed.

4.1.9.2 Surface roughness

Fig. 4.16 reveals the differences in the result of the R_a at a different scale of delivery pressure. The higher delivery pressure reduced friction between the abrasive grit and the work material, preventing pre-mature abrasive grit breakage due to superior temperature control. Additionally, it reduced the amount of chips that are loaded onto the wheel, improving the surface quality. On the other hand, the high-pressure coolant supply produced a white mist surrounding the grinding zone region. One advantage of using cryogenic cooling was that the LN_2 shields the workpiece during grinding, preventing surface oxidation. A percentage reduction in R_a by 7–9% in the range of pressure (2 to 4 bar) of the LN_2 coolant was found. At maximum pressure, the value of surface roughness was low, which was due to more coolant at the grinding zone. Beyond 4 bar pressure, the

spray of liquid nitrogen through the nozzle diminished the visibility of the worker at the contact zone area.

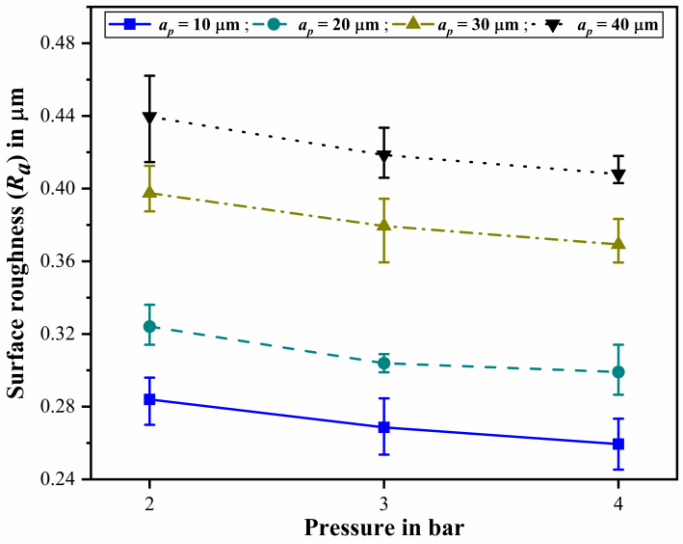

Fig. 4.16: Surface roughness (R_a) versus delivery pressure under different downfeed.

4.1.10 Grinding environment on change in table feed rate for grindability indices

Grinding experiments were conducted on AISI D2 tool steel with an alumina wheel in different table feed rates at a constant downfeed of 40 µm under dry, wet and cryogenic cooling. Results are discussed in this section.

4.1.10.1 Grinding force

Fig. 4.17 shows dry, wet, and cryogenic grinding forces increase with table feed rate. The F_t and F_n forces magnitude in cryogenic environments were less than in dry and wet environments. Cryogenic cooling reduces grinding force by 54-64% and 38-45% in F_t, 44-55% and 31-35% in F_n over dry and wet cooling at different table feed rates (6, 9 and 12 m/min) using an alumina wheel, respectively. Compared to a low table feed rate (6 m/min), the grinding force has a much greater magnitude when applied at 12 m/min. Because of this, alumina grits have a greater contact area with the workpiece, which increases friction.

Therefore, it increased the temperature at the interface zone area. The temperature was significantly lowered by cryogenic cooling, and the workpiece became less ductile as a result of the low temperature, which decreased the grinding forces. Similarly, Manimaran et al. [30] stated that grinding force increases with an increase in table feed rate while grinding stainless steel 316 material. They reported less grinding force under cryogenic grinding than dry and wet grinding.

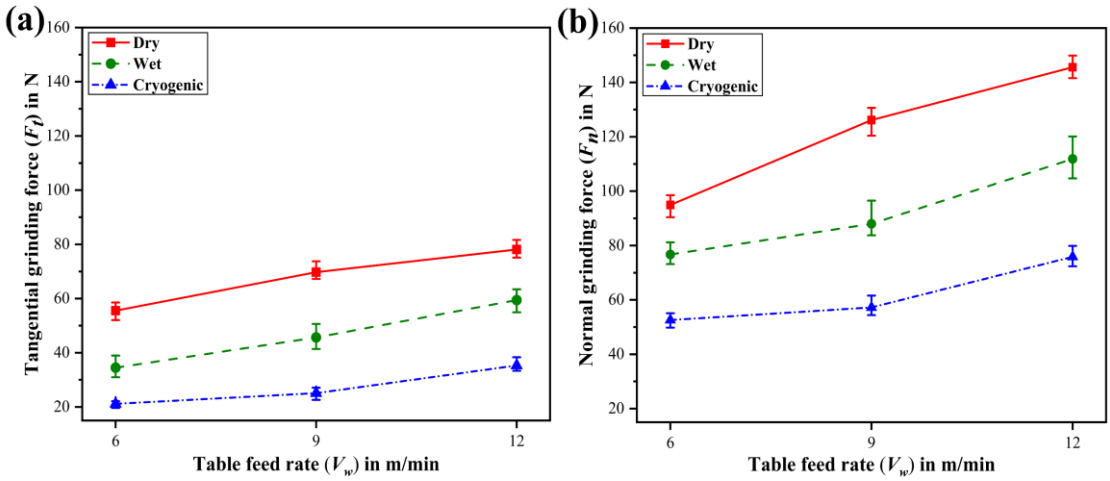

Fig. 4.17: Grinding forces versus table feed rate under different environments.

4.1.10.2 2D and 3D surface roughness

Fig. 4.18 demonstrates the variations in surface roughness (R_a and R_q) values at various table feed rates. The surface roughness for each of the three conditions exhibited an upward trend as the table feed rate rises, according to Fig. 4.18 (a) and (b). The magnitude of surface roughness among the three conditions is substantially smaller at the 6 m/ min table feed rate. The surface roughness, measured in R_a and R_q, was consistent across all conditions, although it became extreme as the table feed rate increased. Compared to dry and wet grinding, LN_2 creates a surface with reduced roughness value even at all points of the table feed rate and a constant downfeed of 40 µm. Because of the lesser temperature, the material may be sufficiently hardened, and a finer (sharper) alumina grit performs the shearing

action [30]. Using cryogenic LN_2 to decrease the work softness minimized the wheel loading, reducing the material's adhesion to the workpiece. In other words, more material is being removed because of the increased table feed rate, which means there is more rubbing surface by the alumina grits, resulting in more contact between the interfacing parts if there is no lubrication effect [225]. Further, it leads to wear out the edges of alumina grits or fracture of the alumina grits. To prevent these consequences, the amount of lubricant should be better. Wet cooling provides the optimum lubrication, whereas it is more challenging to reach the alumina wheel and workpiece interface at a higher table feed rate. One of the most important benefits of using cryogenic cooling is that the liquid nitrogen shields the contact zone area and offers better surface finish. Cryogenic cooling improved roughness (R_a and R_q) values over dry and wet grinding by 41-52% and 40-50%, and 23-38% and 24-37%, respectively. Such results also agree with the finding of Manimaran et al. [226].

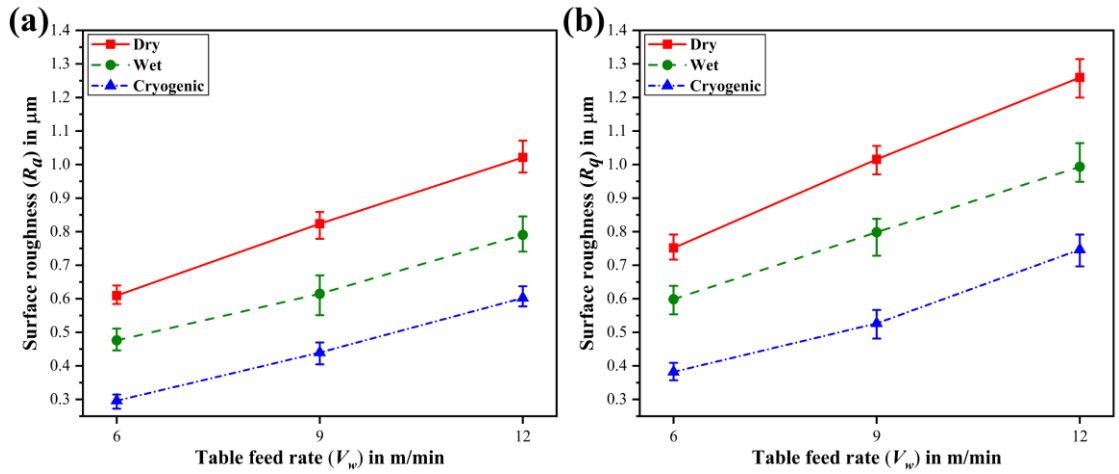

Fig. 4.18: Surface roughness (R_a and R_q) versus table feed rate under different environments.

The 3D approach to better examine surface quality considers that actual surfaces are inherently 3D physical objects. Therefore, the surface-related occurrence also appears in three dimensions. The only reasonable parameters of 3D surface image were extracted from

a particular ground surface mark. These parameters are illustrated. Fig. 4.19 reveals the both parameters of the 3D surface image inside the chosen section under three different grinding environments. They are arithmetic average or mean height (S_a) and root-mean square height (S_q). 3D surface roughness (S_a and S_q) parameters were opted to investigate a more reasonable roughness parameter and to assess the influence of the grinding parameters on the surface characteristics of ground samples under different environments. According to the findings, 3D parameters (S_a and S_q) are better able to characterize the effect of the grinding factors on the surface quality. Among these 3D parameters, S_q is the best option owing to its high sensitivity [227]. Fig. 4.19 shows the line diagram of the 3D surface roughness parameters with respect to the table feed rate on the ground AISI D2 tool steel surface. S_a and S_q rise with an increase in table feed rate.

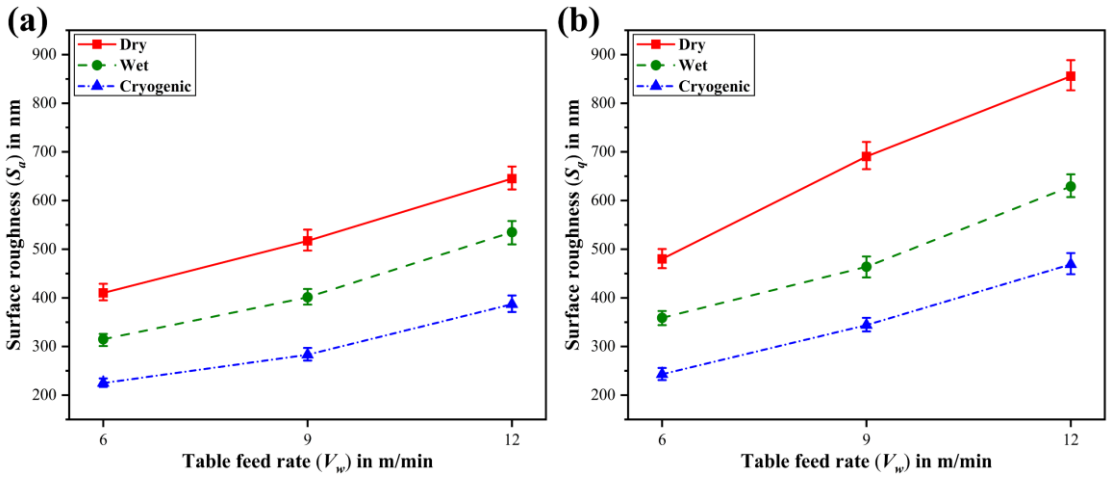

Fig. 4.19: Surface roughness (S_a and S_q) versus table feed rate under different environments.

Poor surface roughness was noticed with an increased table feed rate during the dry grinding operation, as displayed in Fig. 4.19 (a) and (b). The results demonstrated that a lesser surface roughness value could be attained when a cryogenic grinding was set at a constant 40 µm downfeed with 2 bar cryogen pressure. Due to temperature dependence, the sharpness of the grit tip improved while using the LN_2 cryogen. The LN_2 coolant

lowered the S_a values by approximately 40-45% in dry and 27-30% in wet environments. Similarly, in the case of S_q, 45-51% and 25-33% reduction was found under the cryogenic condition in comparison with dry and wet conditions, respectively.

4.1.10.3 Bearing area curve analysis

Fig. 4.20 represents the surface height of the ground workpiece surface at the bearing area in dry, wet, and cryogenic grinding with constant cryogen pressure of 2 bar. For a better understanding of the surface characteristics over the ground surface, the effect of topographic features (3D) on $\eta_{0.05}$ revealed the surface height at the intersection point on the bearing area curve of a 5% ratio, as displayed in Fig. 4.20.

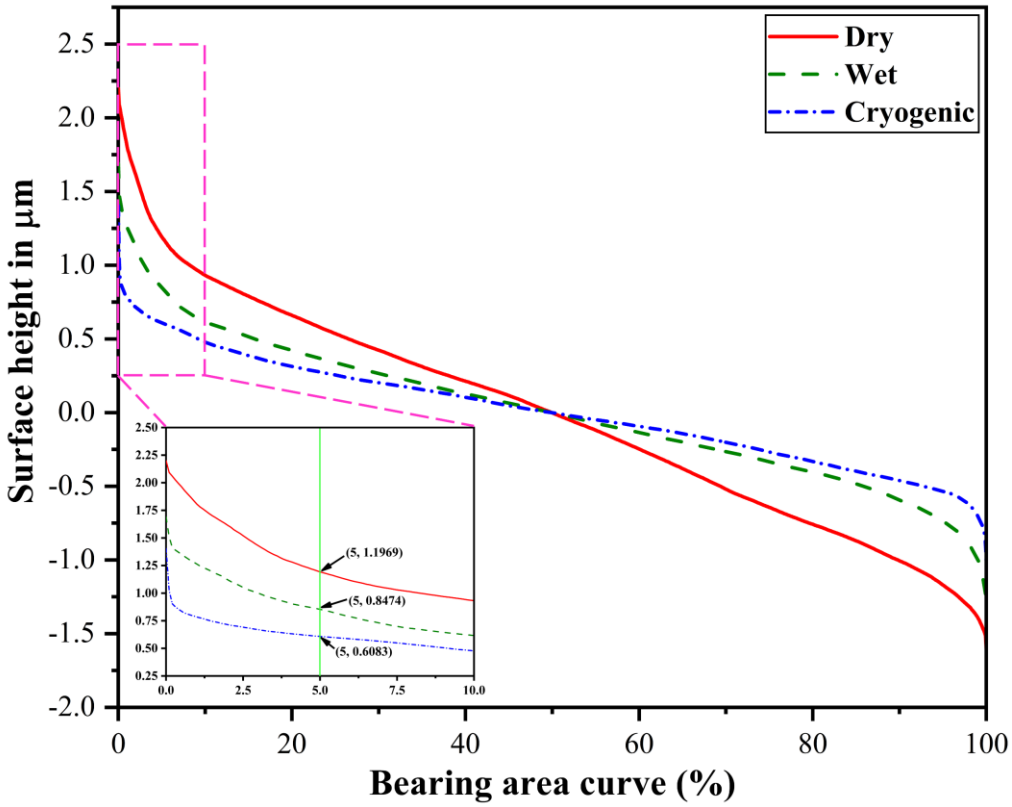

Fig. 4.20: Variation in surface height under dry, wet, and cryogenic environments.

The coordinate point at a 5% bearing area is shown in this figure. These coordinates reflected the surface height under dry, wet, and cryogenic conditions, which were 1.1969, 0.8474, and 0.6083 µm, respectively. Higher surface heights mean more spiky ridges in the

surface profile, resulting in a poor bearing property. This caused a lower value of surface bearing index in dry than in other conditions. In addition, the topographic features are associated with the impact of grit edge sharpness induced through cryogenic cooling, in that a cryogen pressure of 2 bar may result in a more pronounced effect of sharper grit edge. Due to more coolant spray in the interface region, increased cryogen pressure improved the sharpness of the abrasive grit's tip. This may cause a reduction in $\eta_{0.05}$ with rising cryogen pressure under the same settings, which leads to an increase in the surface bearing index.

According to the EUR 15178N standard, assessing the surface quality of finished surface by functional indices, i.e., surface bearing index (*Sbi*) and core fluid retention index (*Sci*), was introduced by Deltombe et al. [228]. These indices are defined by this mathematical formula:

The surface bearing index, *Sbi,* is defined to characterize the bearing characteristic of a surface. A surface with a higher *Sbi* offers superior bearing properties. The equation for calculating the *Sbi*:

$$Sbi = \frac{S_q}{\eta_{0.05}} \tag{4.1}$$

where S_q: root mean square (RMS) deviation; $\eta_{0.05}$: surface height at 5% bearing area.

The core fluid retention index, *Sci*, is defined to characterize the property of fluid retention in the core zone. A greater *Sci* indicates that the surface can retain enough lubricants in the core zone, which is essential for better lubrication. The equation for calculating the *Sci*:

$$Sci = \frac{1}{S_q}\frac{V_v(h_{0.05}) - V_v(h_{0.08})}{(M-1)(N-1)\Delta x \Delta y} \tag{4.2}$$

where $V_v(h_{0.05})$: void volume of the surface heights, $h_{0.05}$; $V_v(h_{0.08})$: void volume of the surface heights, $h_{0.08}$; M and N indicate the number of sampling points in the x and y

directions, and Δx and Δy are the sampling intervals.

The effects of table feed rate on *Sbi* and *Sci* functional parameters were studied and illustrated in Fig. 4.21. *Sbi* and *Sci* of different environments have a similar pattern, in particular Fig. 4.21 (a) and (b). It is clear from Fig. 4.21 (a) that the *Sbi* values under different environments increased with the increase in the table feed rate. This is most likely the result of the *Sbi*, which, according to the definition provided in above paragraph, is proportional to the S_q roughness parameter and inversely related to the surface heights (at 5% bearing area). The increase in table feed rate generally deteriorated the surface quality. Thus, S_q increased with the rise of the table feed rate. In addition, $\eta_{0.05}$ is correlated with the topographical characteristics as well as the height distribution. The height distribution and topographical characteristics variations are typically minimum for the same processing method. Therefore, *Sbi* increased with the increase in table feed rate. The findings also reveal that cryogenic grinding increased the *Sbi* at high table feed rates, indicating a better bearing surface property.

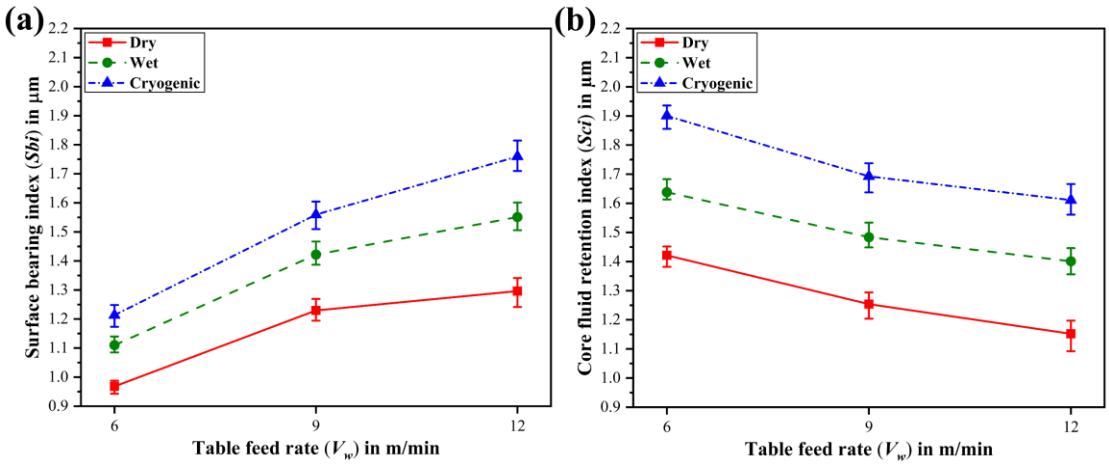

Fig. 4.21: Variation in surface functional indices with change in table feed rate.

On the other hand, Fig. 4.21 (b) shows the variation in *Sci* decreases with an increase in table feed rate under different environments. This may be a result of the inverse proportionality between the *Sci* and S_q. As previously stated, the S_q rises as the table feed

rate increases. Then, the *Sci* increases against the table feed rate. When compared to dry and wet grinding, it was seen that the *Sci* in cryogenic grinding is higher. This signified that the surface created by cryogenic grinding is more helpful for the fluid stored to lubricate the interfacing parts. Chen et al. [229] reported that higher *Sci* means better fluid retention quality in the core region.

4.1.10.4 Grinding temperature

The variations of that temperature developed between the alumina wheel–workpiece interface area with the variation in table feed rate are displayed in Fig. 4.22. It was seen that the lowest temperature was recorded with cryogenic cooling and a gradual rise in temperature was noticed with an increased table feed rate.

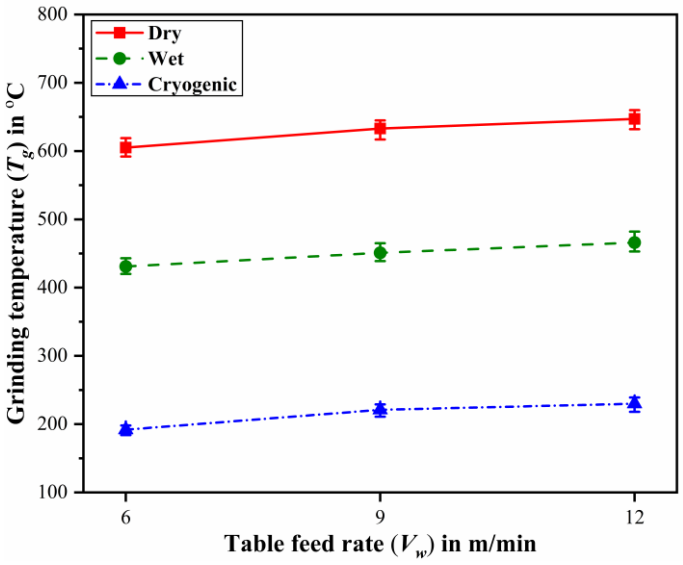

Fig. 4.22: Grinding temperature versus table feed rate under different environments.

Comparing cryogenic cooling to dry and wet cooling environments, the temperature was reduced to about 64-69% and 50-56%, respectively. The grinding process occurred at a 6 m/min table feed rate, producing a low grinding temperature of approximately 7, 8, and 17% over dry, wet, and cryogenic grinding at a 12 m/min table feed rate, respectively. The main reason is that coolants find difficulty reaching the grinding zone due to the air barrier

at high work speeds (as discussed in Chapter 2) for increasing grinding temperature concerning the increment of table feed rate from 6 to 12 m/min.

4.1.10.5 Microhardness

The material near the cutting edge is plastically distorted and pulled in the cutting direction during the grinding process. The ground surface hardness is significantly greater than in the base metal due to work hardening in the distorted layer. Work hardening and elevated temperature during machining affect the surface hardness of the workpiece [230].

Fig. 4.23 illustrates the comparative microhardness measurement results for a table feed rate of 6 m/min, 9 m/min, and 12 m/min under various environments concerning depth beneath the ground surface. Observation reveals that the hardness near the ground surface is higher as compared to subsurface hardness. It is due to the material near the edge of abrasive grains being plastically distorted at a higher strain rate. Also, the high grinding temperature is responsible for the thermal strain experienced near the ground surface. Because of this, the effect of work hardening is influential near the ground surface, resulting in greater hardness at the top surface than below the ground surface[32]. In addition, dry grinding has the maximum hardness of the ground surface, followed by wet and cryogenic grinding. This is responsible for the generation of hardened layers on the ground surface. Abhimanyu et al. [231] also pointed out that high hardness variation was observed near the ground surface of AISI D2 tool steel after dry grinding owing to the work hardening effect. Under wet cooling compared to dry, less hardness was observed on the ground surface caused by sufficient lubrication and cooling in the abrasive wheel and work material interface [26]. On the other hand, in the case of cryogenic grinding, lower hardness was observed at the surface and subsurface due to a lower strain hardening effect over the workpiece because of the generation of lower temperature at the interface zone area (alumina wheel-workpiece) than dry and wet grinding. However, with depth beneath the

ground surface, the hardness becomes reduced due to the low thermally affected and distorted layer. Similar results were obtained by Gajrani [232]. He reported that the workpiece hardness near the surface is highest under dry than cryo-MQL and MQL. It was mainly due to the work hardening effect, resulting in a reduction in the workpiece hardness beneath the surface.

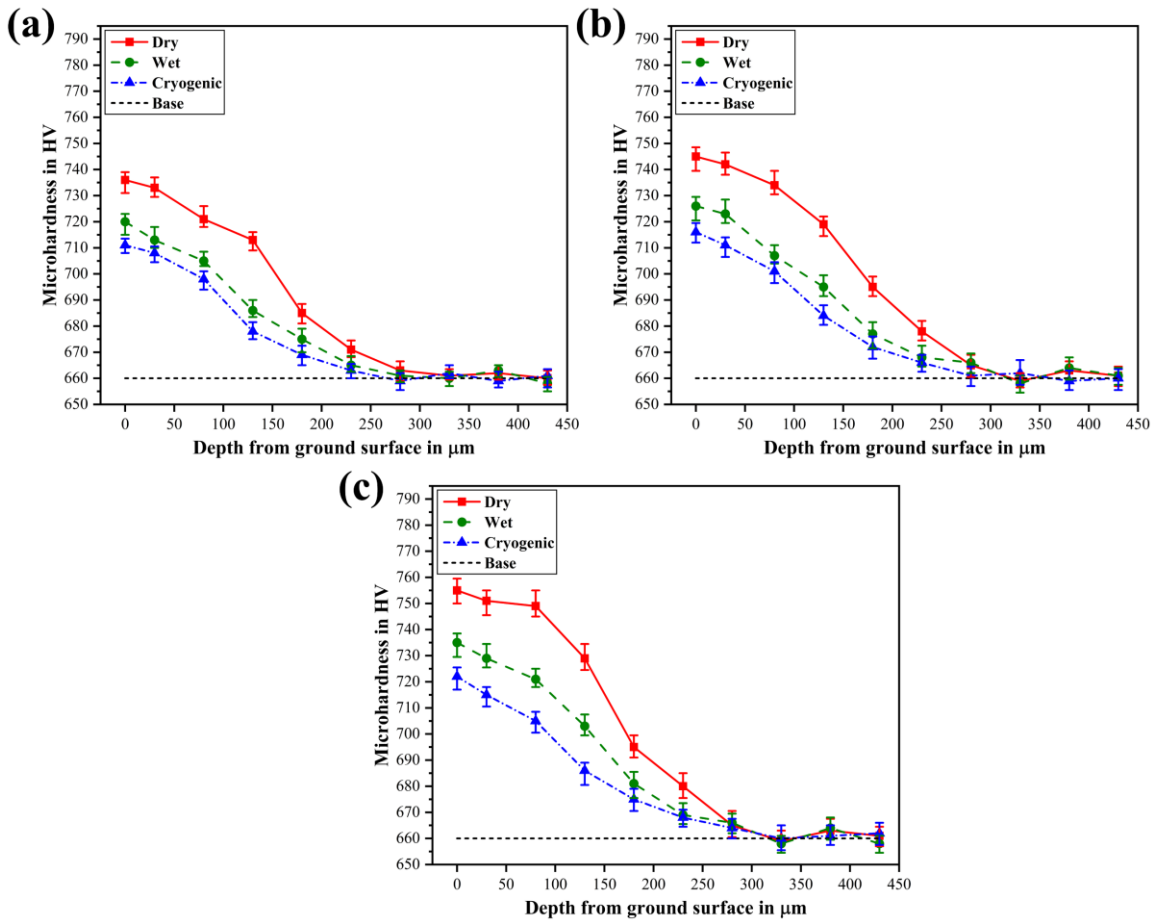

Fig. 4.23: Microhardness variation along the depth beneath the ground surface for different environments at a table feed rate of (a) 6 m/min; (b) 9 m/min; and (c) 12 m/min.

4.2 Performance analysis of grinding parameters under Cryo-MQL environment for ground AISI D2 tool steel

Section 4.2 studied the application of four eco-friendly lubricants such as soybean oil, soybean oil-based deionized water emulsion, 0.5 wt.% Al_2O_3 NFs, and 1 wt.% Al_2O_3 NFs in Cryo-MQL grinding of AISI D2 tool steel. This section examined tribological features such as thermo-physical properties, namely, thermal conductivity, dynamic viscosity, surface tension, density, pH value, and wettability analysis, to optimize the Al_2O_3 NPs concentration in the base fluid. The grinding experiments are conducted using the Cryo-MQL with Al_2O_3 NFs approach, and the optimal concentration (0.5 wt.% and 1 wt.%.) of NPs is identified from the investigation of thermo-physical characteristics of NFs. The quality and stability features of the prepared lubricants have been addressed through the results of micrographs by the sedimentation method. After that, the experiments' results highlighted a significant improvement in all grinding response parameters, i.e., grinding force, specific grinding energy, surface roughness, surface topography, chip morphology and grinding temperature, under the Cryo-MQL environment.

4.2.1 Lubricants selection

In order to get the best lubricating properties and heat extraction from the grinding zone, it is crucial to use the appropriate cutting fluids for MQL under Cryo-MQL grinding. Therefore, four different eco-friendly lubricants, including soybean oil (SO), soybean oil-based deionized water emulsion (SO+DW), Al_2O_3 NFs (0.5 wt.%), and Al_2O_3 NFs (1 wt.%) were selected (refer to Fig. 4.24). Today's food oil market is dominated by soybean oil, a biodegradable vegetable oil. Approximately 80% of the annual production of soybean oil is used for human consumption. A further 6% is used for animal feed, while the remaining (14%) is used for non-food purposes (such as lubricants, soap, fatty acids, coatings, etc.)

[233]. Fig. 4.25 shows the chemical structures of soybean oil. Linoleic and linolenic acids, as well as polarity head groups, are present in large amounts in soybean oil, which enhances the anti-wear and anti-friction properties [234], [235]. On the other word, deionized water was needed to enhance the cooling performance in the grinding zone owing to very low volatility. By using the Millipore purification systems, deionized water was obtained.

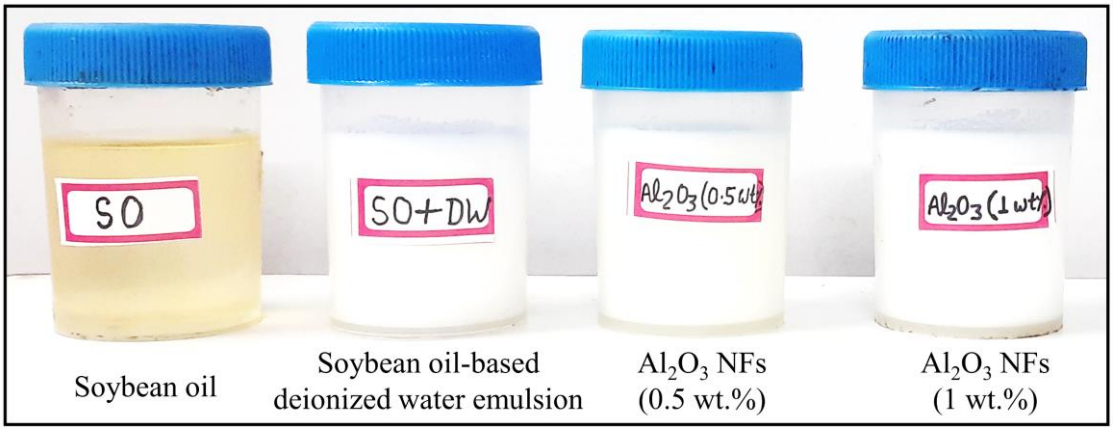

Fig. 4.24: Different lubricants utilized for MQL under Cryo-MQL grinding.

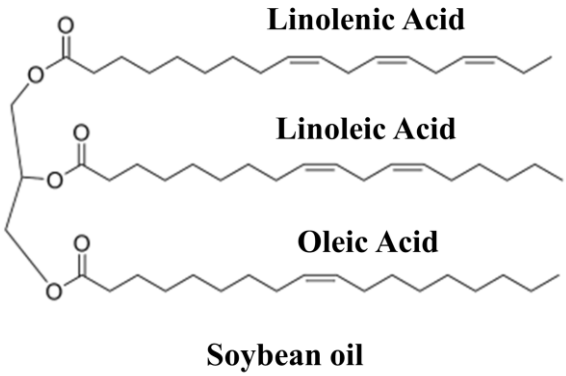

Fig. 4.25: Chemical structures of soybean oil.

Generally, Al_2O_3 NPs are known as metal oxides. Al_2O_3 NPs are quickly dispersed to base fluid, i.e., soybean oil because of their greater surface energy [236]. In the present work, a small amount of Al_2O_3 NPs (0.5 and 1 wt.%) was added to the eco-friendly vegetable oil-based deionized water emulsion to improve the cooling performance. In this NFs, vegetable oil is the leading lubricating agent because it produces a strong absorption

lubricating layer over the ground surface. Hence, Al_2O_3 NFs are considered eco-friendly lubricants. Table 4.1 revealed the thermo-physical properties of MQL lubricants.

Table 4.1: Thermo-physical properties of MQL lubricants.

Lubricants	**Thermo-physical properties**		
	Thermal conductivity (W/mK)	Dynamic viscosity (centipoise)	Density (kg/m^3)
SO	0.19	42	923
SO+DW	0.515	2.1	996
Al_2O_3 NFs (0.5 wt.%)	0.625	3.8	1000
Al_2O_3 NFs (1 wt.%)	0.688	4.7	1003

Transmission Electron Microscopy (TEM) is an effective instrument for analyzing nanoparticle distribution, size, and shape. The TEM image of Al_2O_3 NPs is shown in Fig. 4.26 (a). The diameter of the primary Al_2O_3 NPs, which were approximately spherical, was between 10 and 50 nm.

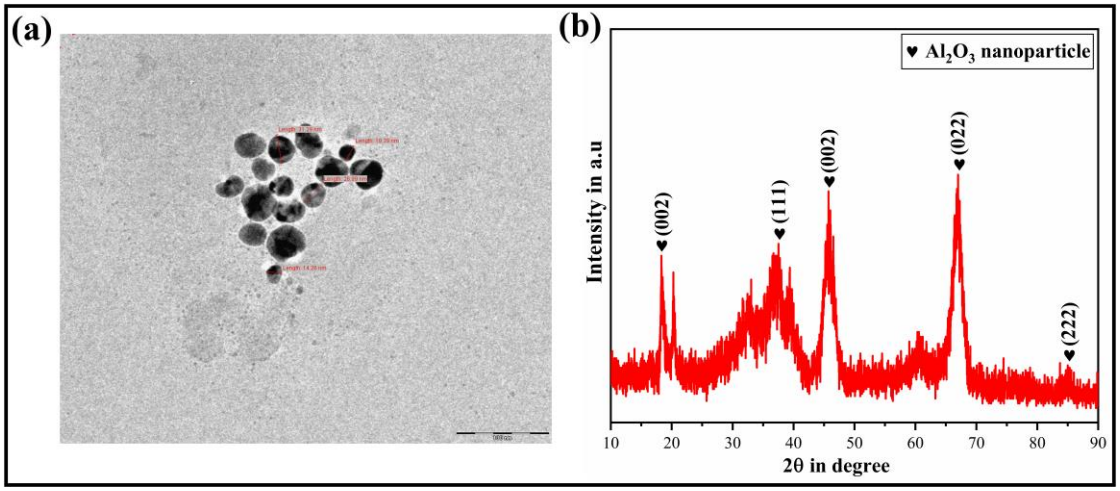

Fig. 4.26: (a) TEM image of Al_2O_3 NPs; (b) XRD pattern of Al_2O_3 NPs.

XRD characterized alumina nanoparticles for phase identification, crystallite size and crystal structure determination. The diffractometer was calibrated to measure in step-scan mode across the two theta ranges (10°-90°). This range was chosen since it included all the

crucial diffraction peaks for analysing the Al_2O_3 NPs. The scanning parameters were 0.02° step size and a 5°/min scan rate. The XRD of Al_2O_3 NPs is depicted in Fig. 4.26 (b). It is shown from the pattern that the Al_2O_3 NPs is with characteristic peaks at 2-theta equal to 18.30°, 37.69°, 45.73°, 66.88°, and 85.27°. The XRD pattern revealed the strong polarity connections between Al and O and the high lattice energy of Al_2O_3 NPs.

4.2.2 Preparation of vegetable oil-based deionized water emulsion and Al_2O_3 NFs

Pure soybean oil, surfactant and deionized water are mixed with commercially available Al_2O_3 NPs. These nanoparticles have a particle size range of 10-50 nm and an assay of 99.99% with a molecular weight of 101.96. Al_2O_3 NFs are produced in two different concentrations (0.5% and 1% by weight). The nanoparticle concentration range is chosen by taking into account the research previously published on optimizing nanoparticle concentration [180], [237].

Fig. 4.27 outlines the steps taken to prepare the vegetable oil-based deionized water emulsion and nanofluids. Base fluid (soybean oil) and emulsifying agent, i.e., surfactant (Tween 20), were mixed into the deionized water. The role of emulsifying agent was to stabilize the emulsion. Surfactant (Tween 20) was supplied by Merck Life Science Private Limited. The amount of vegetable oil, surfactant, and deionized water was taken about 10 ml, 0.5 ml, and 200 ml, respectively. For proper mixing in emulsion, the emulsion was stirred by a magnetic stirrer (IKA India Private Limited) for 30 min. Then, it was further processed using ultrasonication (probe-type sonicator) to the mixture for 2 hour time duration until a stable emulsion was obtained. Sonication was completed by ultrasonic probe sonicator (Ultra Autosonic India Pvt, Ltd. India). In this way, an emulsion of vegetable oil-based deionized water was obtained. After that, the Al_2O_3 NPs were mixed

with soybean oil-based deionized water emulsion to make the nanofluids using the same procedures by a two-step method (refer to Fig. 4.27). A sodium lauryl sulfate (SLS) with a $1/10^{th}$ weight fraction of NPs is added to the Al_2O_3 NFs to form stability. Using an ultrasonic probe sonicator, the probe controller has been chosen for the on (25 s) and off (5 s) cycles to properly mix the emulsion and Al_2O_3 NPs. For the stable suspension of Al_2O_3 NPs in an oil-water emulsion, 240 times of the on and off cycles have been performed at room temperature. Table 4.2 outlines the probe sonication parameters employed for this purpose.

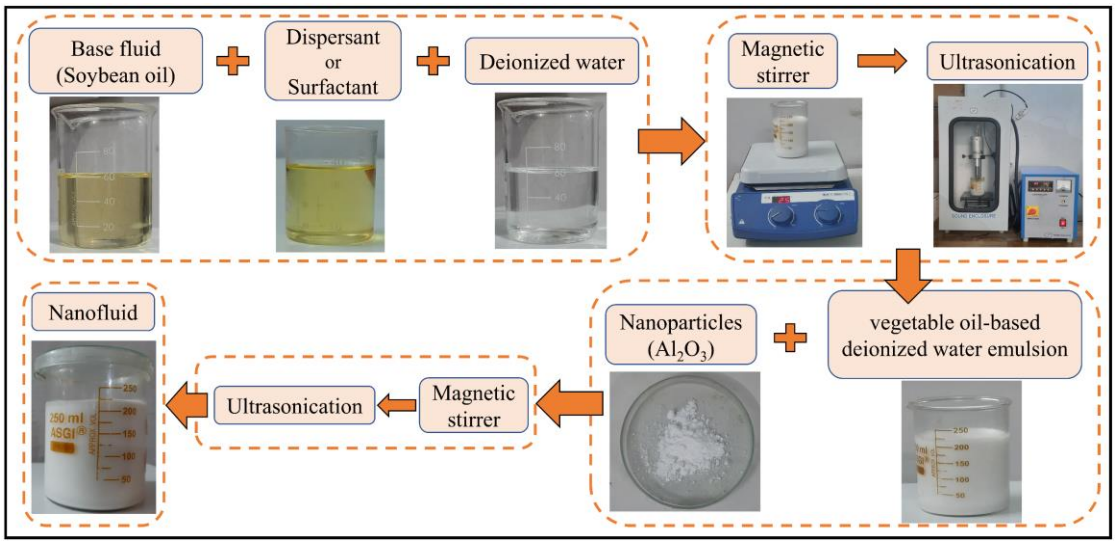

Fig. 4.27: The steps followed for the preparation of vegetable oil-based deionized water emulsion and nanofluid.

Table 4.2: Probe sonication parameters.

Attributes	Values	Attributes	Values
Working frequency	21 kHz	Cycles	240
Pulse on time	25 s	Working temperature	25 °C
Pulse off time	5 s	Working voltage	230 V, 50 Hz

The resulting vegetable oil-based deionized water emulsion and nanofluids can be used in various applications such as lubrication, heat transfer, and cooling. The concentration of

Al_2O_3 NPs used will depend on the application, and it is typically in the 0.5 wt.% and 1 wt.%. Careful attention to detail is necessary to ensure that the resulting emulsion is stable and meets the desired thermo-physical properties for the intended application.

4.2.2.1 Apparent friction coefficient

The significance of the friction coefficient in finishing processes lies in its ability to offer crucial quantitative details regarding the mode of lubrication in the grinding zone. The following formula describes the apparent friction coefficient:

$$\mu = \frac{F_t}{F_n} \tag{4.3}$$

where μ is the apparent friction coefficient; F_t is the tangential force and F_n is the normal force.

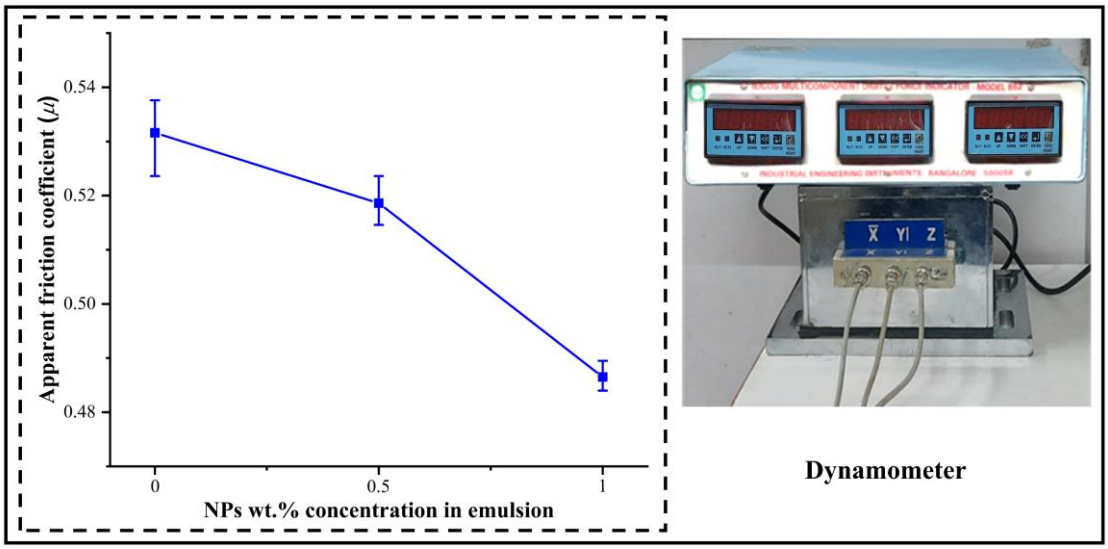

Fig. 4.28: Variation in apparent friction coefficient with Al_2O_3 NPs concentrations in emulsion.

Fig. 4.28 displays the measured apparent friction coefficient results for various concentrations of NPs in emulsion. The addition of NPs into the emulsion has led to a reduction in the friction coefficient. This occurs due to forming of a fluid layer between the

workpiece and the grinding wheel. This leads to better lubrication and less frictional force. Using Al_2O_3 NFs (1 wt.%) in a grinding operation achieved the lowest friction coefficient of around 0.487, as determined by the dynamometer instrument, generating the grinding force, i.e., tangential force and normal force. Mao et al. [238] reported that Al_2O_3 NPs possess the unique ability to penetrate cutting interfaces, resulting in improved heat transfer capabilities. This can be attributed to the significantly higher thermal conductivity than other liquids. The outcomes indicated that adding NPs to the base fluid, mainly Al_2O_3, reduces friction and provides anti-wear properties through rolling and sliding mechanism.

4.2.2.2 Thermo-physical properties of vegetable oil-based deionized water emulsion and Al_2O_3 NFs

The thermo-physical properties of lubricants, i.e., SO+DW emulsion and NFs with 0.5 wt.% and 1 wt.% concentration of Al_2O_3 NPs, are measured by their thermal conductivity, dynamic viscosity, surface tension, density, pH value, and wettability analysis.

4.2.2.2.1 Thermal conductivity

The Hot Disk Thermal Constants Analyzer (Hot Disk, TPS 500) was used to measure the thermal conductivity of the lubricants. Fig. 4.29 illustrates the measured thermal conductivity value obtained from the experiment. The addition of deionized water to base fluid such as vegetable oil leads to an increase in thermal conductivity, as water contains a higher thermal conductivity compared to oil. Additionally, the addition of NPs to the emulsion can further enhance the thermal conductivity of the nanofluid, as NPs can act as heat conductors and increase the effective thermal conductivity of the mixture. The thermal conductivity of the emulsion and nanofluid is influenced by various factors such as nanoparticle concentration, temperature, and particle size distribution. Therefore, the thermo-physical characteristics of vegetable oil-based emulsions and NFs need to be

carefully characterized and optimized to ensure their effective use in heat transfer applications. Similarly, Kong and Lee [238] concluded that Al_2O_3 NFs exhibit enhanced thermal conductivity compared to their base fluids (water), which can be ascribed to the high thermal conductivity of the NPs and their ability to form a stable suspension in the base fluid. It was found that higher thermal conductivity can effectively enhance the performance of heat transfer.

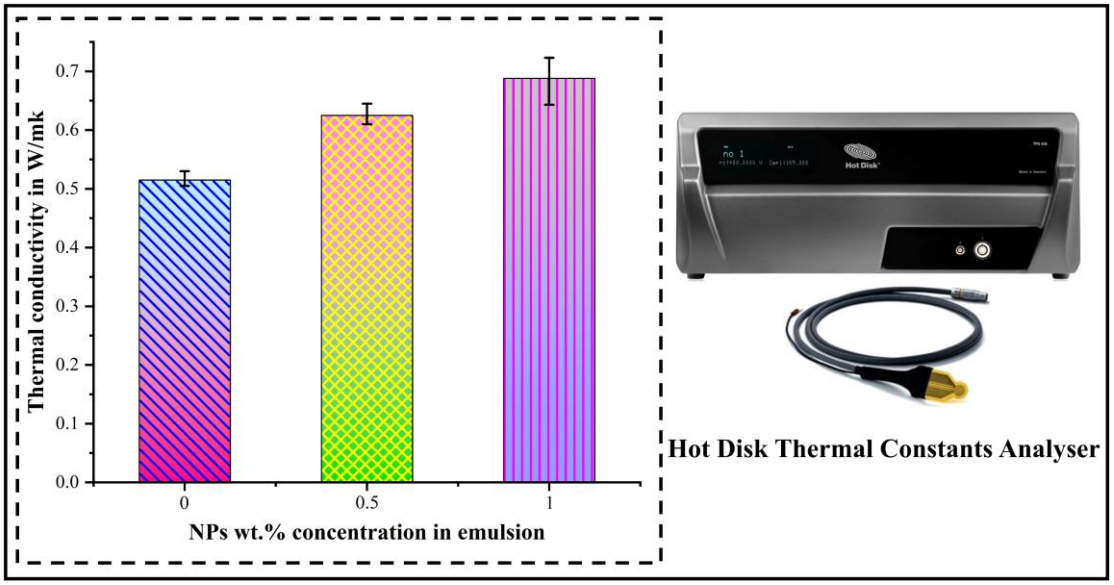

Fig. 4.29: Variation in thermal conductivity of nanofluids with different wt.% concentration of Al_2O_3 NPs.

4.2.2.2.2 Dynamic viscosity

Dynamic viscosity is a measure of the internal friction of a fluid, and it is directly related to the fluid's flow rate. The higher the dynamic viscosity of the emulsion or nanofluid, the more difficult it is for the particles to move freely, which affects the suspension's stability and heat transfer. Therefore, the dynamic viscosity of the base fluid, emulsion and nanofluids plays an important role in their physical behaviour and performance in various applications, such as stability of the suspension, heat transfer, lubrication, and energy storage. By studying the role of dynamic viscosity in these fluids, researchers can develop

strategies to enhance their stability and heat transfer efficiency, leading to improved performance and sustainability.

The dynamic viscosity of the lubricants was measured using a DV1 viscometer (BROOKFIELD) with an accuracy of ±1%. Fig. 4.30 reveals the variation in dynamic viscosity of NFs with different wt.% concentarion of Al_2O_3 NPs. From Table 4.1, it was noticed that SO has maximum dynamic viscosity as compared to other lubricants. The addition of Al_2O_3 NPs in the SO+DW emulsion increased dynamic viscosity. Increasing the concentration of Al_2O_3 NPs from 0 to 1 wt.% may result in the accumulation of NPs in the SO+DW. This can have an impact on the lubricant's ability to form a film. It was also observed from the study presented by Wang et al. [180] that the dynamic viscosity increased with an increase in the addition of Al_2O_3 NPs concentration (wt.%) in the pure palm oil as base fluid.

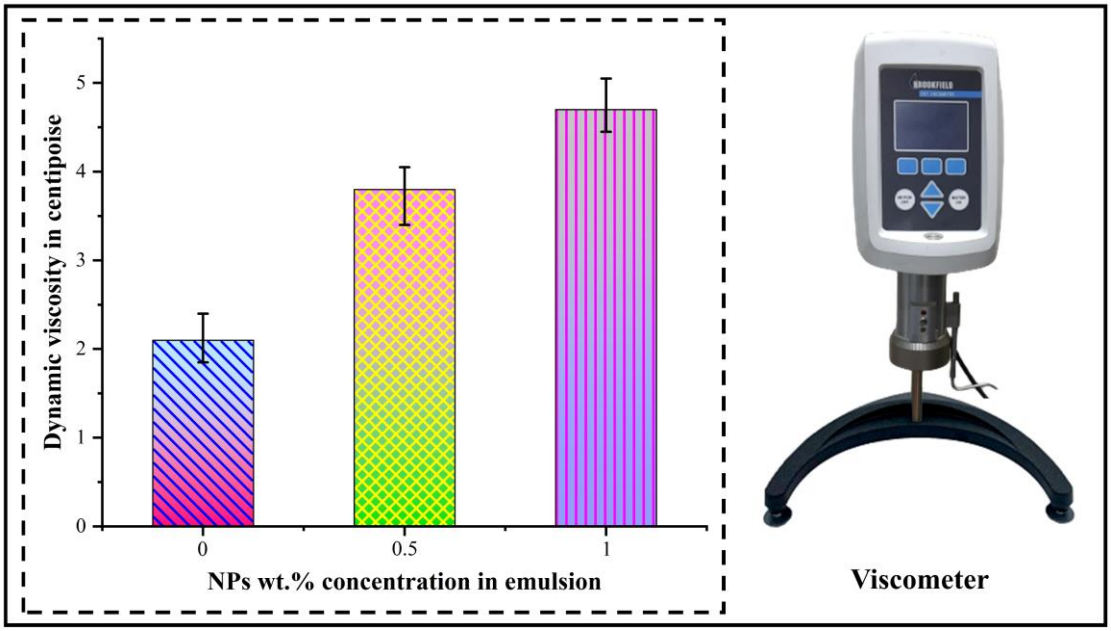

Fig. 4.30: Variation in dynamic viscosity of nanofluids with different wt.% concentration of Al_2O_3 NPs.

4.2.2.2.3 Surface tension

Surface tension plays a crucial role in the formation and stability of emulsions and nanofluids. An emulsion is a mixture of two immiscible liquids, such as oil and water, stabilized by a third substance known as an emulsifier. The emulsifier works by reducing the interfacial tension between the two liquids, allowing them to mix and form a stable emulsion. Similarly, in the nanofluids, which are suspensions of nanoparticles in a base fluid, surface tension helps to prevent the nanoparticles from agglomerating and settling out by creating a repulsive force between them. This repulsion is due to the reduction in the interfacial tension between the nanoparticles and the base fluid, which allows them to remain suspended for longer periods.

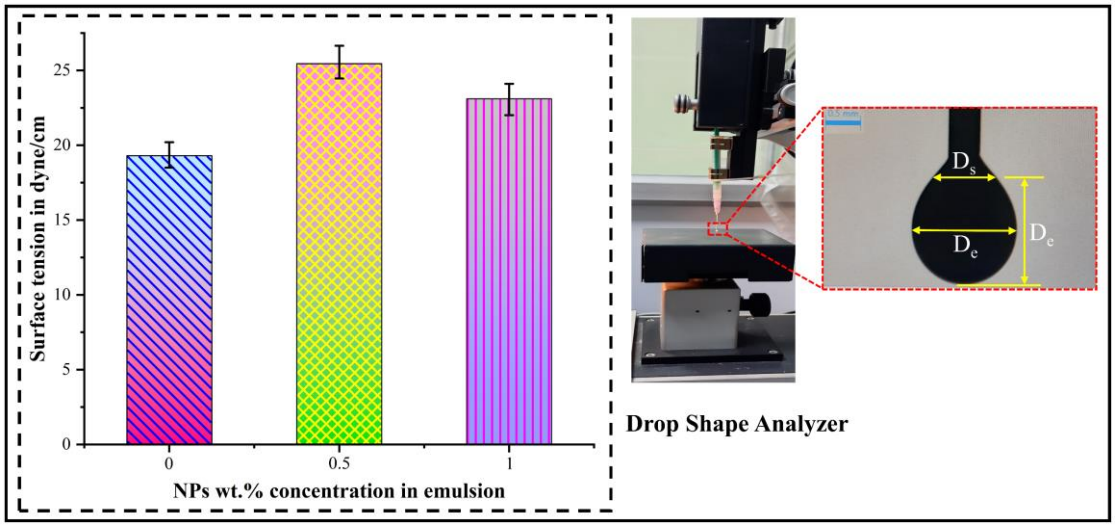

Fig. 4.31: Variation in surface tension of nanofluids with different wt.% concentration of Al_2O_3 NPs.

According to Fig. 4.31, due to intermolecular repulsive forces between the Al_2O_3 NPs, the surface tension decreased as their concentration in the emulsion increased. This happens because nanoparticles can adsorb onto the interface between the two liquids and create a repulsive force that opposes the cohesive forces of the liquids. As reported in a recent investigation, the presence of a long-chain surfactant in nanofluids led to the creation of a

monolayer, which resulted in stronger electrostatic repulsive forces between Al_2O_3 NPs [236]. The pendant drop method was used to measure the surface tension of SO, SO+DW emulsion, and nanofluids with different concentrations, as reported by Gupta et al. [239]. An image of a pendant drop shape was taken at the needle's end using a Drop Shape Analyzer (KRUSS Goniometer, Germany). This image was used to calculate the surface tension by the following equation [239]:

$$\sigma = \frac{g \triangle \rho D_e^2}{H} \tag{4.4}$$

where σ: interfacial tension; $\triangle \rho$: density difference between the fluid phases; D_e: equatorial diameter of the drop; H: correction factor which is related to the shape factor of the pendant drop, *S*, defned as:

$$S = \frac{D_s}{D_e} \tag{4.5}$$

where D_s: drop diameter measured horizontally at a distance D_e away from the apex of the drop.

Therefore, surface tension values were obtained in increasing order for SO, SO+DW emulsion, Al_2O_3 NFs (1 wt.%), and Al_2O_3 NFs (0.5 wt.%), as depicted in Fig. 4.31. SO+DW emulsions significantly increased surface tension compared to pure vegetable oil (SO) because of the presence of two hydrogen (H) and one oxygen (O) atom in deionized water, making a strong link between them.

4.2.2.2.4 Density

Density plays a significant role in determining the fluid's behaviour and properties. The density of vegetable oil-based deionized water emulsion is lower than that of pure water due to the presence of oil droplets in the emulsion. On the other hand, the density of nanofluid is higher than that of the base fluid due to the addition of nanoparticles, as shown

in Fig. 4.32. The density of nanofluid increases with increasing nanoparticle concentration and decreasing temperature [240]. The density of SO+DW emulsion, NFs with 0.5 wt.% and 1 wt.% concentration of Al_2O_3 NPs are 996.58, 1000.11, and 1003.62 kg/m^3, respectively. The presence of emulsifiers can also affect the density of the mixture as they can increase the stability of the emulsion and alter its physical properties. Therefore, lubricants with higher densities can provide better cooling and lubrication, resulting in improved machining performance.

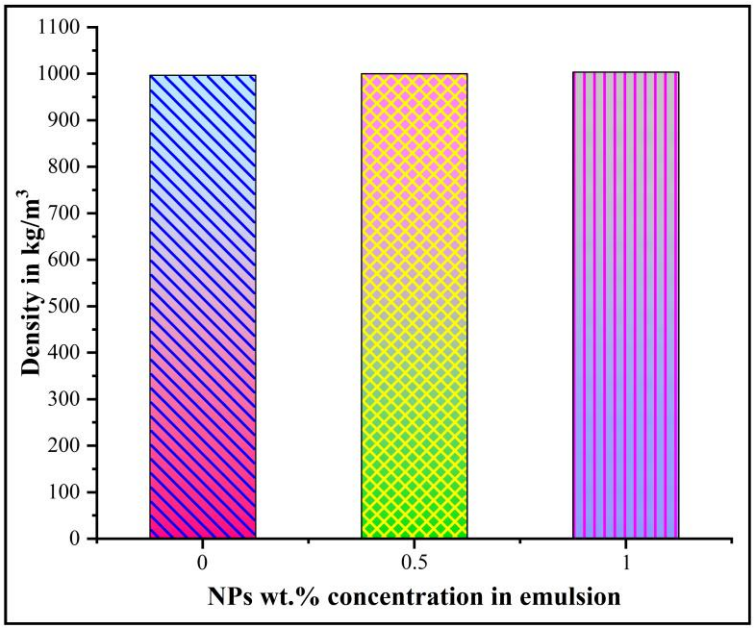

Fig. 4.32: Variation in density of nanofluids with different wt.% concentration of Al_2O_3 NPs.

4.2.2.2.5 pH value

Fig. 4.33 shows the pH value of different wt.% concentration of Al_2O_3 NPs and the arrangement of a Digital pH Meter (ISO-TECH SYSTEM, ITS-201) for measuring the pH value. The pH values can influence the uniform dispersion of NPs in NFs and the stability of the NFs, as well as their thermal conductivity, dynamic viscosity, and density. In this test, the average pH value of Al_2O_3 NFs with different concentrations (0.5 wt.% and 1

wt.%) was compared to the isoelectric point (IEP) of Al_2O_3 NPs. The Derjaguin-Landau-Verwey-Overbeek (DLVO) theory [241] states that NPs tend to be unstable, form clusters, and precipitate when the pH value is equal to or close to the isoelectric point. The IEP for Al_2O_3 NPs lies at a pH of about 9.6 [236]. From Fig. 4.33, the difference between IEP for Al_2O_3 NPs and the pH value of (0.5 and 1 wt.%) Al_2O_3 NFs is noticed by nearly 2.1 and 1.4. Based on DLVO theory, Al_2O_3 nanofluid with 0.5 wt.% is more stable than Al_2O_3 nanofluid with 1 wt.%.

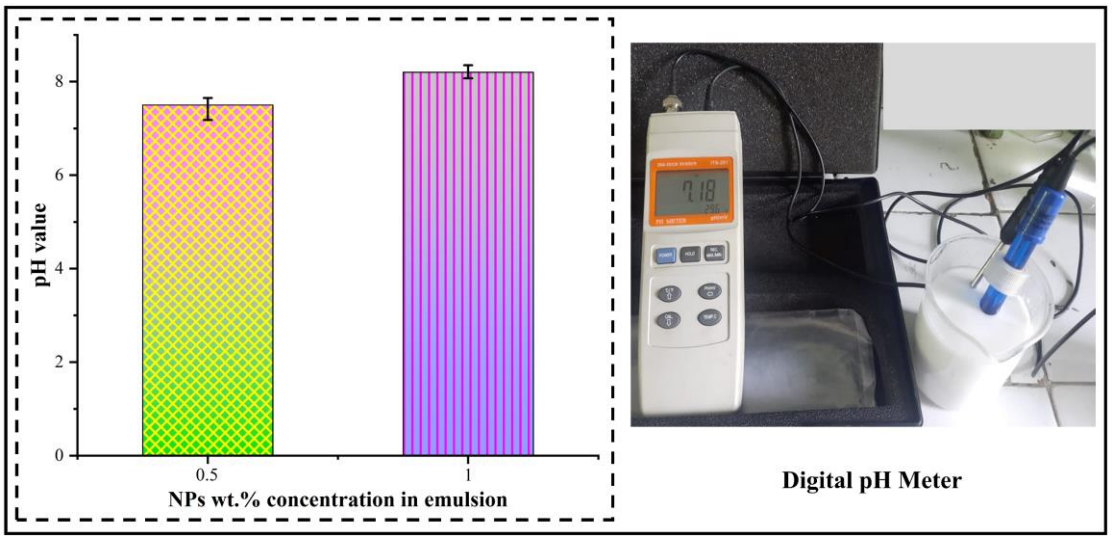

Fig. 4.33: Variation in pH value of nanofluids with different wt.% concentration of Al_2O_3 NPs.

In another way, the dispersion properties of Al_2O_3 NFs with different wt.% concentrations were evaluated using the conventional sedimentation method. The stability of NFs is intimately correlated with the NFs' sedimentation characteristics, which are of the utmost importance and simplest method. A sedimentation picture of Al_2O_3 NFs with 0.5 wt.% and 1 wt.% concentration in test beakers taken by a camera is also a usual method for observing the stability of NFs after 5 hours to 28 hours (refer to Fig. 4.34). In the case of Al_2O_3 NFs (0.5 wt.%), these NFs were observed after 5 hours from fresh preparation, and the next observation occurred after 28 hours from fresh preparation. The gap between the

two red dotted lines presented the area of settle-down of NPs in NFs. A similar procedure was followed for Al_2O_3 NFs (1 wt.%). It was concluded that Al_2O_3 NFs (0.5 wt.%) are more stable than Al_2O_3 NFs (1 wt.%). Zhu et al. [242] measured the graphite suspension's stability using a sedimentation balance method.

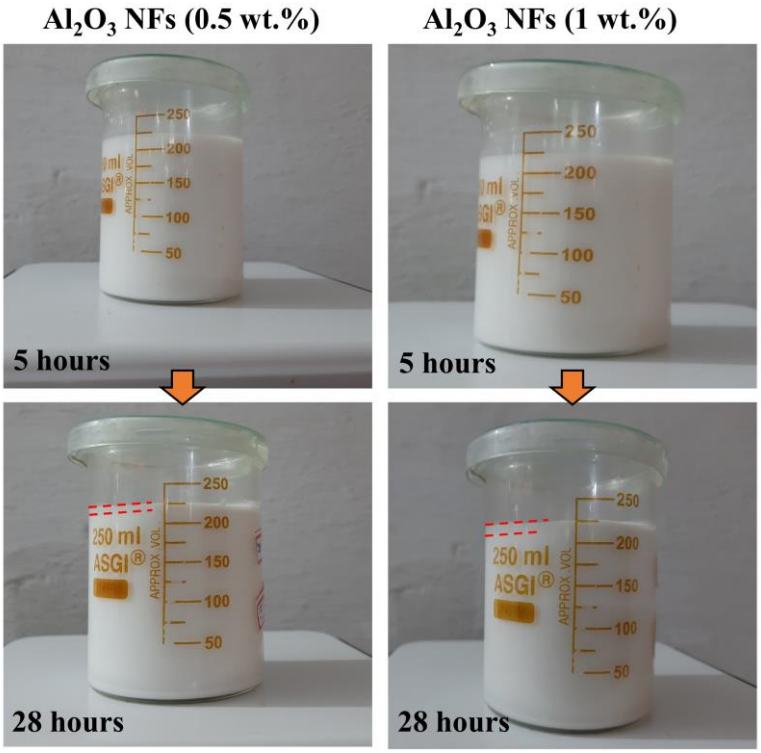

Fig. 4.34: Sedimentation process for Al_2O_3 NFs after 5 hours and 28 hours.

4.2.2.2.6 Wettability analysis

Wettability is an important thermo-physical property that determines the extent to which a liquid can spread over a solid surface using a Drop Shape Analyzer system (refer to Fig. 4.35). The wettability of a surface can be characterized by the contact angle formed through the liquid droplet on the surface, as seen in Fig. 4.35 (a). When a liquid droplet comes into contact with a solid surface, an angle is produced between the tangent of the droplet and the surface. This angle is referred to as the contact angle. In most applications, the air was always considered as the III phase. The workpiece and liquid droplet were considered as phases I and II, respectively (refer to Fig. 4.35 (a)).

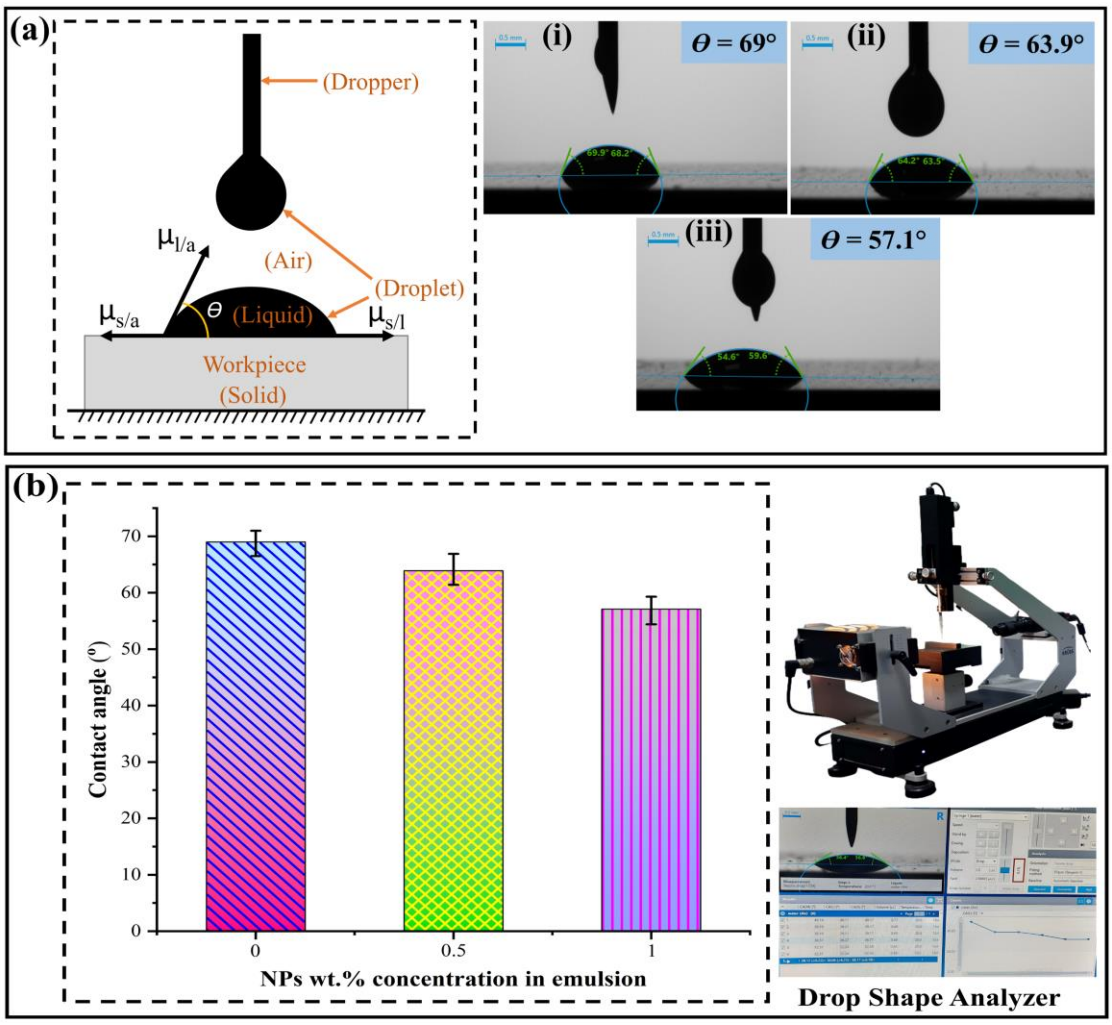

Fig. 4.35: (a) Schematic diagram for wettability analysis and contact angle of different lubricants: (i) SO+DW emulsion; (ii) 0.5 wt.% of Al_2O_3 NFs; (iii) 1 wt.% of Al_2O_3 NFs; (b) Variation in contact angle of NFs with different wt.% concentration of Al_2O_3 NPs.

Generally, the evaluation of the theory of surface tension may clarify the contact angle theory. The surface tension of three distinct interfaces were assessed as solid-air ($\mu_{s/a}$), solid-liquid ($\mu_{s/l}$), and liquid-air ($\mu_{l/a}$), respectively. The relationship between the equilibrium contact angle (Θ) and surface tension of various phases is represented by Thomas Young's equation [243]. A mathematical expression is given by the relation:

$$\cos(\Theta) = \frac{\mu_{s/a} - \mu_{s/l}}{\mu_{l/a}} \tag{4.6}$$

This model assumed that the size of the liquid droplet was small so that gravity could be negligible. For contact angle measurements, the surface of the solid substrate must be flat and homogenous. The surface's wetting property is described as follows: if the Θ is less than 90°, the material's behaviour is hydrophilic, increasing the wetting area; if the Θ is more than 90°, the material's behaviour is hydrophobic, resulting in less wetting area.

Fig. 4.35 shows the schematic diagram for wettability analysis and depicts the contact angle values for nanofluids at different NPs concentrations ranging from 0 to 1 wt.% with a pictorial view of the Drop Shape Analyzer. A sessile drop method was utilized to determine the contact angles of various lubricants. Before the wettability test, acetone was used to clean the ground surface. Further, lubricant through a dropper was dropped on the ground surface. The lubricant droplet image was captured and noted the contact angle value. The addition of Al_2O_3 NPs in emulsion (SO+DW) indicated a lower contact angle. In Fig. 4.35 (b), a study that compared different lubricants, it was observed that Al_2O_3 NFs with 1 wt.% concentration exhibited a minimum contact angle, indicating a higher wetting ability on the surface than the emulsion and Al_2O_3 NFs (0.5 wt.%). A similar trend was reported by Makhesana et al. [244] and Roushan et al. [243] in contact angle for 0 to 1 wt.% concentration of NPs. A smaller contact angle indicated that the lubricant droplet has the potential to spread over more surface area, showing improved lubrication properties of the NFs. Therefore, based on the experimental results, it can be concluded that the concentration of 1 wt.% Al_2O_3 NPs provides the most effective lubrication effect, followed by 0 and 0.5 wt.% Al_2O_3 NPs.

It is concluded from the results that an increased concentration of Al_2O_3 NPs leads to a reduction in the coefficient of friction. However, this increase in concentration also corresponds to increases in thermal conductivity, dynamic viscosity, density, and pH value, but surface tension increases at a concentration of 0–0.5 wt.% Al_2O_3 NPs, after which

surface tension slightly reduces. From the measured contact angle, it was stated that the Al_2O_3 NPs added to the emulsion improved wettability from 0 to 1 wt.% concentration. Thus, determining the optimum concentration of NPs in the emulsion is essential for improving grinding performance.

4.2.3 Effect of Cryo-MQL environment on grinding force

In the grinding process, grinding force is an essential technical parameter. This parameter relates to the service life of the grinding wheel, specific grinding energy, and surface roughness. It is described as the force needed to remove material during grinding. However, it also reflects the lubrication performance of various grinding fluids used during the grinding operation. Fig. 4.36 shows the grinding forces of the different lubricants under MQL and Cryo-MQL environments. Grinding force is divided into tangential force, F_t, and normal force, F_n, for analysis. The trend of grinding force (F_t and F_n) for four different lubricants in MQL and Cryo-MQL environments measured by a dynamometer is shown in Fig. 4.36. The grinding force was found to be in the order of low to high as Cryo-MQL < MQL, and the grinding force of the lubricants in MQL and Cryo-MQL environments appeared by order of SO+DW > Al_2O_3 (0.5 wt.%) > SO > Al_2O_3 (1 wt.%). The excessive negative rake angle of unidirectional rotation alumina grits and the high apparent friction coefficient of the grit-work-chip interface cause the highest grinding force in SO+DW emulsion. Additionally, Al_2O_3 NPs can help to reduce friction at the abrasive wheel and the workpiece interface, resulting in reduced grinding forces and improved surface quality [245]. However, for grinding in the Cryo-MQL environment, the F_t for SO, SO+DW, Al_2O_3 (0.5 wt.%), and Al_2O_3 (1 wt.%) was reduced by 3.64%, 9.27%, 9.39% and 25.66%, respectively, over MQL grinding at the wheel speed of 39.42 m/s and downfeed of 40 µm. Similarly, the F_n was lowered by 3.52%, 4.71%, 4.40% and 12.87%, respectively, as

compared to MQL grinding.

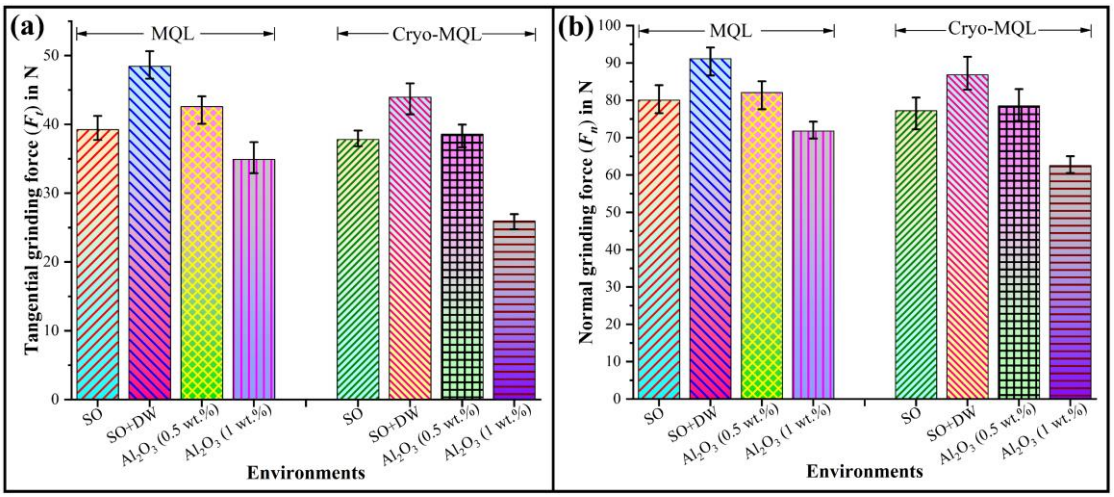

Fig. 4.36: Variation in grinding force with different lubricants under MQL and Cryo-MQL environments: (a) F_t; (b) F_n.

Cryo-MQL is more efficient than MQL due to utilizing LN_2 as a coolant. During the Cryo-MQL environment, the grinding zone area experiences boundary lubrication and cooling effect (by LN_2 coolant), improving the shearing action. The primary reason for this is the high-pressure lubrication under MQL environments and low boiling temperature coolant (LN_2) under cryogenic environments, which enhances grindability by lowering the grinding temperature, sliding friction and wheel loading. Therefore, Cryo-MQL recorded the minimum grinding force by increasing elastic-plastic deformation in the abrasive grit edge [158]. With the introduction of NPs, the Al_2O_3 NPs (1 wt.%) have the lowest grinding force compared to other lubricants under MQL and Cryo-MQL. It happens due to the unique properties of Al_2O_3 NPs (1 wt.%), such as high thermal conductivity and low contact angle, which enable enhanced heat dissipation and lubrication effect [246].

4.2.4 Effect of Cryo-MQL environment on specific grinding energy

All manufacturing sectors focus on reducing energy consumption in producing finished products. This has led to the growth of innovative methods and technologies to optimize

energy usage and increase process efficiency, eventually resulting in cost savings and reduced environmental impact [247]. Several researchers have stated that the measure of grinding efficiency can be determined by using the specific grinding energy concept. The energy required to remove a unit volume of material is known as specific grinding energy. During the grinding process, specific grinding energy is significantly related to the grinding wheel service life and the surface quality of the workpiece. This energy also signifies the lubricating action occurring in the grinding zone region. Sufficient grinding fluid lubrication in the grinding zone effectively decreases the friction between the wheel and workpiece, reducing the grinding force and generating low specific grinding energy [248]. A decrease in specific grinding energy during the process indicates more efficient workpiece machining and is environment-friendly. The effect of various lubricants on specific grinding energy is presented in Fig. 4.37.

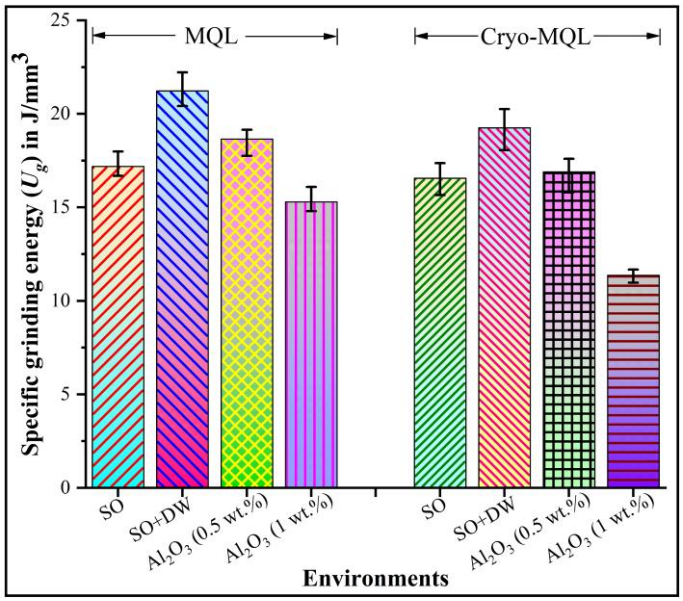

Fig. 4.37: Variation in specific grinding energy with different lubricants under MQL and Cryo-MQL environments.

Based on the experimental results (refer to Fig. 4.37), lubricants under Cryo-MQL decreased the specific grinding energy by 3.64%, 9.27%, 9.39%, and 25.66%, respectively,

compared with lubricants under MQL. Under both environments, vegetable oil (SO) with deionized water as a lubrication medium has poor lubrication conditions at the grinding zone area and high energy consumption during the grinding operation. The lubricating effects of Cryo-MQL using SO lubricants were better than SO+DW emulsion. A higher concentration of Al_2O_3 NPs in SO+DW emulsion under Cryo-MQL was very effective because of the simultaneous generation of cooling and lubrication effects during the grinding of AISI D2 tool steel.

4.2.5 Effect of Cryo-MQL environment on surface roughness

Surface roughness refers to the irregularities and variations in a workpiece's surface texture. The Mitutoyo roughness tester measures the surface roughness on the ground surface produced by randomly distributed abrasive grains. The decreased surface roughness enhances the ground sample's physical, mechanical, and tribological qualities. Several standard roughness parameters, i.e., R_a, R_q, and R_z, describe quantitive information of surface quality. Generally, surface roughness is influenced by the wheel wear rate, adhesion of microchips and grits, and lubricating conditions during the grinding [249].

Fig. 4.38 demonstrates that R_a, R_q, and R_z display similar trends for all investigated conditions. The combination of MQL and LN_2 coolant reduced the surface roughness by 19.56%, 8.81%, 17.01%, 25.02% in R_a parameter, 18.40%, 10.78%, 18.13%, 20.75% in R_q parameter, and 11.26%, 15.49%, 16.46%, 16.52% in R_z parameter compared to the SO, SO+DW, Al_2O_3 (0.5 wt.%) NFs, and Al_2O_3 (1 wt.%) NFs in MQL environment, respectively. The R_a, R_q, and R_z results showed that the best surface roughness is achieved under the Al_2O_3 (1 wt.%) NFs grinding environment with R_a of 0.304 μm, R_q of 0.393 μm and R_z of 2.137 μm. For this reason, the Al_2O_3 NPs can also help to disperse heat generated from the grinding zone area, which can reduce the risk of thermal damage to the work material. Furthermore, Al_2O_3 NPs can act as a filler, filling in microcracks and other

imperfections in the workpiece surface. This can result in a smoother and more uniform surface finish.

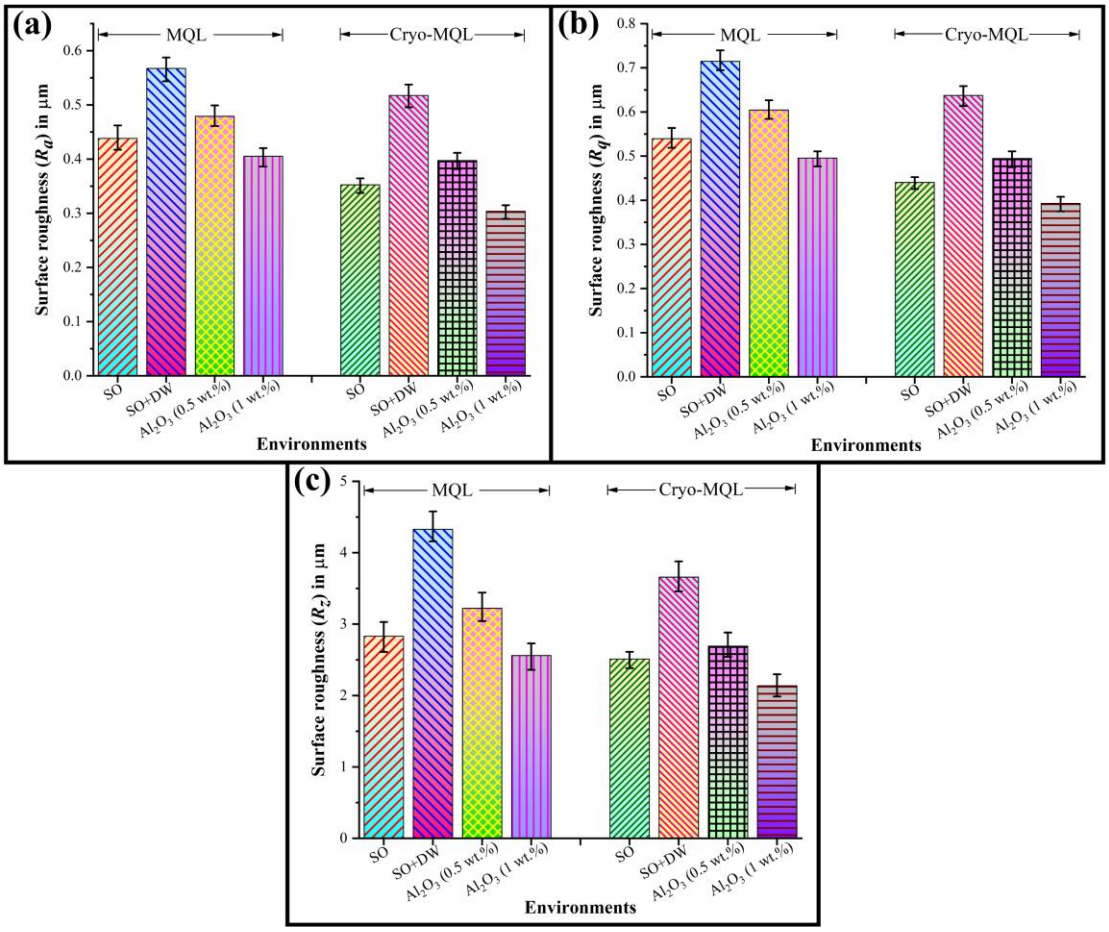

Fig. 4.38: Variation in surface roughness with different lubricants under MQL and Cryo-MQL environments: (a) R_a; (b) R_q; (c) R_z.

Similar results were obtained by Setti et al. [250]. They added Al_2O_3 NPs of 40 nm average size with different volumetric concentrations in water as the grinding fluid and sprayed Al_2O_3 NFs on Ti-6Al-4V alloy during the grinding experiment. A better surface finish was observed over the ground surface by Al_2O_3 NPs than coolant and pure water, and the grinding force and wheel abrasion were significantly reduced. Also, the NPs may be used to dress the grinding tool during the grinding process. If NPs separate the wheel's bonding material from it, new active grains become visible in the grinding zone. As Cui et

al. [251] pointed out, the lubricant layer between grinding wheel-work surfaces effectively lowers friction and wheel wear out, improving surface quality. Additionally, the reduction in temperature by LN_2 coolant and high thermal conductivity of Al_2O_3 NFs protected against the workpiece surface thermal degradation under Cryo-MQL environments.

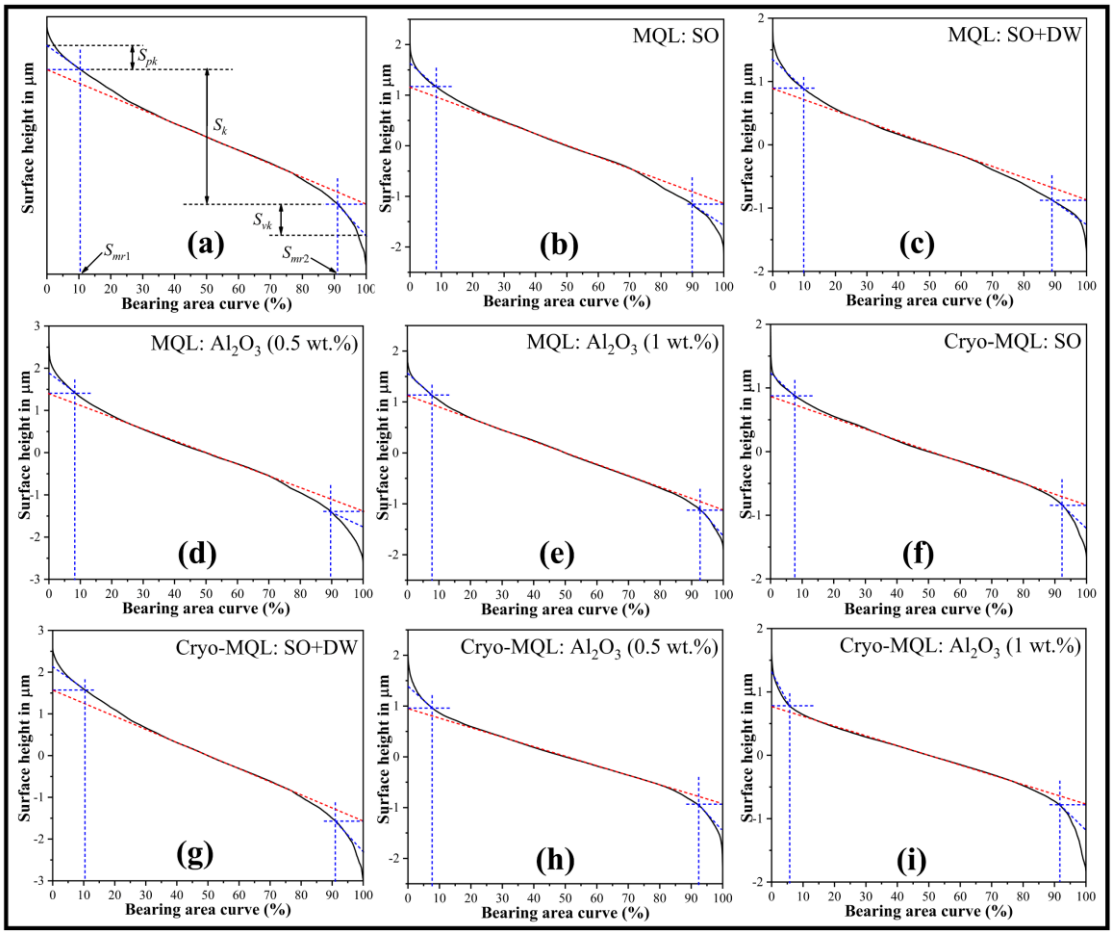

Fig. 4.39: Bearing area curve of ground sample with different lubricants: (a) Functional parameters of the bearing area curve; (b) MQL: SO; (c) MQL: SO+DW; (d) MQL: Al_2O_3 (0.5 wt.%) NFs; (e) MQL: Al_2O_3 (1 wt.%) NFs; (f) Cryo-MQL: SO; (g) Cryo-MQL: SO+DW; (h) Cryo-MQL: Al_2O_3 (0.5 wt.%) NFs; (i) Cryo-MQL: Al_2O_3 (1 wt.%) NFs.

A graphical approach for assessing surface roughness, particularly in surface engineering applications, is the bearing area curve (BAC) analysis, also known as the Abbott-Firestone curve. Bearing area refers to the state where two physical surfaces are in

contact. This state provides qualitative information regarding the components' wear resistance and anti-friction properties [252]. Fig. 4.39 shows the BAC profile of the ground sample in MQL and Cryo-MQL grinding with various lubricants. These curves are segmented into three distinct regions using functional parameters for better understanding. Based on ISO 25178-2 standard [253], all functional parameters (S_{pk}, S_k, S_{vk}, S_{mr1}, and S_{mr2}) used in the BAC analysis are shown in Fig. 4.39 (a), which are informative. The reduced peak height, S_{pk}, is indicated by the upper part of the BAC profile. This refers to the average height of the peaks that extend beyond the roughness core profile.

The reduced peak height, S_{pk}, functional parameter describes the surface conditions in terms of quickly worn-out spikes during the running-in operation. The middle part of the BAC profile represents the core roughness depth, S_k. S_k describes the core roughness of a surface after it has undergone a run-in period, and this parameter is also important for understanding the load-bearing capacity of the finished surface. The lower part of the BAC profile represents the reduced valley depth, S_{vk}, which shows the retained lubricant. The upper material ratio, S_{mr1} and lower material ratio, $S_{mr2,}$ represent the percentage of the BAC profile that intersects with the upper and bottom limits of the core roughness, respectively [254]. The bearing area ratio or core material ratio (S_{mr2}-S_{mr1}), S_{mrk}, indicates the wear resistance and anti-friction characteristics of the ground sample.Table 4.3 represents the functional parameters of ground surface (i.e., S_{mr1}, S_{mr2}, and S_{mrk}) determined from the BAC profile.

According to the data presented in Table 4.3, it was observed that the 1 wt.% Al_2O_3 NFs have a higher bearing area ratio (86.12%) under Cryo-MQL environments than MQL environments. In other words, the bearing properties of the ground surface depend on the slope of the BAC profile, core roughness depth and tribo-characteristics of the lubricants. Temperature also affects the anti-wear and anti-friction characteristics of the sliding

components. However, Cryo-MQL grinding, which used LN_2 as a coolant, produced better anti-friction and anti-wear characteristics than MQL grinding for various lubricants.

Table 4.3: Functional parameters of ground surface derived from bearing area curve profile.

Environments	Lubricants	S_{mr1} (%)	S_{mr2} (%)	$S_{mrk} = S_{mr2} - S_{mr1}$ (%)
MQL	SO	8.39	89.97	81.58
	SO+DW	9.93	88.92	78.99
	Al_2O_3 (0.5 wt.%) NFs	8.25	89.72	81.47
	Al_2O_3 (1 wt.%) NFs	7.81	92.43	84.62
Cryo-MQL	SO	7.69	92.39	84.70
	SO+DW	10.49	91.02	80.53
	Al_2O_3 (0.5 wt.%) NFs	7.67	92.31	84.64
	Al_2O_3 (1 wt.%) NFs	5.77	91.89	86.12

4.2.6 Effect of Cryo-MQL environment on ground surface topography

Fig. 4.40 illustrates the changes in the surface characteristics of the ground surface with different lubricants. In the MQL technique, the insufficient absorption ability of the lubricating film of the SO + DW emulsion has led to the microchip sticking to the entire ground surface, causing noticeable side flows, deep scratches, and adhesion. Due to the low thermal conductivity of SO + DW emulsion (refer to Fig. 4.29), the grinding zone area experienced a higher temperature than other lubricants. This can cause the major portion of grinding chips on the alumina wheel to become smeared or loaded, further redeposited over the ground surface. Large numbers of uneven abrasive grits distributed discretely composed the grinding wheel surface. As a result, deep scratches and grooves were produced on the ground surface along the grinding marks direction, and also side flows by the ploughing action of abrasive grits were found, as shown in Fig. 4.40 (c). A nearly good surface texture

was achieved compared to SO+DW emulsion. The reason for this is attributed to increased thermal conductivity and dynamic viscosity.

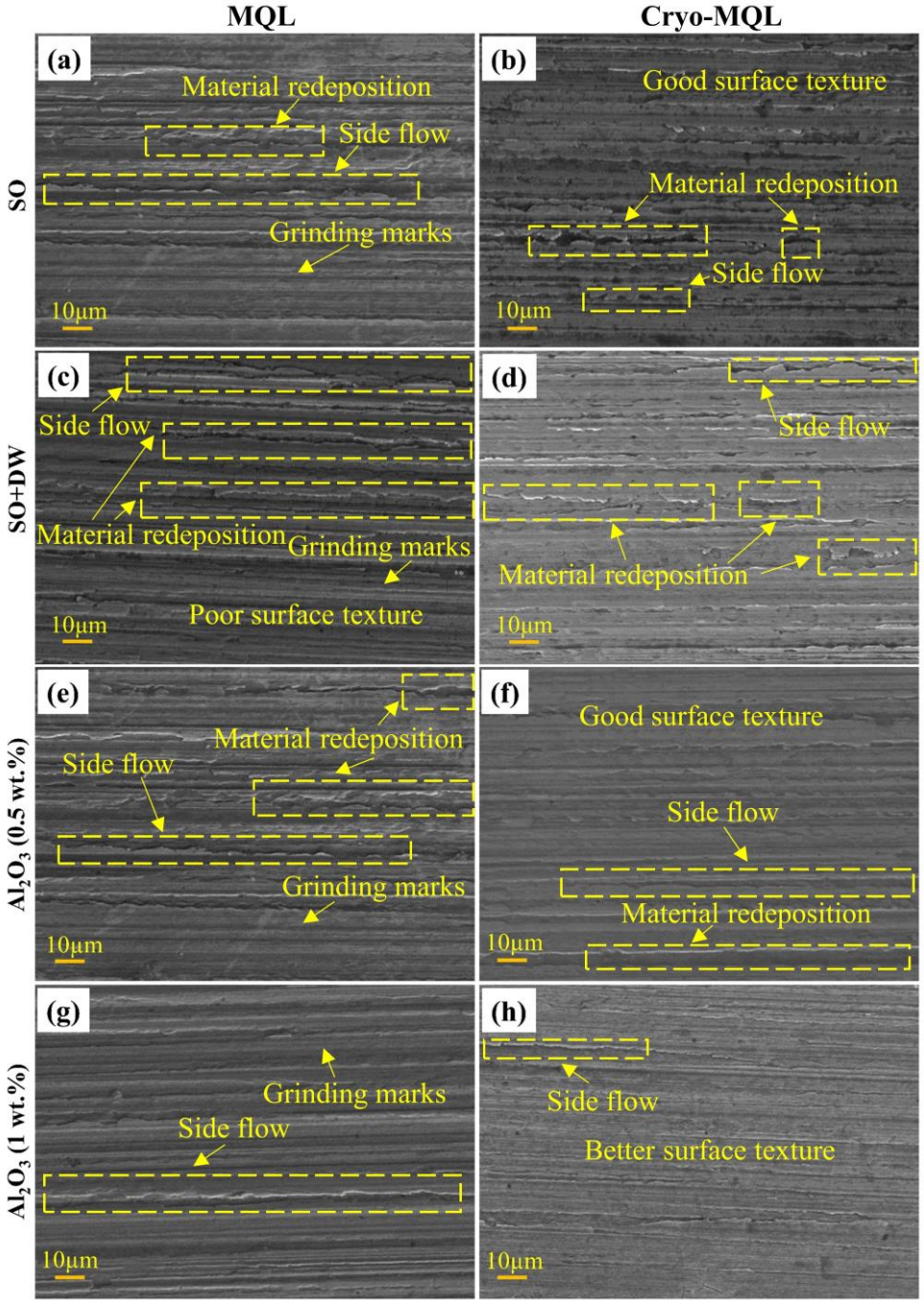

Fig. 4.40: Surface morphology of work material under MQL and Cryo-MQL environments.

Cryo-MQL is a hybrid technique where the lubricant mixture can cool and lubricate the grinding zone, significantly enhancing surface texture and minimizing grinding marks [158]. Good lubrication with LN_2 lowers the evaporation of lubricants and maintains the

lubrication film strength in the grinding zone, resulting in a finer surface. Because the decrease in grinding temperature improves the ground surface, resulting in less crest flattening the asperities.

Application of Al_2O_3 NFs in MQL and Cryo-MQL grinding resulted in a better surface morphology than SO+DW MQL. This improvement suggests that the presence of Al_2O_3 NPs helps to reduce adhesion between the abrasive grain and workpiece by providing effective lubrication through rolling and sliding phenomena and uniform cooling through mass heat transfer from the grinding zone, which consequently lowers the grinding force and friction [255]. On the other hand, Fig. 4.40 (h) shows the best surface texture in comparison to all lubricants owing to the higher concentration of Al_2O_3 NPs and LN_2 coolant under the hybrid Cryo-MQL grinding process.

Three-dimensional surface topography provides a more accurate and detailed representation of the physical features of the ground surface. Because 3D topography allows for the identification and analysis of topographical features, such as peaks and valleys heights, that may not be apparent in 2D morphology. Fig. 4.41 depicts 3D surface topography images obtained using AFM instruments operating in different environments: MQL and Cryo-MQL. AFM analysis obtained the most optimal surface roughness measurements for a ground sample with 1 wt.% Al_2O_3 NFs-based Cryo-MQL grinding. This method provided superior impact of cooling and lubrication, resulting in a small average roughness (S_a: 0.202 µm), low root mean square roughness (S_q: 0.24 µm), and small area peak-to-valley height (S_t: 1.468 µm), as illustrated in Fig. 4.41 (h).

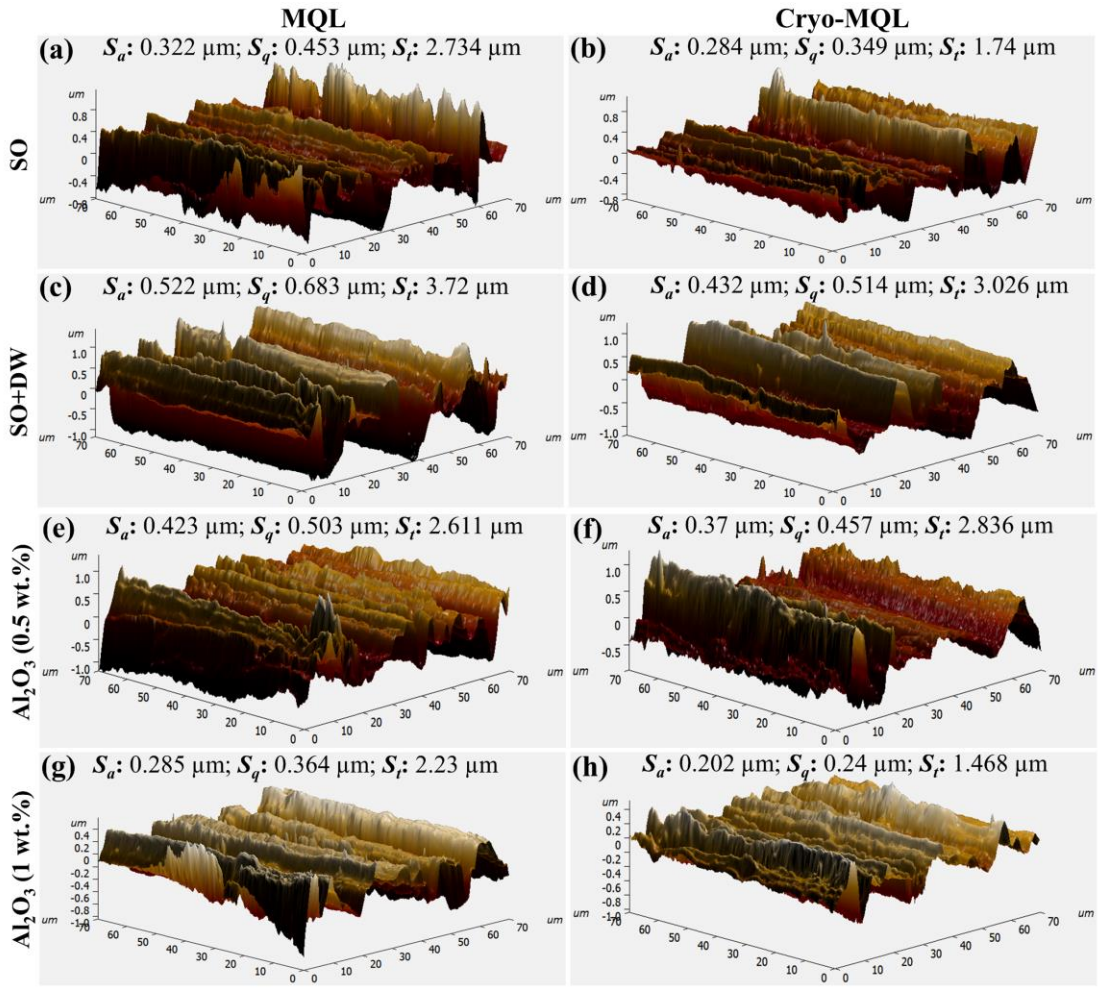

Fig. 4.41: 3D surface topography of ground AISI D2 tool steel under MQL and Cryo-MQL environments.

4.2.7 Effect of Cryo-MQL environment on chip morphology

Chip morphology is essential for the grindability of the work material. Grinding chip morphology, size, and shapes are significantly impacted by the combined influences of the mechanical properties of the work material and the abrasive wheel, as well as the grinding parameters, particularly the grinding environments, downfeed, table feed rate, and wheel speed. Grinding chips produced for different lubricants during MQL and Cryo-MQL grinding of AISI D2 tool steel were collected on carbon tape. These chips were then analyzed under SEM to investigate the chip formation process, lubrication, and cooling effects, as illustrated in Fig. 4.42.

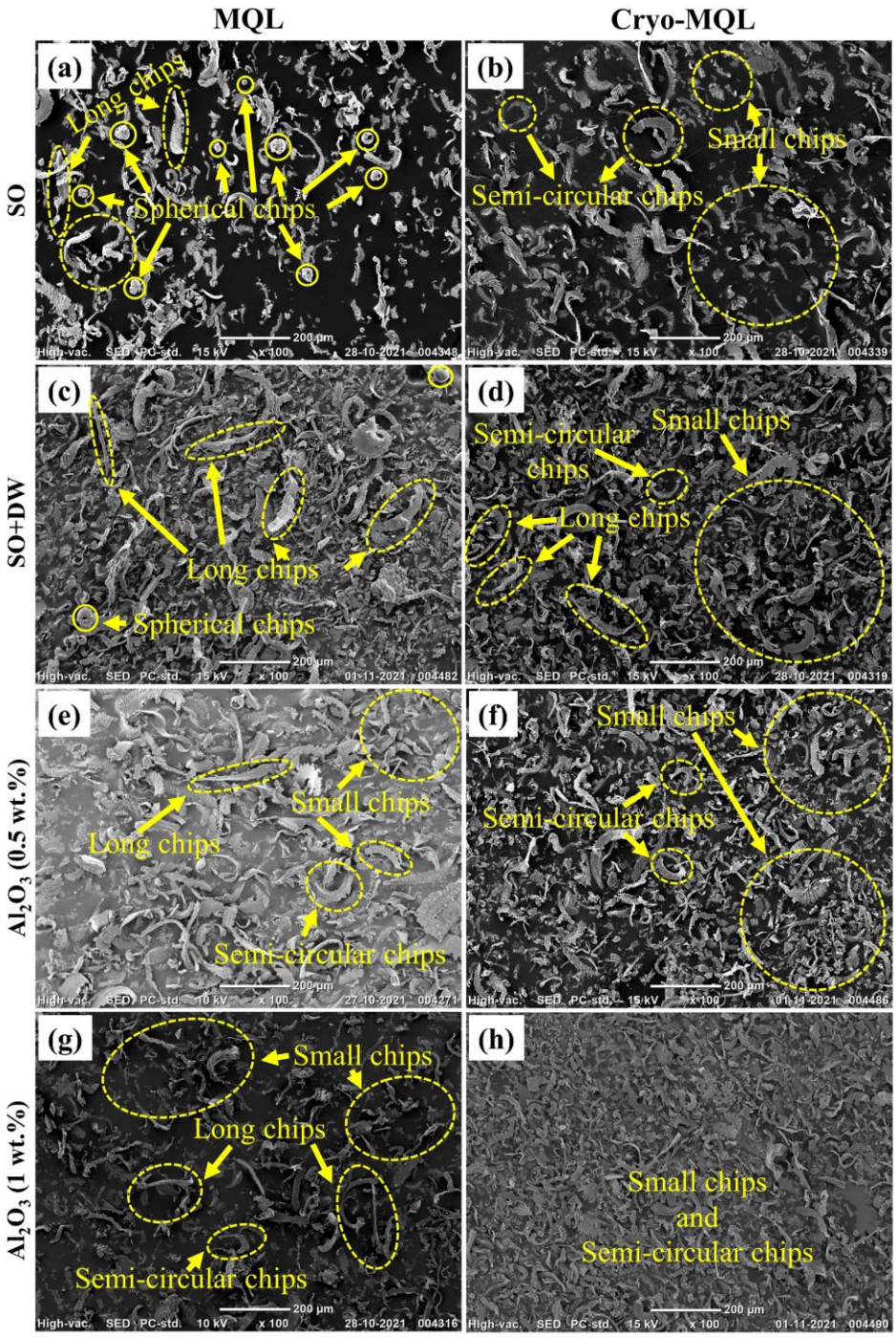

Fig. 4.42: Chip morphology of work material under MQL and Cryo-MQL environments.

Because of its thermo-mechanical characteristics, AISI D2 tool steel has low heat dissipation capabilities. Consequently, an extensive amount of heat is generated in the grinding zone area. Thus, during SO as base fluid and SO+DW emulsion under MQL grinding, long continuous and spherical chips were formed, as shown in Fig. 4.42 (a, c). It

happened because of the low thermal conductivity in comparison to the Al_2O_3 NFs. When Al_2O_3 NPs are added to the vegetable oil-based deionized water emulsion used in MQL grinding, they can form a lubrication boundary layer at the grinding zone, reducing friction at the wheel-workpiece interface and grinding force. This, in turn, reduces the temperature generated during the machining process and increases the proportion of small chips while reducing the proportion of long chips.

During the Cryo-MQL grinding, C-type or semi-circular chips were observed as the temperature was decreased by the LN_2 jet. This phenomenon can be attributed to the frozen effects of cryogenic cooling. Additionally, the reduced temperature can also decrease the plastic deformation of the work material during grinding, leading to the formation of smaller chips. These observations suggest that a combination between better lubrication and cooling performance can effectively control chip morphology, size, and shape during Cryo-MQL grinding. However, based on the results shown in Fig. 4.42 (h), it can be inferred that utilising Al_2O_3 NPs with 1 wt.% concentration improved chip breakability, thus suggesting the superior grindability performance of AISI D2 tool steel.

4.2.8 Effect of Cryo-MQL environment on grinding temperature

Fig. 4.43 compares the grinding temperature generated in various lubricants, including SO, SO+DW emulsion, Al_2O_3 (0.5 wt.%) NFs and Al_2O_3 (1 wt.%) NFs under MQL and Cryo-MQL environments. As discussed earlier, less thermal conductivity produces maximum heat under SO-based grinding, causing more wheel wear and poor surface integrity than other lubricants. Compared to SO-based grinding, the temperature was lower when a SO+DW emulsion was sprayed in the grinding zone. In comparison to SO and SO+DW grinding, Al_2O_3 NPs were seen to significantly reduce grinding temperature. The lowering in grinding temperature with Al_2O_3 NFs is credited to the greater thermal

conductivity, as detailed in Table 4.1.

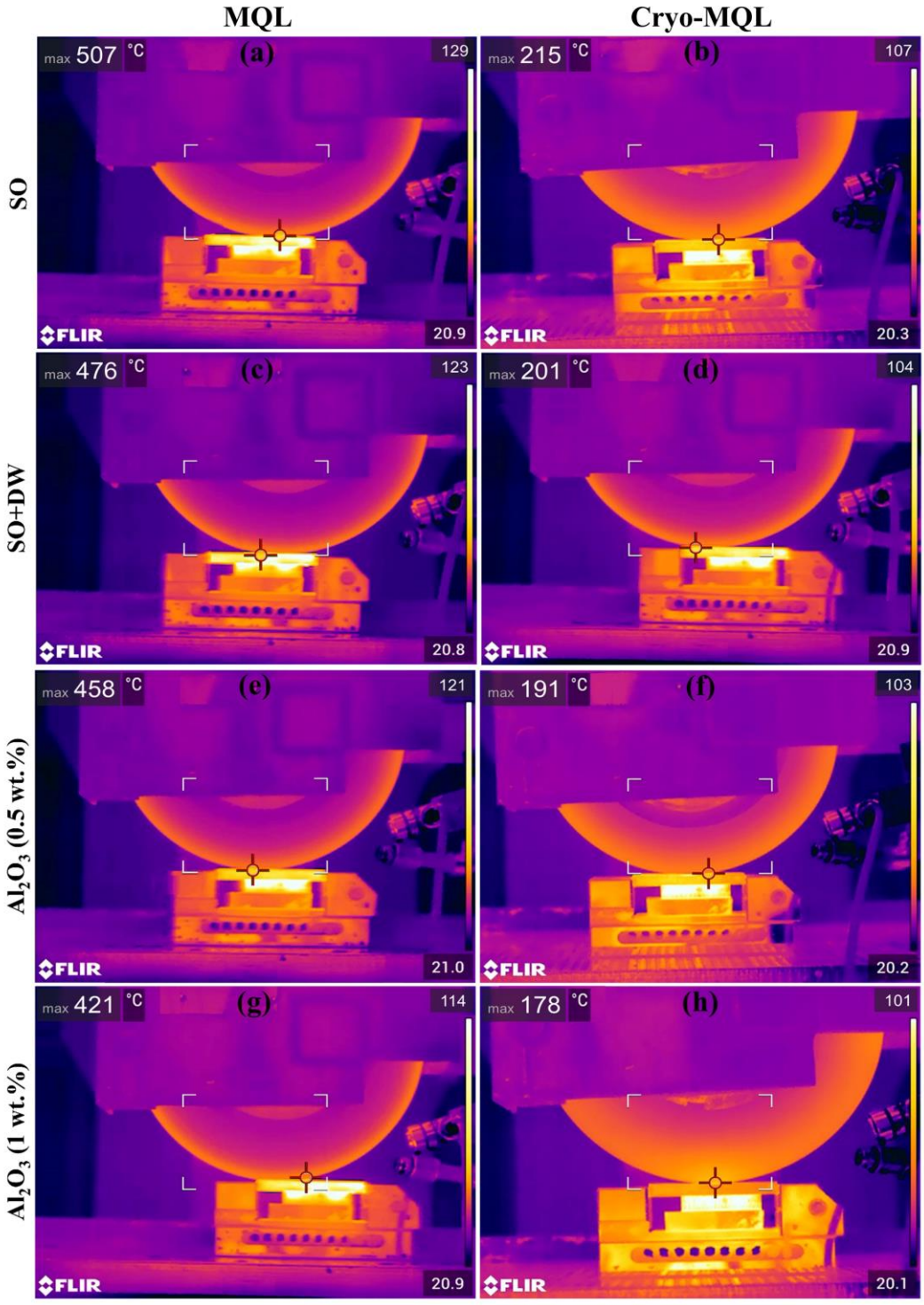

Fig. 4.43: Variation in grinding temperature with different lubricants under MQL and Cryo-MQL environments.

On the other hand, nanofluid has better lubrication properties, enhancing the tribological

properties between the grinding wheel and workpiece interfaces and retaining the abrasive grains for a long period. It is crucial to use the appropriate concentration (wt.%) of NPs. It is supported by thermal conductivity analysis, which demonstrates that increasing the concentration raises thermal conductivity as the dynamic viscosity of the concentration (from 0 to 1 wt.%) of NPs in emulsion increases. On the other hand, LN_2 coolant in Cryo-MQL resulted in significantly lower temperatures at the grinding zone compared to MQL environments. This temperature reduction can provide several benefits, such as improved surface finish, increased tool life, and reduced thermal damage to the ground surface.

4.2.9 Sustainability Assessment: Pugh Matrix Approach

In modern manufacturing sectors, the use of cutting fluids plays a vital role in the efficient production of products with appropriate quality. Presently, various techniques for the application of cutting fluid are available, and a secure and eco-friendly manufacturing process requires a crucial evaluation of the sustainability of each technique before implementation. Sustainable manufacturing, characterized by green efficiency, entails adopting economically efficient and eco-friendly technologies with broader social implications. This approach minimizes waste, reduces negative environmental impacts, and helps in the development of a healthy working environment. It encompasses various manufacturing parameters such as environmental and worker safety, product quality, process efficiency, total cost, etc.

This section uses the Pugh matrix sustainability assessment on MQL and Cryo-MQL techniques to decide the best among these two cooling environments during the grinding operation of AISI D2 tool steel by considering environmental impact, operator safety, coolant cost, setup cost, surface finish, specific energy consumption, grinding temperature, grinding force, and coolant recycling and disposal. To assess sustainability in manufacturing processes, the Pugh matrix decision-making sustainability assessment

technique is preferred by many researchers [256], [257], [258], [259]. According to the importance of each quality parameter, a weight criterion as mathematical numbers ranging from -2 to +2 was assigned. Here, dry grinding was referred to as a datum or reference line for comparing the other two conditions. Its factors are denoted by "S" and receive a total score of zero. Scores were allocated based on the worst-to-best criterion, with "-1" for inferior outcomes and" +1" for better results, and much superior and much inferior results were assigned a score of +2 for the best and -2 for the worst, respectively. Total scores for all conditions, i.e., MQL and Cryo-MQL grinding, are calculated by summing up the scores of all sustainability assessment factors, as represented in Table 4.4. Compared to dry grinding, MQL and Cryo-MQL grinding scored "-1" regarding environmental impact. Because under the MQL and Cryo-MQL, the MQL uses a small quantity of lubricants at high pressure, which emits minimal emissions of harmful gases that harm the environment. At the same time, cryogenic coolant (LN_2) evaporates into the atmosphere and does not harm the environment due to its properties. As to operator safety scoring, MQL and Cryo-MQL were given a "+1" score, producing efficient cooling and debris-flushing capabilities. In the case of MQL, only a small amount of lubricant was used with compressed air; a score "-1" was given to the coolant cost. However, in Cryo-MQL grinding, the score "-2" was given for coolant cost due to the use of liquid nitrogen coolant and lubricants with compressed air. For setup cost, "-1" and "-2" scores were given to the MQL and Cryo-MQL, respectively. The MQL setup includes an air compressor, flow control valve, air control valve, lubricant reservoir, air atomizing spray nozzle, etc. On the other hand, the Cryo-MQL setup has two additional major parts, namely, dewar and nitrogen gas cylinder with MQL setup. Therefore, Cryo-MQL setup cost is high. When the graphs of experimental results were examined, it was seen that Cryo-MQL have better results than MQL grinding in terms of surface roughness, specific energy, grinding temperature and

grinding force. Therefore, MQL and Cryo-MQL grinding were given "+1" and "+2" scores for surface finish, specific energy consumption, grinding temperature, and grinding force, respectively. Further, for coolant recycling and disposal, a score of "-1" was provided for MQL and Cryo-MQL because dry grinding has better results due to the absence of coolant.

Table 4.4: Pugh matrix comparison for MQL and Cryo-MQL techniques.

Sustainability assessment factors	Dry	MQL	Cryo-MQL
Environmental impact	S	-1	-1
Operator safety	S	+1	+1
Coolant cost	S	-1	-2
Setup cost	S	-1	-2
Surface finish	S	+1	+2
Specific energy consumption	S	+1	+2
Grinding temperature	S	+1	+2
Grinding force	S	+1	+2
Coolant recycling and disposal	S	-1	-1
Total +	0	+5	+9
Total -	0	-4	-6
Score	0	+1	+3

Also, in MQL and Cryo-MQL environments, cleaning, filtering, and minimizing the harmful effects of the coolant used, resulted in enhancement in manufacturing cost. Now, after the summation of positive and negative scores in both cases, the final scores are achieved. The MQL receives a final score of +1, and the Cryo-MQL gets a final score of +3. The technique with the highest total score is deemed the best. Thus, this clearly indicates that the Cryo-MQL technique is superior in terms of sustainability compared with the MQL. Therefore, from a sustainability point of view, Cryo-MQL grinding proves economically and socio-technologically beneficial. All these results are displayed in the Kiviat diagram in Fig. 4.44 and sustainability assessment scores are plotted in Fig. 4.45.

"In summary, the Cryo-MQL system is more efficient than the MQL, offering enhanced lubrication, cooling, and process adaptability, leading to improved grinding performance and productivity.

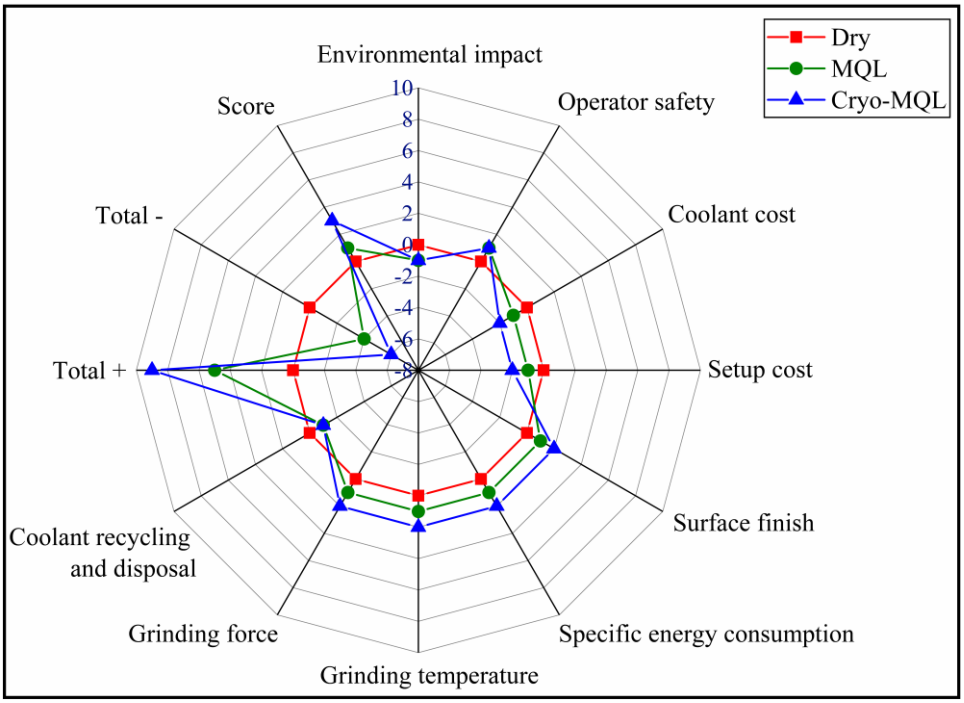

Fig. 4.44: Kiviat diagram based on the Pugh Matrix for sustainability assessment.

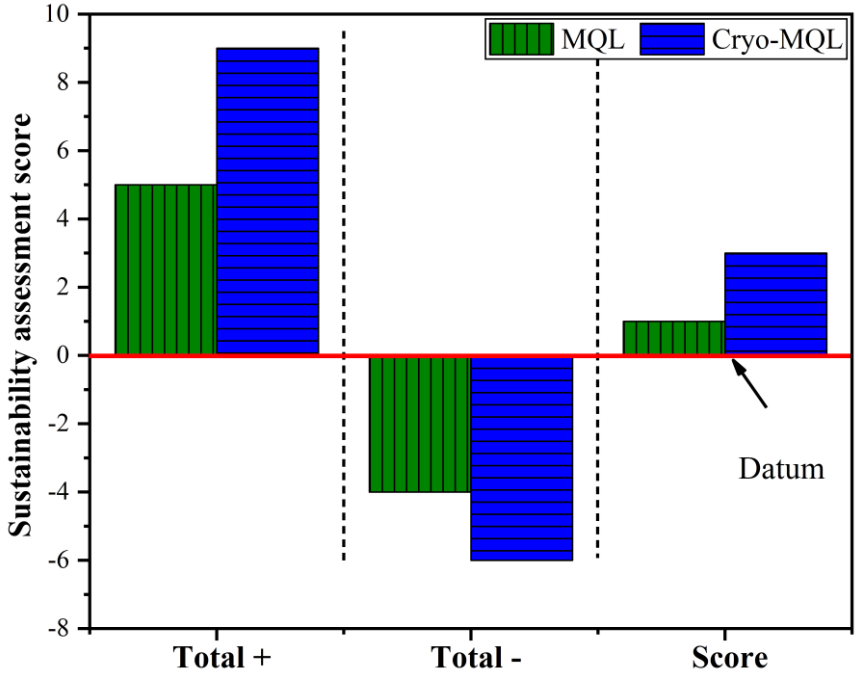

Fig. 4.45: Sustainability assessment scores.

4.3 Performance analysis of magnetic BN and HL parameters under various environments for ground AISI D2 tool steel

The production rate of grinding is significantly impacted by thermal damage. The MBN technology has proven itself as the most suitable alternative to the grinding industry for detecting thermal damage concerning the cost of production and fast analysis with high accuracy. The present section explores the application of novel non-destructive techniques, such as the MBN technique. It is used to characterize the surface integrity and qualitatively assess the thermal damage of AISI D2 tool steel under different environmental conditions. The experiment was conducted with ten environments: dry, wet, MQL: SO, MQL: SO+DW emulsion, MQL: Al_2O_3 NFs (0.5 wt.%), MQL: Al_2O_3 NFs (1 wt.%), Cryo-MQL: SO, Cryo-MQL: SO+DW emulsion, Cryo-MQL: Al_2O_3 NFs (0.5 wt.%), Cryo-MQL: Al_2O_3 NFs (1 wt.%) at a higher downfeed of 40 µm. Combining Cryo-MQL with the MBN technique may result in effective grinding and rapid characterization of the ground sample, shortening the product cycle time. The effect of grinding temperature on the ground surface was examined in terms of microstructure, microhardness, and microchips. Apart from this, BN, and HL outcomes like root mean square (RMS), peak, average permeability, coercivity, and MBN and HL envelopes were correlated with surface property, i.e., microhardness under different environments. The detailed magnetic BN and HL parameters used in the magnetic characterization for ground samples are given in Chapter 3, section 3.3, subsection 3.3.3.

4.3.1 Effect of thermal damage on ground surface under different environments

The grinding process raises temperatures over the workpiece by the rubbing, ploughing, and shearing actions of the grinding wheel that has randomly oriented abrasive grains with

a high negative rake angle. Overheating during grinding results in thermal damage to the surface in the form of oxidation, burning, and the creation of microcracks.

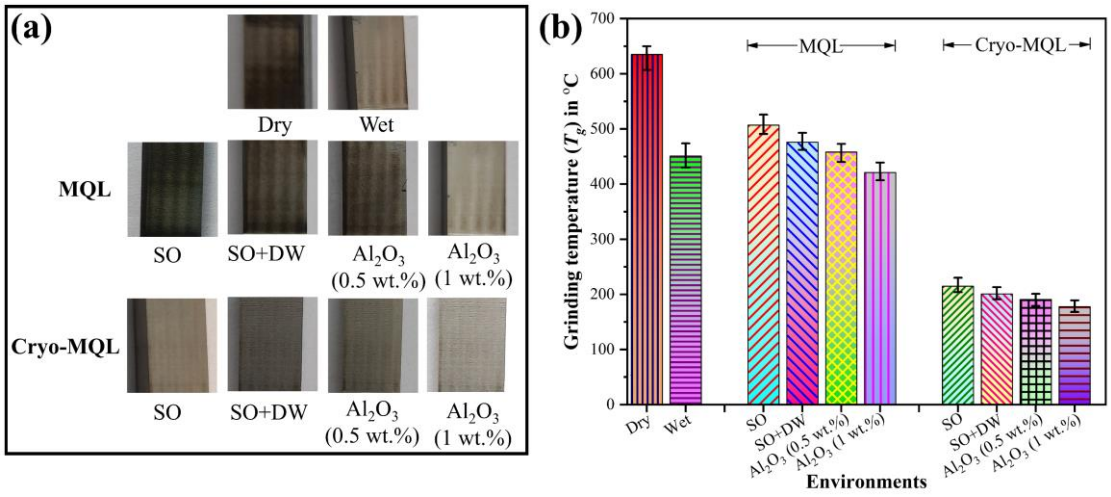

Fig. 4.46: (a) Thermally damaged ground samples; (b) Variation in grinding temperature under different environments.

Fig. 4.46 (a) and (b) show the thermal damage inflicted on ground samples and measured grinding temperature value under different grinding environments. Thus, it is clearly indicated from Fig. 4.46 (a) and (b) that a higher temperature (635 °C) has more thermal damage, and a lower temperature (178 °C) has very low or negligible thermal damage. A lower grinding temperature was obtained at a higher downfeed under Cryo-MQL with Al_2O_3 NFs (1 wt.%), as revealed in Fig. 4.46 (b). This is because the LN_2 coolant in cryogenic cooling and Al_2O_3 NFs in MQL have extracted the maximum amount of heat from the grinding zone. During the grinding process using NFs, Al_2O_3 NPs produced a rolling effect than the sliding action between the grinding wheel and workpiece, resulting in lower friction force and low heat penetration in the ground sample. As seen in Fig. 4.46 (a), dry grinding caused severe grinding burns on the ground sample because cooling and lubricating conditions were absent. Similarly, a high surface roughness value was obtained in the dry mode, as mentioned in Chapter 4 (section 4.1). It was mainly due to generating

more heat, which produced blunt edges of abrasive grits, causing more rubbing and ploughing than shearing phenomena. Clearly, a substantial quantity of heat permeated the sample after dry grinding. Further, MQL-SO has poor surface quality due to its thermo-physical properties (refer to Table 4.1) [260].

4.3.2 Effect of thermal damage on microhardness under different environments

Microhardness is the hardness of a material as examined by pressing an indenter such as a Vickers or Knoop indenter into the material's surface under a 10 to 1000 g load. The microhardness measurement makes it possible to easily evaluate the microstructural change that has occurred in the ground's surfaces. Generally, the microhardness of a material is directly dependent on its microstructural features, which can include plastic deformation, phase transformation, grain boundaries, grain refinements, etc. As part of the experimental analysis, microhardness measurements were performed on the ground sample's surface layer to analyze how the grinding environments influence the final surface layer hardness, which is frequently observed for ground surfaces. This study conducted a microhardness measurement on a cross-section of the ground's surface. The load magnitude was set to 100 gm per 10 s dwell time for analyzing the microhardness.

Fig. 4.47 represents the change in microhardness as a function along with a depth from the ground surface using the alumina grinding wheel under dry, wet, SO MQL, SO+DW MQL, Al_2O_3 (0.5 wt.%) MQL, Al_2O_3 (1 wt.%) MQL, SO Cryo-MQL, SO+DW Cryo-MQL, Al_2O_3 (0.5 wt.%) Cryo-MQL, Al_2O_3 (1 wt.%) Cryo-MQL grinding. In the grinding, work material goes through several abrasive grits action. Hence, the ground surface is plastically deformed and thermally damaged in the shearing direction, resulting in the hardness of the ground surface being much higher than the base metal (660 HV). Further, it was

exponentially diminishing with increasing subsurface depth up to base metal hardness. The reason is to minimize the work-hardening effect along with subsurface depth.

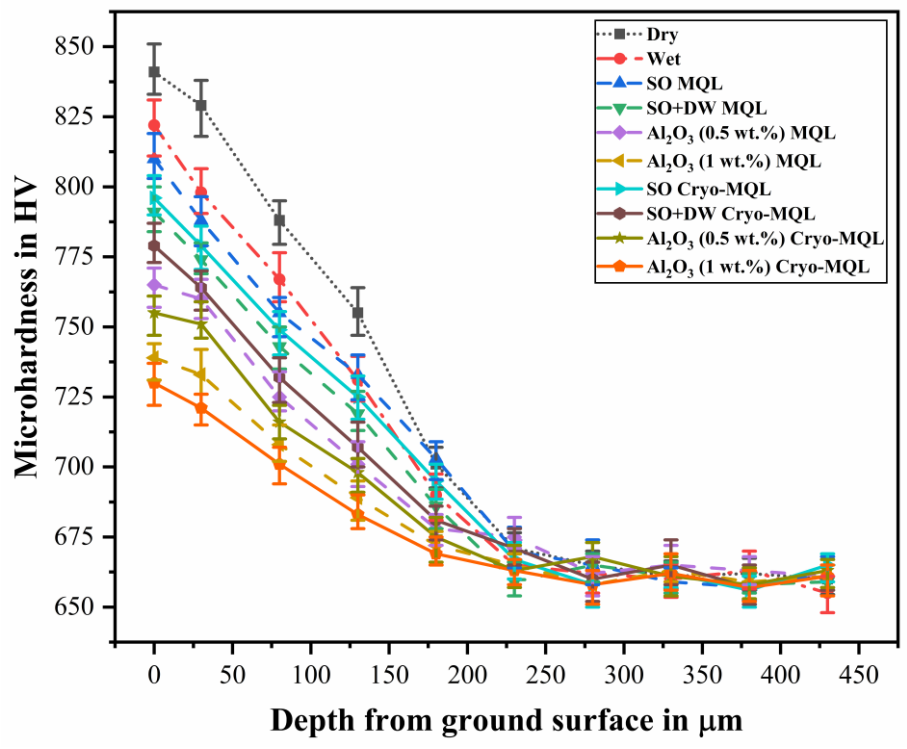

Fig. 4.47: Microhardness of ground surface and subsurface under various grinding environments.

Fig. 4.47 also showed that maximum hardness was observed in dry grinding as compared to other environments. It was mainly due to high heat penetration in the ground surface, which induced large grain refinement in the plastic deformation region. The small grain is improved strength of the plastically deformed layer, providing higher hardness on the ground surface and subsurface of the sample. Meyers and Chawla [261] explained the fundamental relation of grain size and hardness with the help of the Hall-Petch effect. Compared to a dry environment, a relatively lower microhardness value was observed in wet, MQL, and Cryo-MQL environments because of lower heat penetration in the ground sample. This may be attributed to the existence of strong anti-friction lubricating tribo-film, which provided effective lubrication in the grinding wheel and work material interface.

This was reducing heat penetration in the ground surface at lower downfeed for the short grinding duration. The grinding with Al_2O_3 (1 wt.%) NFs lubricant under the Cryo-MQL environment produced the lowest microhardness variation, as illustrated in Fig. 4.47. Similar results (dry > MQl > Cryo-MQL) were reported by Gajrani [232]. This happened due to the cushion by LN_2, the rolling effect of NPs and a uniform protective lubricating boundary layer between the grinding wheel and workpiece. Consequently, this reduced the friction force and heat penetration in the ground surface, contributing to a more consistent lower microhardness value across the ground surface. Similarly, Wang et al. [180] observed the rolling effect of Al_2O_3 NPs on the ground surface during the grinding of the GH4169 workpiece, resulting in anti-friction and anti-wear.

4.3.3 Analysis of ground sample by magnetic BN parameters under different environments

Process variables in grinding, such as downfeed, table feed rate, and grinding environments, are critical in producing thermal damage incurred to the machined surface (discussed in Sections 4.1 and 4.2). Grinding burns on the ground surface, which are thermal damage, change the ferromagnetic material's domain wall movement when an external magnetic field is applied and, as a result, significantly impact BN signal emission. Fig. 4.48 indicates the effect of grinding environments on BN signal, i.e., RMS and peak under different MFI. It clearly observed that BN RMS and peak increased with increased magnetic field intensity at a constant magnetizing frequency (MF) of 25 Hz, table feed rate of 9 m/min and downfeed of 40 µm. BN RMS and peak varied from 0.005–0.077 mV and 0.034–0.717 mV, respectively. Maximum RMS and peak values were obtained under an Al_2O_3 (1 wt.%) Cryo-MQL environment, which were higher, about 155-270% in RMS and 173-370% in peak than the RMS and peak values of dry grinding. RMS and peak values were found in dry, wet, SO MQL, SO+DW MQL, Al_2O_3 (0.5 wt.%) MQL, Al_2O_3 (1 wt.%)

MQL, SO Cryo-MQL, SO+DW Cryo-MQL, Al_2O_3 (0.5 wt.%) Cryo-MQL, Al_2O_3 (1 wt.%) Cryo-MQL about 0.029 and 0.239, 0.03 and 0.293, 0.032 and 0.303, 0.037 and 0.355, 0.049 and 0.471, 0.065 and 0.61, 0.035 and 0.321, 0.041 and 0.399, 0.054 and 0.54, and 0.074 and 0.696 mV, at MFI of 500 Oe, respectively.

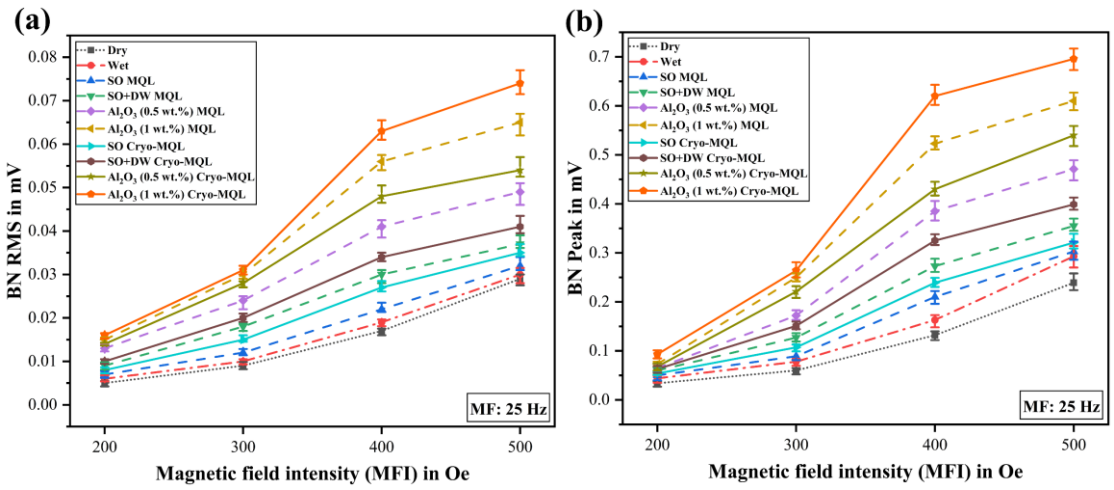

Fig. 4.48: Variation in BN RMS and BN Peak with magnetic field intensity (MFI) under different environments.

Generally, effectiveness of MBN analysis depends upon the process parameters such as MF and MFI. When the MFI was applied to the ground sample, the MF of this field affects the penetration depth into the work material. As MF increases, then decreases the depth penetration of the magnetic field, means low coverage of an area of penetration [262]. In other words, minimum subsurface was covered by a magnetic field at a higher frequency, resulting in a few grains boundary response to magnetic domain wall movement and overall pulse generation was infected. Shrivastava et al. [56] reported that the motion of domain walls becomes less due to thermal damage or plastic-deformed grain boundaries, which act as obstacles. Hence, poor BN responses in terms of lower rms and peak value obtained. On the other hand, magnetization energy was provided by an external magnetic field to the magnetic domain walls motion. More magnetic energy was developed with an increase MFI. Increase in MFI provides more acceleration for movement and rotation of magnetic

domain walls. Apart from this, cooling and lubrication effects significantly influence the surface quality. By this effect, the occurrence of thermal damage over the surface was less due to their thermos-physical properties of lubricants, as discussed in previous section 4.2.

From the discussion with Fig. 4.47 and Fig. 4.48, it was concluded that the RMS and peak values of ferromagnetic material AISI D2 tool steel mainly depend on the hardness of that material. Because higher hardness means more grains with small size in a ferromagnetic material, acting as a hurdle for domain wall motion, resulting in less values of RMS and peak. Many authors reported that BN signal was affected by the number of domain wall movement under the external magnetic field. According to Jiles [263], grain size significantly influences the BN response. If grain size becomes smaller, the number of domain walls increases, which produced smaller BN amplitude. The second influencing parameter of the BN signal was the hardness of work material. Santa-Aho et al. [264] reported that an increase in hardness of the material results in an increase in dislocation density, which restricts the motion of domain walls and leads to low BN response. For better understanding, BN responses correlate with surface integrity indices like microhardness variation of the ground samples (refer to Fig. 4.49). Fig. 4.49 illustrates the relationship between BN RMS and microhardness under different grinding environments, i.e., dry, wet, SO MQL, SO+DW MQL, Al_2O_3 (0.5 wt.%) MQL, Al_2O_3 (1 wt.%) MQL, SO Cryo-MQL, SO+DW Cryo-MQL, Al_2O_3 (0.5 wt.%) Cryo-MQL, Al_2O_3 (1 wt.%) Cryo-MQL, at a constant MFI of 450 Oe and MF of 25 Hz. RMS decreases with the increase in the microhardness of the ground samples of various environments. This variation may be attributed to the rise in the volume fraction of grain boundaries, which hinders the motion of magnetic domain walls and causes a decrease in RMS value. According to the Hall-Petch relationship, grain size is inversely proportional to microhardness, and the same is true for the relationship between the MBN signal and microhardness [265]. A polynomial

link was found between RMS and microhardness of several environmental-based samples (RMS = 2.7458-0.0065 × $HV_{0.1}$ + 3.8865 × 10^{-6} × $HV_{0.1}^2$) with a correlation coefficient (R^2 = 0.9990).

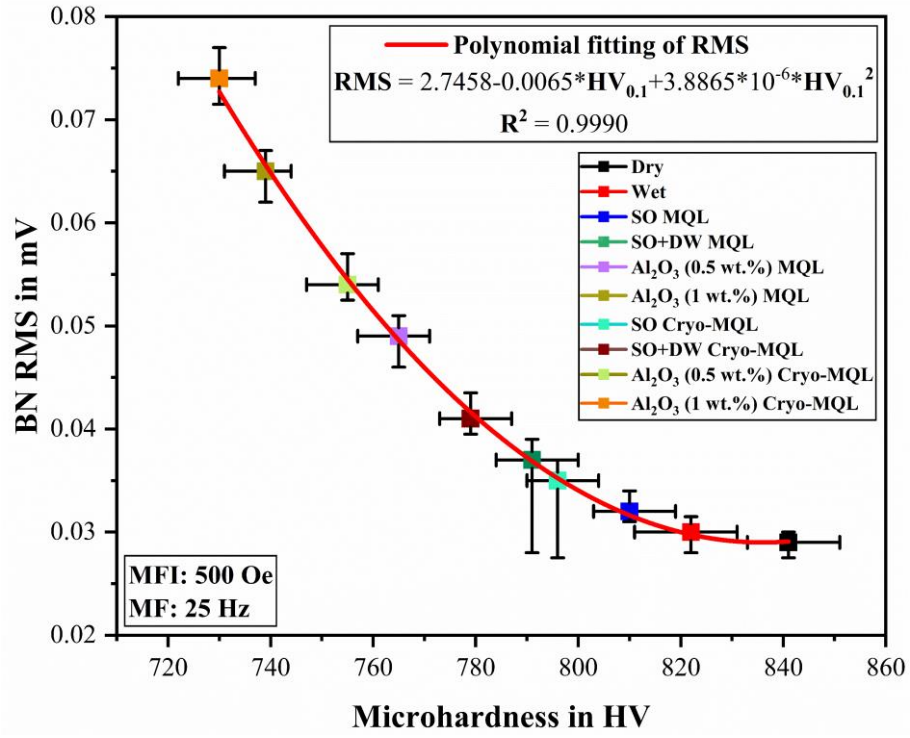

Fig. 4.49: Correlation between RMS and microhardness of ground samples under different environments.

Fig. 4.50 shows the variation in the average envelope of the MBN signal under different grinding environments A single peak MBN envelope was observed under each grinding environment after MBN analysis over the ground samples. This indicated no drastic microstructural changes to long depth occurred in the ground surface under different environments. Gurruchaga et al. [266] also reported a single peak MBN envelope. They investigated the effect of grain size on MBN envelope shape. As seen from Fig. 4.50, the MBN envelope peak shifted towards higher field strength with low RMS amplitude under dry grinding than in other environments. This shift results from more severe thermal damage, which increases the number of grain boundaries and causes an increase in small

grain size. Because these grain boundaries restrict the domain wall, stronger magnetic fields were needed to allow the domain wall to cross these pinning sites. Conversely, the MBN envelope under Al_2O_3 NFs-based grinding gets shifted towards the left side due to lower thermal damage than dry grinding. Furthermore, the shape of the MBN envelope changes with the increase in hardness, as shown in Fig. 4.50.

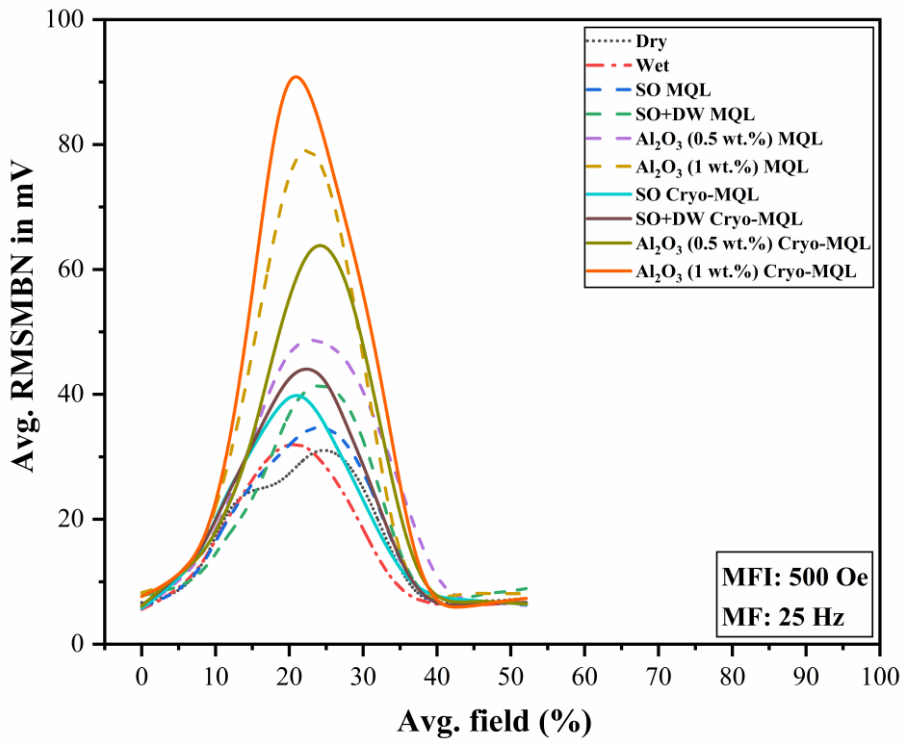

Fig. 4.50: Average of MBN envelope under different grinding environments.

4.3.4 Analysis of ground sample by magnetic HL parameters under different environments

Hysteresis loop study of the ground surfaces was carried out over a broad range of MFI (MFI: 200, 300, 400, and 500 Oe) with a constant MF of 0.1 Hz and a wide range of MF (MF: 0.05, 0.1, 0.15, and 0.2 Hz) with a constant MFI of 450 Oe. The findings of the experiment showed that HL properties, such as average permeability and coercivity, varied when ground samples were exposed to various temperatures. Fig. 4.51 presents the changes in the average permeability of ground samples under variable MFI and MF conditions.

Permeability is the ability of a ferromagnetic substrate to enable magnetic field generation. Fig. 4.51 (a) shows the increasing trend of average permeability with respect to MFI variation. Compared to grinding environments, minimum average permeability was found under dry grinding. In contrast, maximum average permeability was obtained in Al_2O_3 NFs (1 wt.%) under Cryo-MQL grinding. These characteristics were reliant on the samples' hardness. Due to the strong magnetizing energy at high MFI, which assures good magnetization and leads to comparable behaviour in all samples, this occurred. Magnetic field also affect the magnetic tribology properties [267]. An increase in MFI raised the penetration depth of the magnetic field into the work material. Hence more volume of the material can get energized to cross the obstacles in the form of grain boundaries to achieve saturation. This causes the average permeability of the ground sample to increase as a result.

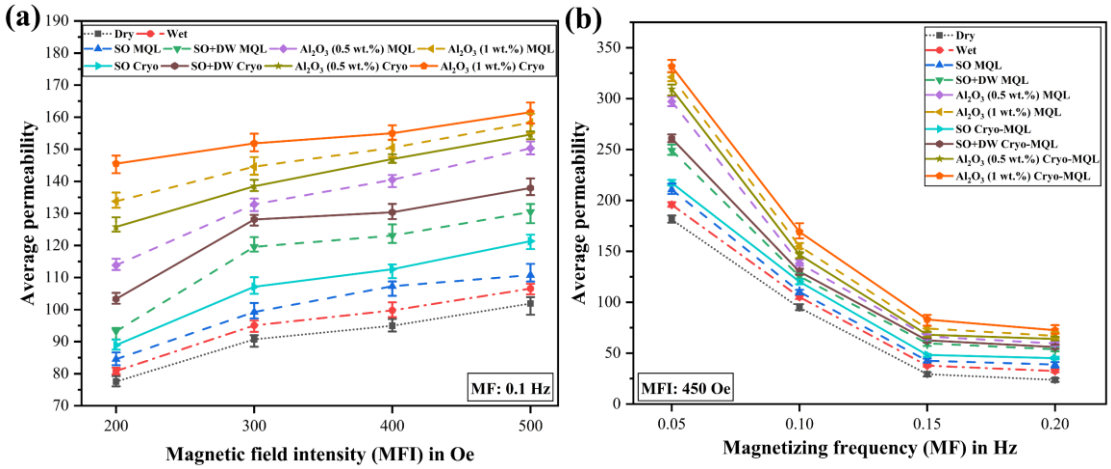

Fig. 4.51: Average permeability with MFI and MF under different grinding environments.

Fig. 4.51 (b) indicates average permeability decreases with an increase in MF. The average permeability value differs greatly between the low-frequency (0.05 Hz) and high-frequency (0.2 Hz). During Cryo-MQL grinding, a high average permeability value was noted, approximately 331.58 at 0.05 Hz MF and 450 Oe MFI. But the low average permeability value was recorded, about 72.28, under the MF of 0.2 Hz MF and MFI of 450

Oe. It depends on the hardness of the ground sample. Aside from that, when the magnetizing frequency is raised, the eddy current damping (i.e., reduction in the strength of the external magnetic field by eddy current) effect rises along with it, limiting the extent to which the magnetic field may penetrate the workpiece; less magnetic field penetration means fewer active domain walls, which in turn reduces the average permeability during the HL process. A similar outcome was obtained by Abhimanyu et al. [231] when they investigated the effect of thermal damage on the surface integrity of work material AISI D2 tool steel using the HL technique. They also reported decreased average permeability with an increase in the MF.

Coercivity is the strength of the applied magnetic field needed to bring the material's magnetization to zero when the specimen's magnetization reaches saturation. It shows the resistivity of the ferromagnetic material to demagnetization. Coercivity is a promising parameter that varies with the material's characteristics, including hardness, stress, phase transformation, magnetizing frequency, and magnetic field intensity.

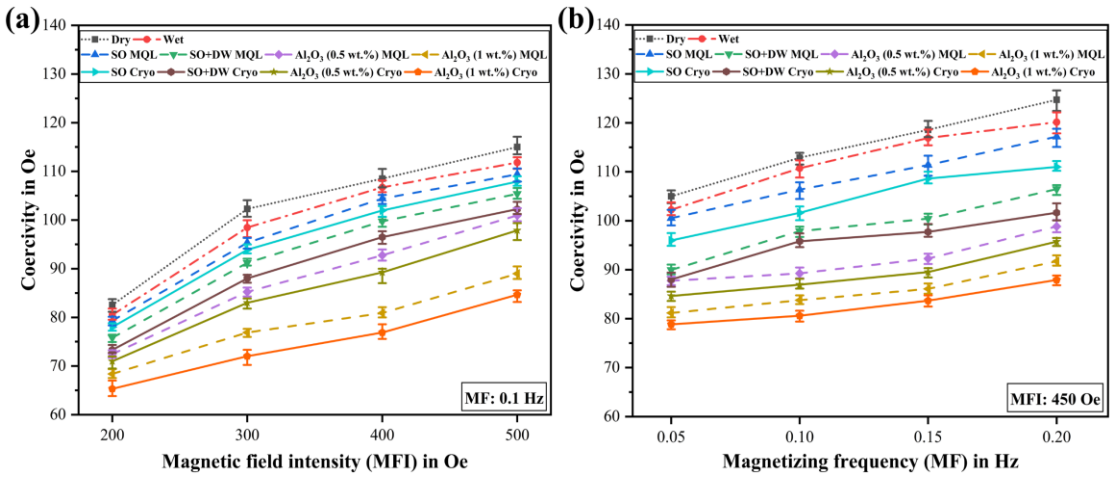

Fig. 4.52: Coercivity with MFI and MF under different grinding environments.

Fig. 4.52 illustrates the variation in coercivity of the ground samples with MFI and MF for different grinding environments. It indicated a significant increase in coercivity with an

increase in the MFI and MF (refer to Fig. 4.52 (a) and (b)). Similar outcomes by Srivastava et al. [62] were reported on the pack carburised low carbon steel work material. Fig. 4.52 reveals the increased coercivity with an increase in MFI. Increased MFI provides more magnetization energy. This energy accelerates magnetic domain wall motion to attain the saturation caused by the external magnetic field. Hence, greater strength of the reverse magnetic field is required after saturation to demagnetize the material. Severe thermal damage provided more hurdles for the magnetic domain wall motion. Therefore, the ground sample required a more energetic magnetic field to attain the saturation of the movement of the magnetic domain wall. This resulted in more coercivity of dry grinding compared to the other environments. As the thermal damage surface decreased, lesser coercivity was noticed, as seen in Fig. 4.52 (a). The coercivity of wet, SO MQL, SO+DW MQL, Al_2O_3 NFs (0.5 wt.%) MQL, Al_2O_3 NFs (1 wt.%) MQL, SO Cryo-MQL, SO+DW Cryo-MQL, Al_2O_3 NFs (0.5 wt.%) Cryo-MQL, Al_2O_3 NFs (1 wt.%) Cryo-MQL at higher MFI were 111.81, 109.4, 105.38, 100.95, 88.98, 107.89, 102.24, 97.87, and 84.66 Oe, respectively, which were reduced by 2.78, 4.88, 8.37, 12.23, 22.63, 6.21, 11.10, 14.90, and 26.39%, respectively, relative to that of dry environment.

Fig. 4.52 (b) depicts the variation in coercivity with increased MF for the ground samples under various environments. A rise in MF reduces the amount of magnetic field penetration into the material, which corresponds to an increase in the reverse MFI required to cause the magnetization to zero after saturation (called coercivity). As a result, coercivity rises as MF rises. Further, the grain refinement and increased hardness upon dry grinding resulted in the formation of more hurdles in the form of more grain boundaries. The magnetic domain wall movement becomes challenging, resulting in the allowance of less penetration of the magnetic field into the ground samples of dry grinding. Thus, the coercivity value was consistently higher in the case of the dry grinding sample in

comparison to the remaining grinding environment samples. Also, increase plastic deformation in the sub-layer of the ground surface resulted in an increase in the coercivity of the ground samples [268]. The results of the analysis of ten ground samples indicated that there was a significant relationship between the coercivity value and the level of thermal damage. Specifically, as the thermal damage increased, the coercivity value also increased. The lower coercivity was obtained in the Al_2O_3 NFs (1 wt.%) under Cryo-MQL grinding owing to negligible phase transformation in the work material.

The hysteresis loop describes the material behaviour during magnetization and demagnetization. The hysteresis curve is drawn between magnetic flux density (B) and magnetizing force (H), as depicted in Fig. 4.53. The change in material properties of ground samples during various grinding environments also affected the shape of the hysteresis loop.

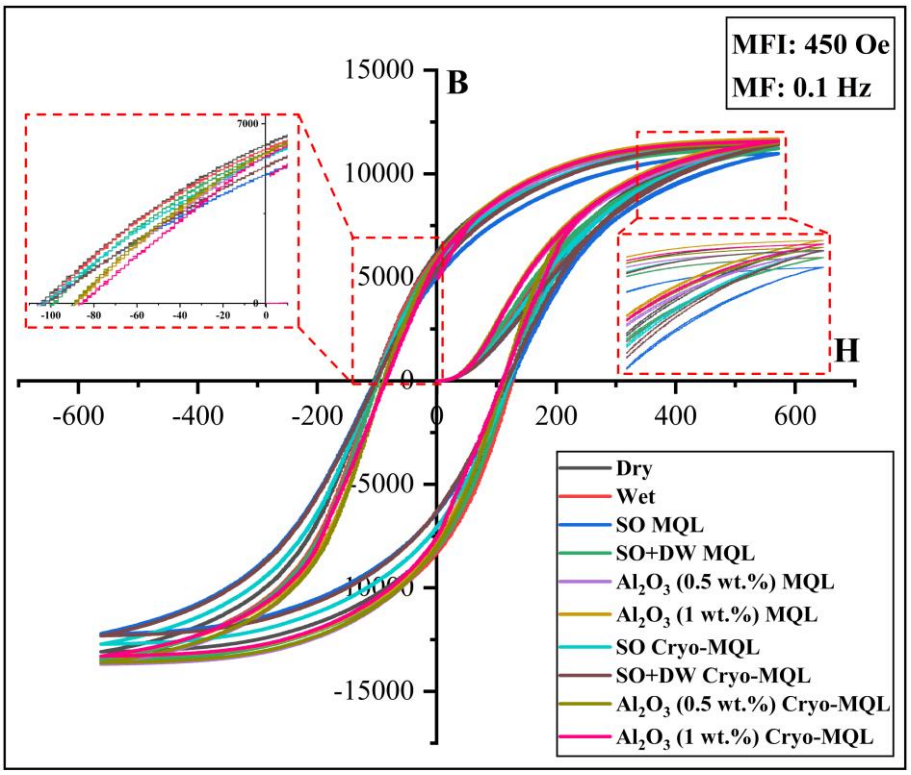

Fig. 4.53: Hysteresis loop envelope for ground samples under different grinding environments.

After applying an external magnetic field to a ferromagnetic material with zero initial magnetic flux density, i.e., negligible magnetic property, the majority of magnetic domains aligned with the direction of the external magnetic field, while some magnetic domains aligned with the opposite direction. The magnetic field intensity exhibited a distinct path from its initial value of zero up to the point of saturation. Moreover, it should be noted that an increase in the external magnetic field does not result in a corresponding increase in magnetic flux density. It is observed that magnetized materials exhibit a deviation from their original path during the process of demagnetization. The region encompassing the processes of magnetization and demagnetization is commonly referred to as the hysteresis loop, which is characterized by a significant loss of energy in a single cycle. Typically, the thermal degradation of ground samples can result in distinct variations in the shape of the hysteresis loop, which can be attributed to the magnetic domain wall motion. Moreover, a shorter and wider hysteresis loop can be achieved for a ground sample with higher hardness due to the presence of a greater number of obstacles that impede the movement of domain walls.

Fig. 4.53 illustrates the hysteresis loop envelope of ground samples at MFI of 450 Oe and MF of 0.1 Hz under different grinding environments. In the present work, as seen in Fig. 4.53, Al_2O_3 nanofluid with 1 wt.% concentration under Cryo-MQL grinding has a long and thin shape of hysteresis loop. It was mainly due to the slightly highest magnetization and demagnetization saturation point while applying the same magnetic field to ground samples. The saturated magnetic flux density was high for it, indicating that this ground sample got more magnetized, followed by the remaining samples under different environments because of its low hardness and less energy lost during the single cycle. As hardness (given in Fig. 4.47) increased, the hysteresis loop changed, resulting in a small and thick shape. Diwakar et al. [55] studied the hysteresis loop analysis on IS 2062 steel

and AISI D2 tool steel work material. They reported a change in the shape of the hysteresis loop. Higher hardness material, i.e., AISI D2 tool steel, compared to lower hardness material like IS 2062 steel, has a short and thick shape of the hysteresis loop.